Effects of electron-electron interaction upon the conductance of nano-systems

Axel Freyn

UNIVERSITE PIERRE & MARIE CURIE
LA SCIENCE A PARIS

spec

THÈSE DE DOCTORAT DE L'UNIVERSITÉ PARIS 6
École Doctorale de Physique de la Région Parisienne
(ED 107)
Spécialité: Physique Théorique

Effets des interactions électroniques sur la conductance de nanosystèmes

Axel Freyn

Thèse dirigée par Jean-Louis Pichard
soutenue le 23 septembre 2008

Jury:
Hélène BOUCHIAT
Patrick BRUNO (rapporteur)
Benoît DOUCOT
Jean-Louis PICHARD (directeur de thèse)
Klaus RICHTER (rapporteur)
Denis ULLMO

to my parents

Acknowledgements

First and for all, I want to thank my thesis advisor, Jean-Louis Pichard for guiding my research during the last three years. Thank you very much for all his patience, his clear explanations of physics and for all the time he spent in discussion with me.

A huge thank you goes also to Yoichi Asada, who motivated the use of the Hartree-Fock theory to understand the non-local effect studied in this work. During his stays in Saclay. I enjoyed our collaboration and discussions. Sadly, Yoichi died in a tragic accident in September 2006.

I would also like to thank Gert-Ludwig Ingold at the "Universität Augsburg". Supervising my diploma thesis, he guided my first steps in research in physics. I enjoyed all our collaboration and discussions.

Thank you also to Rodolfo Jalabert and Dietmar Weinmann at the IPCMS in Strasbourg, for the collaborations and interesting discussions during the last three years.

Thank you of course to all my friends and my family for their love and support. I enjoyed all the time we spent together – it was never sufficient.

The financial support from the "Studienstiftung des deutschen Volkes" (accademic science foundation of Germay), the network "Fundamentals of nanoelectronics" of the European Union (with Contract No. MCRTN-CT-2003-504574), and from the french "Triangle de la Physique" is gratefully acknowledged.

Abstract

In this thesis, the non-local effect of local electron-electron interaction upon the transport in low-dimensional quantum models is studied. At zero temperature, the transport through an interacting nano-structure is described by the scattering approach, using an effective scattering matrix. However, when the interactions are important inside the nano-structure, the effective one-body scatterer describing the nano-structure cannot be determined from the internal properties of the nano-structure only, but is influenced also by external scatterers in the leads.

In this thesis, these interaction-induced non-local effects are studied in three different models, using the Hartree-Fock theory to describe the interaction.

Looking at two interacting nano-structures coupled by a non-interacting lead, we show that the scattering matrices of the nano-structures are effectively coupled via Friedel-oscillations in the lead.

It is sufficient to study a single interacting nano-structure in series with an one-body scatterer to obtain non-local contributions to the quantum conductance. Replacing the second nano-structure by an Aharonov-Bohm scatterer, we show that the scattering matrix of the nano-structure depends on the magnetic flux in the Aharonov-Bohm scatterer.

Extending our study to two dimensions, the influence of the non-local effect upon the images obtained by Scanning Gate Microscopy is considered. Using the non-local effect, we show that the importance of electron-electron interactions inside a nano-structure can be detected from the these images.

Résumé

Dans cette thèse, l'effet non-local des interactions locales électron - électron sur le transport est étudié dans des modèles de dimensions réduites. À température nulle, le transport au travers d'une nanostructure où les électrons interagissent peut être décrit par une matrice de diffusion. Néanmoins, si les interactions sont importantes à l'intérieur de la nanostructure, le diffuseur effectif à un corps qui décrit la nanostructure ne dépend pas seulement des paramètres internes de la nanostructure, mais aussi des diffuseurs qui existent dans les conducteurs en contact avec la nanostructure.

Ces effets non-locaux induits par l'interaction sont étudiés dans trois modèles différents, en utilisant la théorie Hartree-Fock pour décrire l'interaction.

En regardant deux nanostructures où les électrons interagissent, on montre que les matrices de diffusion des deux nanostructures sont effectivement couplées par les oscillations de Friedel qu'elles engendrent dans les conducteurs externes.

Pour observer les effets non-locaux dans la conductance quantique, il suffit de regarder une seule nanostructure où les électrons interagissent en série avec un diffuseur à un corps. En remplaçant la deuxième nanostructure par une boucle attachée, nous montrons que la matrice de diffusion de la nanostructure dépend du flux magnétique au travers de la boucle.

En étendant l'étude à des modèles bidimensionnels, l'influence de l'effet non-local sur les images obtenues par un microscope à effet de grille est étudiée. En utilisant l'effet non-local, on peut détecter l'importance des interactions locales électron - électron dans ces images.

Abstract

In this thesis, effects of local electron-electron interaction upon transport in low-dimensional quantum models are studied. At zero temperature, the transport through a nano-structure can be described by the scattering approach [15, 31, 40] to quantum transport. This approach remains correct even when the electron-electron interactions inside the nano-structure become important. In order to use the scattering approach in the presence of electron-electron interactions, it is necessary to describe the transport properties of the nano-structure by the ones of an effective one-body scatterer which depends on the internal parameters of the nano-structure, including the interaction strength.

But a new phenomenon appears when local electron-electron interactions become important inside the nano-structure: the effective one-body scatterer describing the nano-structure cannot be determined from the internal properties of the nano-structure only, but it will be influenced by the presence of external scatterers which are attached to the leads in the vicinity of the nano-structure: The usual combination law to obtain the scattering properties of multiple one-body scatterers in series from the scattering matrices of the single one-body scatterers is no longer valid in the presence of local electron-electron interactions. This thesis is devoted to the study of these interaction-induced non-local contributions to quantum transport.

There are a number of different techniques for calculating transport through interacting nano-structures. As an analytical solution is impossible for almost all models, it is necessary to use approximate or numerical methods in order to describe transport in the presence of local electron-electron interactions. Examples for the numerical methods include the "Numerical Renormalization Group"-technique, which was originally introduced by Wilson [80] to solve the Kondo problem. This algorithm allows to obtain expectation values of quantum operators inside the nano-structure as a function of the temperature. From these expectation values, it is possible to deduce the transport properties of the nano-structure [54]. However, the NRG-algorithm is limited to the study of a small interacting region coupled to perfect electron bathes, and it is not easily possible to include the effects of external scatterers into this formalism.

Another exact numerical method, which is suitable for one-dimensional systems only, is given by the "Density Matrix Renormalization Group"-algorithm (DMRG) [78, 79], which allows to obtain ground state properties at zero temperature. However, it is very difficult to generalize the DMRG-algorithm to higher-dimensions. In order to obtain the transport properties from the DMRG-calculations, the so-called

"embedding method" can be used [50, 67]: The effective one-body scattering matrix which describes the nano-structure can be related to the persistent current in an infinitely large ring, which is composed of the nano-structure and a noninteracting one-dimensional lead. For finite ring sizes, the persistent current being obtained from the DMRG calculations [50], it is possible to obtain the persistent current of an infinite ring by extrapolating these results.

In this work, we use the Hartree-Fock approximation [7, 26] to describe the electron-electron interaction. The Hartree-Fock approximation can be used to determine an effective one-body Hamiltonian, from which the effective one-body scatterer describing the transport through the interacting nano-structure can be obtained. It has been shown [6] by comparison with exact results obtained from DMRG calculations [52], that for short interacting nano-structures the quantum conductance obtained from the Hartree-Fock approximation can be in good agreement with the exact conductance obtained by the "Embedding method" and the DMRG calculations. In this thesis, we restrict ourselves to such short nano-structures. For the nano-structures studied in this thesis, it is possible to perform one part of the Hartree-Fock calculations analytically, and only use numerical calculations to obtain the self-consistent solution of the Hartree-Fock equations. This approach can help to understand the effects which appear in the model, as it is possible to identify different regimes using these analytical expressions.

In the first chapter, we review some physics related to our work, and present a short overview of the concepts and techniques used in this work.

In the second chapter, we introduce the model for the interacting nano-structure (in the following, referred to as "nano-system") which is used throughout this thesis. We use spin polarized electrons (spinless fermions) and neglect the spin degree of freedom. The nano-system is studied first in the absence of external scatterers. The Hartree-Fock calculations are compared with exact DMRG results, and the relation to the Kondo problem [28] is discussed. In some parameter regimes, the Hartree-Fock theory reproduces the effects obtained by NRG or DMRG-calculations, whereas there are some other parameter regimes, in which the Hartree-Fock theory fails to describe the physics.

Hereafter, we study the influence of different external scatterers: In the third chapter, two identical nano-systems are coupled by an ideal non-interacting lead of length L_C. The presence of the interaction inside the two nano-systems leads to a deviation from the usual combination law for one-body scatterers. This deviation is analyzed as a function of the distance L_C between the two nano-systems. We show that the deviation from the combination law is only important for small distances L_C, and falls of to zero for large distances L_C between the two nano-systems.

In order to obtain non-local contributions to the quantum conductance it is sufficient to study a single interacting nano-structure in series with an arbitrary non-interacting one-body scatterer. Such a setup is studied in chapter 4, where the interacting nano-system is coupled in series with an Aharonov-Bohm scatterer, modelled

by an attached ring, which is threaded by a magnetic flux Φ: If the local interactions inside the nano-system are important, the effective one-body scattering properties of the nano-system depend on the magnetic flux threading the Aharonov-Bohm ring. A particular interesting situation occurs when the geometry of the Aharonov-Bohm ring is adjusted such that its scattering properties at the Fermi energy are independent of the magnetic flux: Without electron-electron interactions inside the nano-system, the total conductance through the complete setup (nano-system and Aharonov-Bohm scatterer) is independent of the flux. But in the presence of local interactions inside the nano-system, the effective scattering matrix of the nano-system does depend upon the flux through the Aharonov-Bohm ring, thus creating flux-dependent oscillation in the total conductance.

So far we have discussed only one-dimensional systems. In the last chapter, we extend our analysis to an interacting nano-structure coupled to two-dimensional leads. Again, we use the nano-system described in chapter 2 to model the interacting nano-structure. This two-dimensional model is motivated by recent experimental results obtained by "Scanning Gate Microscopy" (SGM). In Scanning Gate Microscopy, the charged tip of an Atomic Force Microscope (AFM) is used as a movable gate. While the AFM-tip is scanned over the surface of the sample, the conductance through the sample is measured between two ohmic contacts as a function of the tip position, in order to obtain an image of the electron transport in a semiconductor heterostructure. If the electron-electron interactions are important inside a small region of the sample (e. g. due to low electron density inside a quantum point contact), the non-local interaction effect discussed in this work changes the obtained SGM-images. In chapter 5, we show that the relative importance of the interaction inside the nano-system can be determined by analyzing these SGM images.

Keywords: quantum transport, mesoscopic transport, electron-electron interaction, Scanning gate microscopy, Landauer formulation of electron transport

Résumé substantiel

Dans cette thèse, les effets des interactions locales entre électrons sur la conductance sont étudiés pour des modèles de dimensions réduites. La conductance d'une nanostructure peut être décrite par l'approche de Landauer du transport quantique [15, 31, 40]. Même si les interactions électron - électron deviennent importantes à l'intérieur de la nanostructure, cette approche reste possible dans la limite de température nulle. Mais dans cette limite, la nanostructure doit être décrite par un diffuseur effectif à un corps, qui dépend des paramètres internes de la nanostructure comme par exemple la force des interactions.

Mais si les interactions locales deviennent importantes à l'intérieur de la nanostructure, un phénomène nouveau apparaît : Le diffuseur effectif à un corps qui décrit la nanostructure ne dépend plus seulement des paramètres internes de la nanostructure, mais aussi des diffuseurs externes qui sont au voisinage de la nanostructure : La loi de composition usuelle qui est utilisée pour déterminer la matrice de diffusion complète de plusieurs diffuseurs à une particule en série n'est plus valable en présence des interactions locales. Cette thèse est dédiée à l'étude de ces contributions non-locales induites par les interactions sur le transport quantique.

Pour calculer le transport au travers des nanostructures en présence des interactions entre électrons, il y a plusieurs techniques théoriques qui peuvent être utilisées. Comme la solution analytique est impossible pour la plupart des systèmes, on doit utiliser des approximations ou des méthodes numériques pour décrire le transport au travers de ces nanostructures. Un exemple de ces méthodes numériques est donné par le "groupe de renormalisation numérique" (Numerical Renormalization Group, NRG), développé par Wilson [80] pour la solution du problème Kondo. Avec cette approche, on peut calculer des valeurs moyennes pour des opérateurs quantiques définis à l'intérieur de la nanostructure en fonction de la température. C'est possible de calculer les propriétés de transport de ces valeurs moyennes [54]. Néanmoins, le NRG est restreint à l'étude d'une petite région avec interaction couplée à un bain d'électrons. La prise en compte des effets d'un diffuseur externe reste difficile dans ce formalisme.

Le "Groupe de renormalisation des matrices de densité" (Density Matrix Renormalization Group, DMRG) [78, 79] est une autre technique numérique qui peut donner des résultats exacts pour des modèles unidimensionnels. Avec DMRG, on peut calculer des propriétés de l'état fondamental à température nulle. Toutefois, une généralisation de cet algorithme pour des conducteurs bi- où tridimensionnels est très difficile. Pour obtenir des propriétés de transport par DMRG, on peut utili-

ser la "méthode de la boucle" (embedding method) [50, 67] : La matrice de transfert effective qui décrit la nanostructure peut être reliée au courant permanent d'une boucle de longueur infinie formée d'un conducteur idéal, dans lequel la nanostructure est intégrée. Pour des longueurs finies, le courant permanent peut être calculé avec DMRG [50]. Pour obtenir le résultat pour la longueur infinie, une méthode d'extrapolation doit être utilisée.

Dans ce travail, nous utilisons l'approximation d'Hartree-Fock [7, 26] pour décrire les effets de l'interaction. L'approximation d'Hartree-Fock peut être utilisée pour obtenir la conductance d'une nanostructure avec des interactions locales. En comparant les résultats exacts basés sur des calculs DMRG on a déterminé [6] la validité de l'approximation d'Hartree-Fock : Si la région avec interaction électrons - électrons reste petite, l'approximation d'Hartree-Fock peut donner de bons résultats pour la conductance au travers de la nanostructure. Dans ce travail, on regarde seulement des nanostructures petites. Pour les modèles étudiés, on peut faire une partie des calculs d'Hartree-Fock analytiquement, la solution auto - consistante des équations Hartree-Fock restant à faire numériquement. Ceci aide a mieux comprendre l'effet étudié et en plus diminue le temps de calcul nécessaire.

Dans le premier chapitre, nous introduisons des phénomènes physiques nécessaires à la compréhension de ce travail et donnons un résumé des concepts utilisés dans cette thèse.

Au chapitre deux, nous introduisons le modèle pour la région où les électrons interagissent qui est utilisé dans cette thèse. Cette région sera appelée le "nanosystème". Nous utilisons des électrons polarisés et négligeons les effets de spin. On commence par l'étude du nanosystème seul, sans diffuseurs externes. Les résultats obtenus par Hartree-Fock sont comparés avec les résultats exacts obtenus par DMRG, et la relation avec l'effet Kondo est discutée. Dans quelques régimes des paramètres, l'approximation d'Hartree-Fock donne les mêmes résultats que NRG ou DMRG, mais il y a aussi des régimes où Hartree-Fock ne décrit pas correctement la physique.

Après cette discussion générale, nous étudions l'influence de diffuseurs externes différents : Dans le troisième chapitre, deux nanostructures identiques où les électrons interagissent sont combinées en série par un conducteur parfait de longueur L_C. La présence des interactions locales introduit des déviations à la loi de combinaison usuelle des diffuseurs en série. Ces déviations sont étudiées en fonction de L_C : Elles sont importantes seulement pour des petites distances L_C, et décroissent vers zéro si la distance L_C entre les deux nanosystèmes augmente.

Pour avoir des contributions non locales à la conductance quantique, il est suffisant d'avoir une seule nanostructure où les électrons interagissent, en série avec un diffuseur arbitraire. Ce modèle est étudié au chapitre 4 pour un nanosystème connecté en série avec un diffuseur Aharonov-Bohm qui est donné par une boucle attachée : Si les interactions locales dans le nanosystème sont importantes, les propriétés effectives de diffusion du nanosystème dépendent du flux magnétique au travers de la boucle. Une situation particulièrement intéressante peut arriver pour quelques géométries

spécifiques de la boucle, où la transmission du diffuseur Aharonov-Bohm à l'énergie de Fermi est indépendante du flux magnétique. Sans interaction électron - électron dans le nanosystème, la conductance totale ne dépend pas du flux. Mais si les interactions deviennent importantes, la conductance du nanosystème dépend du flux au travers de la boucle, introduisant des oscillations de la conductance totale en fonction du flux.

Jusqu'ici, seulement des systèmes unidimensionnels ont été étudiés. Dans le dernier chapitre, nous regardons une nanostructure où les électrons interagissent, couplée à des conducteurs bidimensionnels. Comme avant, nous utilisons le nanosystème décrit au chapitre 2. L'étude de ce modèle bidimensionnel est motivée par des expériences récentes faites en "microscopie à effet de grille" (SGM). Dans la microscopie à effet de grille, la pointe chargée d'un "Atomic Force Microscope" (AFM) est utilisée comme grille mobile. On mesure la conductance entre deux contacts ohmiques connectés à la nanostructure en fonction de la position de la pointe chargée, pour créer une image de la distribution et du transport des électrons dans un gaz d'électrons bidimensionnelles. Si les interactions électron - électron sont importantes dans une partie de la structure (par exemple grâce à une densité réduite dans un contact quantique ponctuel), l'effet non local discuté dans cette thèse change les images SGM. Au chapitre 5, nous montrons qu'on peut déterminer l'importance relative des interactions à l'intérieur du nanosystème en analysant les images SGM.

Mots clés : transport quantique, transport mésoscopique, interaction électron - électron, microscopie à effet de grille, Formule de Landauer pour le transport des électrons

Contents

List of Figures

1 Introduction

1.1 Review of some fundamental phenomena

1.1.1 Mesoscopic regime

The important length scales of mesoscopic physics are given by the thermal length L_T and the phase coherence length L_ϕ.

The length scale $L_T \propto 1/T$ exists due to the fact that electrons of different energies around the Fermi energy contribute to the conductance. The width of this energy range is $\propto k_B T$ for a finite temperature T. L_T is given by the length on which a free fermion at the Fermi energy propagates during a time $\hbar/(k_B T)$.

L_ϕ gives the typical length scale on which an electron can propagate without loosing phase coherence, either by scattering at an localized magnetic impurity or by an inelastic scattering process with another electron.

The mesoscopic range is defined by the condition

$$L \leq \min(L_\phi, L_T)\,, \tag{1.1}$$

where L describes the relevant length scales of the problem, for example the size of the studied sample.

In typical experiments, mesoscopic phenomena are observed for samples of sizes up to a few hundred nanometers, at very low temperatures in the range of a few hundred milli-Kelvins.

1.1.2 Non-local effects driven by Friedel-oscillations

When a charged impurity is introduced into a system of electrons, it induces a oscillating change of the electron density in the surrounding electron gas. At zero temperature, this change of the electron density δn, called Friedel oscillations, can be described by an asymptotic decay of the form

$$\delta n(r) \propto \frac{\cos(k_F r + \delta)}{r^d}\,, \tag{1.2}$$

for a d-dimensional model of non-interacting fermions with the Fermi vector k_F. The density $n(r) = \langle c_r^\dagger c_r \rangle$, where $c_r^\dagger$ and c_r are the creation and annihilation operators at the position r.

The non-local effect we want to discuss in this work is essentially driven by the Friedel oscillations: Describing by the Hartree-Fock approximation a nano-structure where the electrons interact and which is coupled to non-interacting leads, the nano-structure Hartree-Fock parameters depend on the local electron density. When an external scatterer is attached to one of the leads at a distance r from the nano-structure, it can induce Friedel-oscillations which change the electron density inside the nano-structure and thus its Hartree-Fock parameters. In one-dimensional models, the Friedel oscillations have a slow asymptotic decay $\propto 1/r$, such that these effects can be important over long distances. The Friedel oscillations decaying as $1/r^2$ in $d = 2$ dimensions, it is necessary in this case to decrease the distance r in order to have significant non-local effects upon the Hartree-Fock parameters.

In chapters 3 and 4, we show a generalization of this concept: Even if the Friedel oscillations $\langle c_r^\dagger c_r \rangle$ vanish and a uniform electron density appears in the model (e. g. at half filling when the setup obeys particle-hole symmetry), it is possible to observe a similar effect when the correlation function $\langle c_r^\dagger c_{r'} \rangle$ (for $r \approx r'$) obeys equivalent oscillations. In the discrete one-dimensional model which we study in this work, we show that the correlation function $\langle c_r^\dagger c_{r'} \rangle$ oscillates as

$$\delta \langle c_r^\dagger c_{r+1} \rangle \propto \frac{\cos(k_F r + \delta_1)}{r^d} \,. \tag{1.3}$$

The nearest-neighbour interaction which will be considered probes both the oscillations of $n(r) = \langle c_r^\dagger c_r \rangle$ and of $\langle c_r^\dagger c_{r+1} \rangle$ at the Hartree-Fock level. While the oscillations $\delta n(r)$ of the density directly change the Hartree correction, the oscillations $\delta \langle c_r^\dagger c_{r+1} \rangle$ influence the Fock energy. Thus, even when the density is uniform, a non-local effect can characterize the Fock corrections via the oscillations of $\langle c_x^\dagger c_{x+1} \rangle$.

This explanation lets us expect that the non-local effect upon quantum transport decays asymptotically as the Friedel oscillations causing it, as $\propto \cos(k_F x + \delta_1)/x^d$ in d dimensions. Later in this work, we will confirm this expectation.

1.1.3 The RKKY-interaction

The RKKY-interaction, named after Ruderman, Kittel, Kasuya and Yosida who described it first, refers to a coupling mechanism of localized magnetic moments in a metal [12, 35, 62, 73, 82]. The magnetic moments are coupled via the conduction electrons of the metal. In metals, there are two different possible realizations of such localized magnetic moments: on the one hand, the spins of two nuclei can be coupled via their hyperfine interaction with the conduction electrons. On the other hand, the spins of two ions can be coupled via the exchange interaction of electrons on their inner shells with the conduction electrons.

For three-dimensional lattices, the effective coupling between two localized magnetic moments $\mathbf{I}_n$ and $\mathbf{I}_m$ separated by a distance $|\mathbf{r}|$ can be described by the effective

Hamiltonian

$$H_{nm}(\mathbf{r}) = \mathbf{I}_n \mathbf{I}_m \frac{4J^2 m^* k_F^4}{(2\pi)^3} F(2k_F|\mathbf{r}|), \tag{1.4}$$

where J denotes the coupling constant between the magnetic moment and the conduction electrons, m^* gives the effective mass of the conduction electrons and $F(x)$ is given by

$$F(x) = \frac{x\cos x - \sin x}{x^4}. \tag{1.5}$$

The effective Hamiltonian (1.4) can be obtained by writing the coupling $\mathbf{I}_i\mathbf{S}$ between one magnetic moment and the spin $\mathbf{S}_i$ of a conduction electron explicitly, and integrating out the conductance electrons. For a detailed derivation of Eq. 1.4 see e. g. [36].

The RKKY-interaction between two localized magnetic moments is important in the study of metals with magnetic order. A analysis of the indirect exchange interaction in $CuMn$-alloys, with a low Mn concentration in Cu is given e. g. by Blandin and Friedel [12].

In $d = 1$ dimensions, Eq. (1.4) gives a long range coupling decaying as $1/r$, with oscillations of period π/k_F. We show in this work that a similar phenomenon contributes also to the quantum conductance of nano-structures inside which electrons interact, when the nano-structures are coupled via metallic wires in which the electron-electron interaction can be neglected. This effect is very general and does not require the presence of the spin degrees of freedom. We will show that the scattering matrix describing an interacting nano-structure depends on the presence of other scatterers in the attached leads. For a distance r between the interacting nano-structure and the second scatterer, this dependence decays as $1/r^d$ and shows oscillations of period π/k_F. The non-local effect upon the quantum conductance of spinless electrons which we study in this thesis is another effect of indirect exchange interactions between interacting nano-structures via conduction electrons, as the RKKY-interaction between local magnetic moments.

1.1.4 The Kondo effect

The Kondo effect is probably one of the most known and studied many-body problems in condensed matter physics. It arises in the study of electron transport in metals at low temperatures: When the resistivity of a metal is measured for decreasing temperature, it will usually fall down too. This is due to the fact that scattering processes between the conduction electrons and between the conduction electrons and the metallic crystal become less and less important for smaller temperature, thus the electrons can travel more easily. However, for many materials, the crystal defects become more important than the lattice oscillations at some low temperature, such that the conductance will saturate at a finite value > 0, depending upon the concentration of defects in the metal.

A special exception is given by superconductors: In these materials, below a critical temperature, the resistance will fall completely to zero. This effect is explained as a many-body phenomenon, in which two electrons are coupled together to act as a single effective particle [9].

Another principally different behavior is observed in metals, when some magnetic atoms are injected into the lattice. In this situation, the resistivity does neither fall to zero, nor saturate to a finite value, but after a minimal value, it increases again when the temperature is lowered further. This phenomenon is the so-called Kondo effect, named after J. Kondo, who succeeded to reproduce theoretically this increase of resistivity in 1964 [37]. Doing higher order perturbation theory in the coupling J between the impurity and the conduction electrons, he showed that the third order term introduces a $\ln T$ contribution to the resistivity. However, it was clear that Kondo's theory could not be correct in the limit $T \to 0$, as the $\ln T$ term diverges for $T \to 0$. Later generalizations of the theory, in which a summation over the leading order terms in $\ln T$ was done, did neither work: For anti-ferromagnetic coupling, this summation results in a divergence of the resistivity already at a finite temperature, which is the so-called Kondo temperature T_K, such that these theories can only be used at temperatures $T > T_K$. In 1975, Wilson developed the non-perturbative "Numerical Renormalization Group" and succeeded to explain the behavior [80]: For temperatures $T < T_K$, the ground state is described by an effective model, having an infinite coupling parameter, such that the impurity spin is bound in a singlet state to the conduction electrons at the spin position.

1.1.5 The 0.7 structure in quantum point contacts

A Quantum Point Contact (QPC) can be realized as a narrow constriction between two two-dimensional electron gases. When the constriction is almost closed, the conductance through the QPC is quantized in units of the conductance quantum $2e^2/h$ [71]. The factor 2 resulting from the spin degeneracy, one observes a conductance quantization in units of e^2/h in the case of polarized electrons. At the lowest conductance step an extra plateau around a conductance of $G = 0.7 \times 2e^2/h$, the "0.7 structure", has been observed in many experiments [68]. Until now there is no general agreement about the precise origin of this effect. However, as the conductance at this structure is not an integer multiple of $2e^2/h$, it cannot be explained in a single particle picture, but a many-body theory is necessary.

There are many different proposed theoretical models which describe the experimentally observed effects of the 0.7 structure. A first explanation is made by assuming a spontaneous magnetization within the contacts. Using density-functional theory, Wang *et al.* [74] succeeded to reproduce the 0.7 structure in the conductance, but the temperature dependence of the 0.7 structure is not correctly reproduced by these calculations. However, with phenomenological models for a gate-dependant spin gap [13, 59, 60], also the magnetic-field and temperature dependence can be

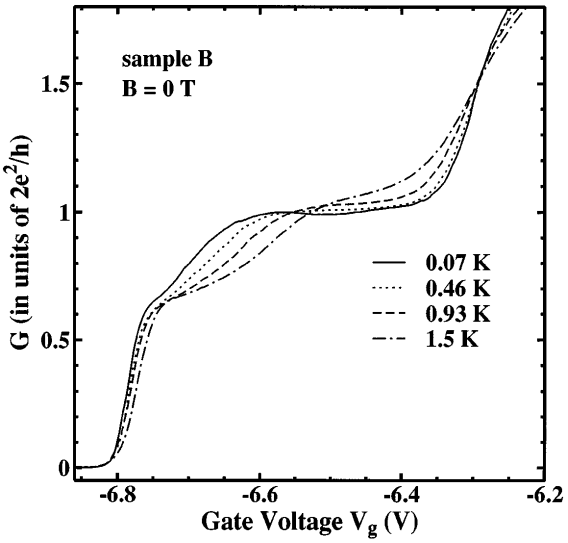

Figure 1.1: The 0.7 structure in an Quantum Point contact in an GaAs/AlGaAs heterostructure at zero magnetic field. For increasing temperature, the plateau at $2e^2/h$ disappears, while the 0.7 structure becomes more pronounced. [From Thomas *et al.* [68]]

reproduced.

Another explanation [19, 29, 47] explains the 0.7 structure by a Kondo effect, treating the QPC as an interacting two-level system for different spins. Also this explanation reproduces the correct magnetic-field and temperature dependence.

In a recent work [42] non-equilibrium Green's function theory was used to study electron transport through a quantum point contact. Taking into account the electron-electron interaction at the Hartree-Fock level, Lassl *et al.* succeeded to reproduce the relevant features of the 0.7 anomaly.

All these explanations have in common that electron-electron interactions play a crucial effect in the appearance of the 0.7 structure. Thus we can expect that the non-local effect which we study in this work will appear in a quantum point contact biased at the 0.7 structure: The electron-electron interactions being important inside the QPC, its transmission properties will depend upon the presence of external scatterers in the attached 2DEGs.

1.1.6 The Coulomb blockade

When a nano-structure is weakly coupled to leads, the electron states inside the nano-structure are well defined and independent of the leads. In this limit, the coupling between the nano-structure and the leads can be described by tunneling barriers. The conductance through the nano-structure is only non-zero when the

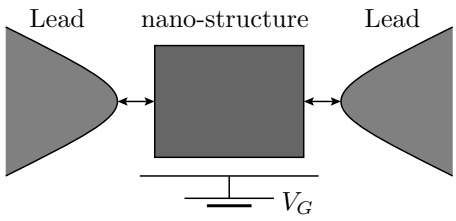

Figure 1.2: Example setup to observe the Coulomb blockade. The nano-structure is weakly coupled to two reservoirs. A gate voltage V_G is applied upon the nano-structure, in order to change the chemical potential inside the structure.

nano-structure has a free state at the Fermi energy E_F. In this situation, electrons can be transmitted through the nano-structure by tunneling from the first lead into the nano-structure, and then into the other lead.

Due to the electron-electron repulsion inside the nano-structure, adding a new electron results in a change of the electrostatic potential inside the nano-structure. For large nano-structures, this change is small and hardly noticeable. However, in small nano-structures and especially at low temperature, this change of the potential can be important, resulting in a gap in the energy spectrum at the Fermi energy. This phenomenon is called "Coulomb blockade", causing a zero conductance unless this gap is compensated by a gate potential applied to the nano-structure.

The Coulomb blockade can be explained using a one-body theory, in which the electron-electron interaction results in a change of the one-body eigenstates inside the nano-structure. Let us define $\Delta\epsilon$ as the mean level spacing between the one-body eigenstates. The energy needed to add an additional electron into the nano-structure can then be given by this mean level spacing $\Delta\epsilon$ plus the repulsion energy between the new electron and the electrons already located inside the nano-structure. This repulsion energy depends on the number N of electrons inside the nano-structure, and can be given by the so-called charging energy E_C, which can be written as

$$E_C = \frac{e^2}{2C}, \tag{1.6}$$

C denoting the effective capacitance which describes the nano-structure. This repulsion energy introduces a gap in the energy spectrum at the Fermi energy, which can block the transport through the nano-structure.

To be able to observe the Coulomb blockade, it is necessary that the charging energy E_C is large compared to the thermal energy k_BT as well as compared to the energy eV for an applied bias Voltage V. Under these conditions, the transport through the nano-structure can be blocked by the Coulomb blockade.

The one-particle energies of the setup shown in Fig. 1.2 are sketched in Fig. 1.3.

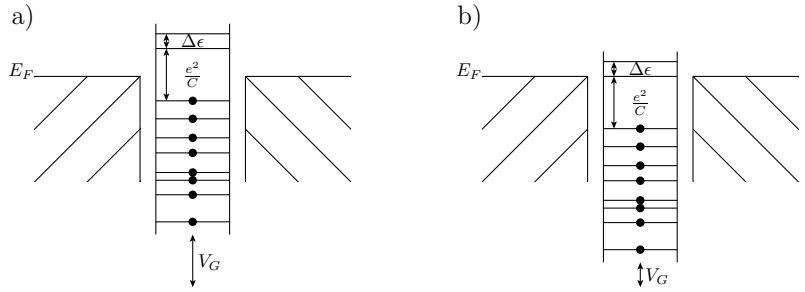

Figure 1.3: The one-particle states of the setup sketched in Fig. 1.2. a) shows the Coulomb blockade with zero conductance, b) gives the resonant situation with optimal conductance.

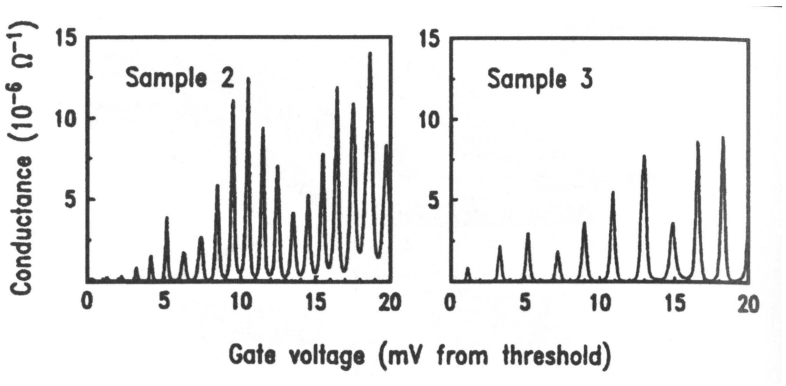

Figure 1.4: Conductance through a nano-structure as a function of the Gate voltage V_G for two samples of different size. Between the conductance peaks, the number N of electrons inside the nano-structure is well defined [After Kastner *et al.* [34]].

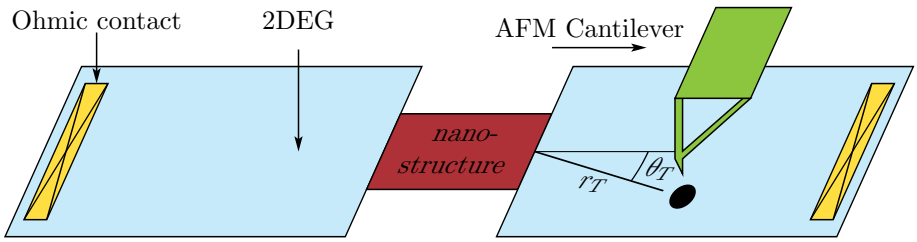

Figure 1.5: The setup of an Scanning Gate Microscope: The nano-structure is connected to two two-dimensional electron gases (2DEG). The charged tip of an Atomic Force Microscope is scanned over these 2DEGs. The conductance is measured between the two ohmic contacts, as a function of the tip position.

In the two leads, the density of states is assumed to be continuous, while inside the nano-structure only discrete states exist.

In Fig. 1.3a we show a situation in which the conductance through the nano-structure is blocked: An electron at the Fermi energy E_F cannot enter into the nano-structure. By changing the applied gate voltage V_G, the states inside the nano-structure can be shifted, until an empty eigenstate appears at the Fermi energy (Fig 1.3b). In this situation, the transport through the nano-structure is possible. When the gate potential is changed further, also this state will be occupied, resulting in a situation similar as shown in Fig. 1.3a, in which the transport through the nano-structure is blocked.

Thus, when the conduction through the nano-structure is measured as a function of the applied gate voltage V_G, one observes a sequence of conductance peaks between which the conductance goes to zero. Typical experimental results such a measurement are shown in Fig. 1.4.

When the coupling between the nano-structure and the leads is increased, the Coulomb blockade disappears: For larger coupling terms, the quantum mechanical fluctuations will smear the distinct electron levels of the nano-structure, resulting in the disappearing of the conductance peaks and valleys.

However, in the presence of strong electron-electron interactions, it is nevertheless possible to observe Coulomb blockade even in the presence of perfect contacts [72].

1.2 Scanning Gate Microscopy

1.2.1 Principle of Scanning Gate Microscopy

Scanning gate microscopy (SGM) [23] is a technique from the class of scanning probe microscopy [10, 11]. In scanning probe microscopy, a tip is scanned over

the surface of the sample in order to obtain an image of the surface. Scanning gate microscopy uses an electrically charged tip above the surface. The charged tip couples capacitively to the electrons in the sample and thus influences electron distribution and electron flow in the sample. During the last years SGM has been used to study a wide range of semiconductor nano-structures inside two-dimensional electron gases (2DEGs). SGM can be used to obtain results on the nanometer scale.

The generic setup of an SGM experiment is shown in Fig. 1.5: The charged tip of the microscope is placed at a position (r_T, θ_T) on top of the heterostructure, locally changing the potential in the 2DEG. SGM images are obtained by measuring the quantum conductance g between two Ohmic contacts connected at both sides of the nano-structure as a function of the tip position, while the tip is scanned above the two-dimensional electron gas.

Scanning gate microscopy has been used to study many different two-dimensional nano-structures. Examples include Quantum Point Contacts [4, 33, 69, 70], open quantum rings [27, 45, 55], quantum dots created in carbon nano-tubes [8, 81] or lithographically defined quantum dots [57]. Also some more complex structures like electron interferometer created by a quantum point contacted and a circular mirror [43] have been studied using SGM.

In oder to reduce the effects of thermal smearing, these measurements are done at liquid helium temperatures $T = 4K$ or even below at $T = 300mK$ [57].

1.2.2 SGM images of branched electron flow

In this work, we are mainly interested in the SGM images of electron flow through a Quantum Point Contact (QPC). Topinka *et al.* studied the electron flow through quantum point contacts biased on the first conductance plateaus [69]. In these measurements, the charged tip was placed in the vicinity of the quantum point contact. They measured the angular dependence of the first conductance modes, by biasing the QPC to the first few conductance plateaus $g(n) = n2e^2/h$ and comparing the measured conductances. For example, if the charged tip is placed at an angle $\theta_T = 0$, only the first conductance mode is affected by the tip potential, but not the second. Experimental results are shown in Fig. 1.6.

In a later work [70], Topinka *et al.* studied the electron flow in the two-dimensional electron gas for larger distances r_T between the tip and the quantum point contact. Example results are shown in Fig. 1.7. Those SGM images show that the electrons which pass through the Quantum point contact flow along narrow, branched strands, they are not spread smoothly. Along these branches, the images show oscillations with a period of half the Fermi wave length $\lambda_F/2$. These branches can be reproduced by numerical simulations, where a disorder background potential is added to the 2DEG [48].

G. Metalidis *et al.* developed a Green's function technique for efficient simulation of images obtained by SGM measurements experiments, ignoring the electron-electron

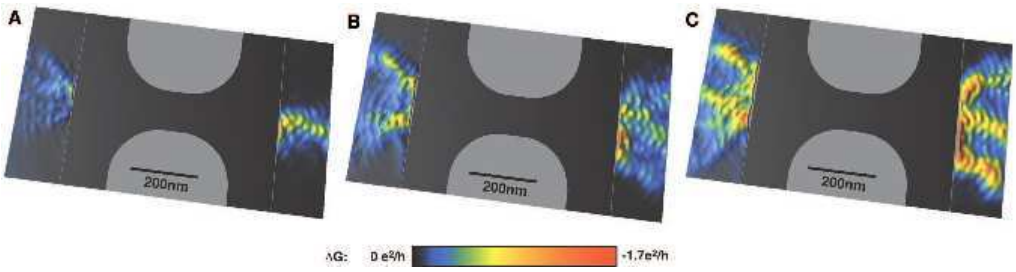

Figure 1.6: Images of electron flow from a QPC of three increasing widths. The images A, B and C show the QPC biased on the first, second and third conductance plateau: The first mode is centered around $\theta_T \approx 0$, the second around $\theta_T \approx \pm\pi/4$. The third plateau can be understood as sum of the first two modes. [From Topinka *et al.* [69]]

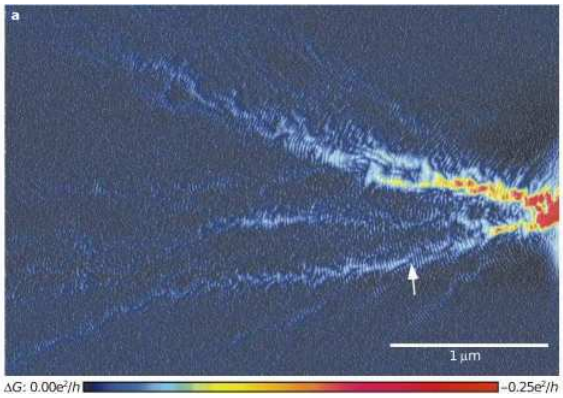

Figure 1.7: Experimental image of branched electron flow in a 2DEG: The QPC is biased on the first conductance plateau $G = 2e^2/h$. The images shows the change of the conductance G as a function of the tip position. Narrow channels of the electron flow appear, and fringes spaced by half the Fermi wave length $\lambda_F/2$ are clearly visible. [From Topinka *et al.* [70]]

interactions [48]. The disorder in the 2DEG is modelled in these calculations by a plane of impurities above the 2DEG. G. Metalidis *et al.* succeeded to reproduce qualitatively all features seen in the experiments, but the magnitude of the effect of the tip in their calculations is much smaller than the one observed in the experiments. This difference can be explained by the fact that the tip is modelled by a delta potential in the numerical simulations, while it has a finite width in experiment, thus scattering the electrons more efficiently. In chapter 5, we will show that including the electron-electron interaction inside the QPC can also increase the magnitude of the conductance decrease induced by the tip.

Although many features of SGM images can be explained using single particle theories, many body effects are expected to be important inside certain nano-structures. Examples include an almost closed QPC around the $0.7 \times 2e^2/h$ conductance structure [68], quantum dots at low electron densities (large factor r_S, the interactions between the electrons are important). In these models, we believe the non-local interaction effects which we will discuss in this work to be important.

However, as the interaction induced effects decay quite fast, it is necessary to place the SGM tip near the nano-structure. These very small distances were not scanned in Refs. [69, 70], but this was done later [4, 20]. In order to be able to approach the nano-structure with the tip, it is necessary that the sample has a clean surface, without top gates. In Refs. [4, 20] the nano-structures were created by using lateral gates instead of top gates, such that is is possible to include the quantum point contact into the region scanned by the tip. In these experiments, Aoki *et al.* placed the tip inside the QPC to obtain SGM images of the inner structure. When the QPC is biased between the conductance plateaus, ring structures appear. For decreasing conductance, the ring diameter increases.

We will analyze the influence of interactions inside the nano-structure upon the SGM images in chapter 5. In our calculation, we ignore disorder and interaction in the leads and use a minimalistic interacting model for the quantum point contact. The decay appearing in the SGM images is different when the electrons interact inside the nano-structure, compared to the situation where the electron-interactions inside the nano-structure are neglected. By analyzing SGM images it is thus possible to detect the importance of the electron-electron interaction inside the QPC.

1.3 Used Methods

1.3.1 Scattering formulation of the conductance

In order to describe quantum transport through a nano-structure, we use the Landauer-Büttiker approach [17, 41]. In this approach, the current through a mesoscopic sample is related to the probability for an electron to be transmitted through the sample. Although the Landauer-Büttiker approach can be generalized to multiple

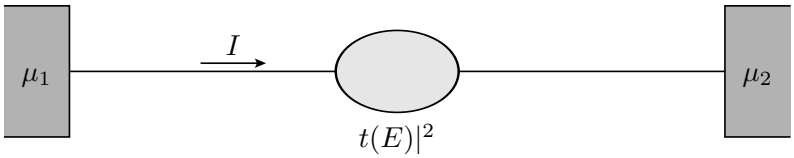

Figure 1.8: Set-up for a two probe measurement of the conductance: The nano-structure is connected by two perfect leads to two electron reservoirs with chemical potential μ_1 and μ_2. The potential difference $\mu_1 - \mu_2$ results in a current I. The only parameter of the nano-structure, which influences the current, is the transmission matrix $t(E)$ describing the transmission through the nano-structure at an energy E.

terminals, we will restrict ourselves to the systems with two leads, as depicted in Fig. 1.8: The nano-structure is connected via ideal leads to two electron reservoirs, which are at different chemical potentials μ_1 and μ_2.

For one-dimensional leads and spin-polarized electrons, the current through the nano-structure from the first to the second lead can be written as

$$I = -\frac{e}{h}\int |t(E)|^2 (f_1(E) - f_2(E))\mathrm{d}E\,, \tag{1.7}$$

where e is the magnitude of the electronic charge, h denotes Planck's constant, $f_i(E) = (1 + \mathrm{e}^{(E-\mu)/k_B T})^{-1}$ denotes the Fermi-Dirac distribution in the i-th lead at a temperature T, and $|t(E)|^2$ gives the transmission probability for electrons to be transmitted from the first to the second lead. At zero temperature, Eq. 1.7 simplifies to

$$I(T=0) = -\frac{e}{h}\int_{\mu_2}^{\mu_1} |t(E)|^2 \mathrm{d}E\,, \tag{1.8}$$

as the Fermi-Dirac distribution is given by

$$f_i(E) = \begin{cases} 1 & \text{if } E - \mu_i < 0 \\ 0 & \text{if } E - \mu_i > 0 \end{cases} \tag{1.9}$$

at zero temperature.

When the difference between the two chemical potentials μ_1 and μ_2 is small, Eq. (1.8) can be linearized to give

$$I = \frac{e^2}{h}|t(E_F)|^2 (V_1 - V_2), \tag{1.10}$$

where $V_i = -\frac{\mu_i}{e}$ denotes the voltage of reservoir i and E_F gives the Fermi energy. The conductance G through the nano-structure is then given by

$$G = \lim_{(V_1 - V_2)\to 0} \frac{I}{V_1 - V_2} = \frac{e^2}{h}|t(E_F)|^2. \tag{1.11}$$

Instead of using the conductance G, it can be useful to introduce the dimensionless conductance g given by $g = h/e^2G = |t(E_F)|^2$ for spinless particles.

The generalization of formula (1.11) to the many-channel case is straight-forward, introducing separate conduction channels α, β in the leads. An electron in channel α in the first lead can then be transmitted to the channel β in the second lead with a probability $|t_{\alpha,\beta}|^2$. In order to obtain the conductance through the nano-structure, it is thus necessary to sum over all incoming and all outgoing conduction channels α, β.

Doing this, we obtain the many-channel conductance formula

$$G = \frac{e^2}{h} \sum_{\alpha,\beta} |t_{\alpha,\beta}(E_F)|^2 = \frac{e^2}{h} Tr(tt^\dagger), \tag{1.12}$$

where Tr denotes the trace of a matrix and t the transmission matrix describing the nano-structure at the Fermi energy.

More detailed reviews of the Landauer-Büttiker conductance formula can be found e. g. in [21, 32].

1.3.2 The Hartree-Fock theory

The complete many-body Hamiltonian can be written as sum of the non-interacting (H_0) and the interacting (H_U) parts,

$$H = H_0 + H_U \,. \tag{1.13}$$

For the tight-binding model of spin-polarized electrons which we use in this thesis the non-interacting part can be written in the general form

$$H_0 = \sum_{\langle p,p' \rangle} t_{p,p'} c_p^\dagger c_{p'} + \sum_p V_p c_p^\dagger c_p \,, \tag{1.14}$$

where $c_p^\dagger$ and c_p are the creation and annihilation operators in second quantization for the site p, $t_{p,p'}$ describes the hopping term between the sites p and p' and V_p the one-body potential on site p. As we take into account nearest-neighbour hopping only, the summation over $\langle p, p' \rangle$ runs only over neighbouring sites p, p'.

The interacting part H_U of the many-body Hamiltonian can be written as

$$H_U = \sum_{\langle p,p' \rangle} U_{p,p'} c_p^\dagger c_p c_{p'}^\dagger c_{p'} \,, \tag{1.15}$$

where $U_{p,p'}$ denotes the interaction between electrons on sites p and p'. Again, we take into account only nearest-neighbour terms for the interaction, such that the summation over $\langle p, p' \rangle$ runs only over neighbouring sites p, p'.

The Hartree-Fock approximation assumes that the many-body ground-state Ψ can be written as a Slater determinant of effective one-body wave functions ψ_α with energies E_α. For a given Fermi energy E_F, all states with energies E_α below E_F are filled at zero temperature.

Thus for N particles, the many-body ground state Ψ can be written in the Hartree-Fock approximation as

$$\Psi(x_1, x_2, \dots x_N) = \begin{vmatrix} \psi_1(x_1) & \psi_2(x_1) & \dots & \psi_N(x_1) \\ \psi_1(x_2) & \psi_2(x_2) & & \\ \vdots & & \ddots & \\ \psi_1(x_N) & & & \psi_N(x_N) \end{vmatrix}, \tag{1.16}$$

where $|\dots|$ denotes the determinant of the matrix.

By minimizing the many-body ground state energy under the condition Eq. (1.16), we obtain the Hartree-Fock equations

$$H_0\psi_\alpha + H_H\psi_\alpha - H_F\psi_\alpha = E_\alpha\psi_\alpha\,, \tag{1.17}$$

which define the single-particle wave-functions ψ_α. The terms H_H and H_F denote the Hartree- and the Fock-correction. The elements of H_H and H_F are given by

$$\langle p|\, H_H\, |p'\rangle = \delta_{p,p'} \sum_{E_\beta<E_F} \sum_{p''} U_{p,p''}\psi^*_\beta(p'')\psi_\beta(p'') \tag{1.18}$$

$$\langle p|\, H_F\, |p'\rangle = \sum_{E_\beta<E_F} U_{p,p'}\psi^*_\beta(p')\psi_\beta(p)\,. \tag{1.19}$$

In order to obtain the Hartree-Fock solution, Eqs. (1.17), (1.18) and (1.19) have to be solved self-consistently. This will be done numerically throughout this work.

The equations (1.18) and (1.19) show that the Hartree- and Fock-corrections are non-zero only between the sites where the interaction is non-zero. Since we neglect the electron-electron interactions in the leads in our model, this are the sites inside the nano-structures only.

A review of the Hartree-Fock approximation can be found e. g. in [7].

An alternative derivation of the Hartree-Fock equations starts from the first-order perturbation theory in U, and adds the condition of self-consistency. These calculations can be formulated also in the Green's function formalism. Of course, the same Hartree-Fock equations are obtained. A detailed derivation is given in e. g. [26].

1.3.3 Numerical solution of the Hartree-Fock equations

In order to obtain the conductance within the Hartree-Fock approximation, we have to include two semi-infinite leads into our models. In numerical calculations, it is

not possible to calculate the single-particle wave-function ψ_α for infinite system sizes. Instead, we use two different techniques to describe the two semi-infinite leads: In one dimension, we first calculate the Hartree-Fock parameters for a model with leads of finite length. Then, it is possible to obtain the limit valid for infinite lead length by an extrapolation procedure. In two dimensions, it is more efficient to formulate the Hartree-Fock theory in terms of Green's functions [26], and to describe the leads by their self-energies.

Extrapolation technique

In order to solve numerically the Hartree-Fock equations in the one-dimensional models, we use an extrapolation technique. Coupling the nano-structure to leads of increasing length, we determine the corresponding Hartree-Fock parameters from Eq. 1.17. The numerical procedure used to solve this system of coupled equations is given in appendix A.7.

The Hartree-Fock parameters obtained from these finite models can be extrapolated to the limit of an infinite model size $L \to \infty$. The precise details of the used extrapolation procedure are given in appendix A.1.

Hartree-Fock theory using Green's function

In the case of a two-dimensional system, the extrapolation method becomes numerically too difficult. It becomes more convenient to use instead a Green's function approach to determine the Hartree-Fock parameters [21].

In the Green's function formulation of the Hartree-Fock theory [21, 26], the Hartree and Fock corrections are included into the Green's function as additional self-energies Σ^H and Σ^F. Also the Hartree-Fock self-energies Σ^H and Σ^F are non-zero only inside the nano-structure. It is thus sufficient to calculate the Green's function elements inside the nano-structure. For a complex energy z, these elements of the Green's function can be given by

$$G^{HF}(z) = \left(z - H_{\mathrm{sys},0} - \Sigma^L - \Sigma^R - \Sigma^H - \Sigma^F\right)^{-1} , \tag{1.20}$$

where $H_{\mathrm{sys},0}$ denotes the non-interacting part of the Hamiltonian of the nano-structure, Σ^L and Σ^R are the self-energies describing the effects of the semi-infinite leads upon the nano-structure, and Σ^H and Σ^F denote the Hartree- and Fock self-energies. The self-energies Σ^L and Σ^R describing the leads are derived in appendix A.5.

The Hartree and Fock self-energies can be obtained from integrals over the Green's

function elements

$$\Sigma^H_{i,i} = \sum_{j,(j\neq i)} \left(-\frac{U_{i,j}}{\pi} \int_{-\infty}^{E_F} \mathrm{d}\epsilon \Im \left(G_{j,j}(\epsilon) \right) \right) \tag{1.21}$$

$$\Sigma^F_{i,j,(i\neq j)} = \frac{U_{i,j}}{\pi} \int_{-\infty}^{E_F} \mathrm{d}\epsilon \Im \left(G_{i,j}(\epsilon) \right) \ , \tag{1.22}$$

$\Im(x)$ denoting the imaginary part of x.

In the two-dimensional model studied in chapter 5, this method allows us to determine the Hartree-Fock solution using a small computer time, since:

- in our study, the electrons interact only between the two sites describing the nano-system. This reduces the Green's function Eq. (1.20) to a matrix of size 2×2.
- the self-energies Σ^L and Σ^R describing the leads are independent of the nano-system and remain unchanged during the Hartree-Fock iterations, it is sufficient to calculate $\Sigma^L(z)$ and $\Sigma^R(z)$ once for each energies z needed in the numerical integration (see A.6).

1.4 Outline

At zero temperature, the conductance through a mesoscopic nano-structure obtained in a two-probe measurement depends only upon the transmission probability $|t_{\mathrm{sys}}(E_F)|^2$ through the nano-structure for electrons at the Fermi-energy E_F. This statement is valid even when the electron-electron interactions inside the nano-structure are important and cannot be neglected. It is possible to describe the scattering properties of the interacting nano-structure exactly by an effective one-body scattering matrix. This has been shown e. g. in [49]. However, this effective one-body scatterer shows an interesting new behavior: For a non-interacting nano-structure, the scattering properties are independent of the additional scatterers in the attached leads. When the electron-electron interaction inside the nano-structure becomes important, the effective one-body scatterer describing the interacting nano-structure depends on the scattering properties of the leads.

In this thesis we want to study the importance of this non-local many-body effect upon the transport properties in spinless models. In chapter 2, we start the study by a discussion of the model for the interacting nano-structure which we use throughout this thesis. This nano-structure, which we call "nano-system" in the following, is shown in Fig. 1.9. In order to include electron-electron interactions into the spinless model, a nearest-neighbour repulsion U is added between the two sites of the nano-system. A applied gate is modelled by the potentials V_G acting on both sites of the nano-system. Additional parameters describing the nano-system are the hopping

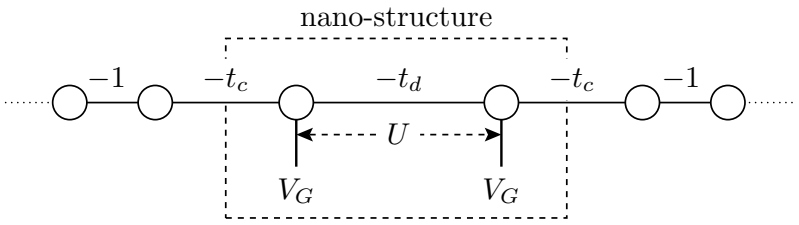

Figure 1.9: The interacting nano-system is modelled by two sites with gate potential V_G, hopping term t_d and nearest-neighbour interaction U. The coupling between the nano-system and the leads is given by t_c. We study at spinless fermions.

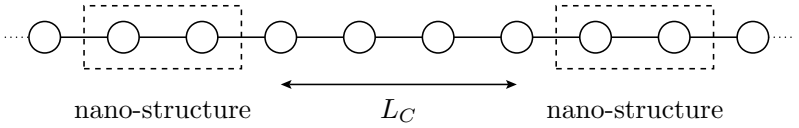

Figure 1.10: Two identical interacting nano-systems are connected by a non-interacting lead of L_C sites.

terms t_d, which couples the two sites of the nano-system, and t_c, which describes the coupling between the nano-system and the attached non-interacting leads.

As a function of the parameters describing the interacting nano-system, this interacting nano-structure can show very different behavior: In the parameter range which we study, exact DMRG (Density Matrix Renormalization Group) calculations show that the Hartree-Fock approximation gives correct results for the quantum conductance of the nano-system. However, the model shown in Fig. 1.9 can be mapped exactly upon an Anderson model [3] with an additional magnetic field which couples to the local impurity. The hopping term t_d is transformed into this local magnetic field. When $t_d \to 0$, a Kondo effect can appear for some set of the parameters V_G, t_c and U. In these parameter ranges, the Hartree-Fock approximation cannot be used to obtain reliable results.

In chapter 3 we consider two identical interacting nano-systems coupled in series, which are connected by a non-interacting lead of length L_C (see Fig. 1.10). Without electron-electron interactions inside the nano-systems, the total transmission through the complete model can be obtained from the usual combination law for one-body scatterers in series. However, if the electrons interact inside the nano-systems, the two scatterers cease to be independent. In this situation, the total conductance through both scatterer is no longer given by the previous combination law, but it is necessary to determine the effective one-body scatterers describing each nano-system in the presence of the other nano-system. As a function of the length

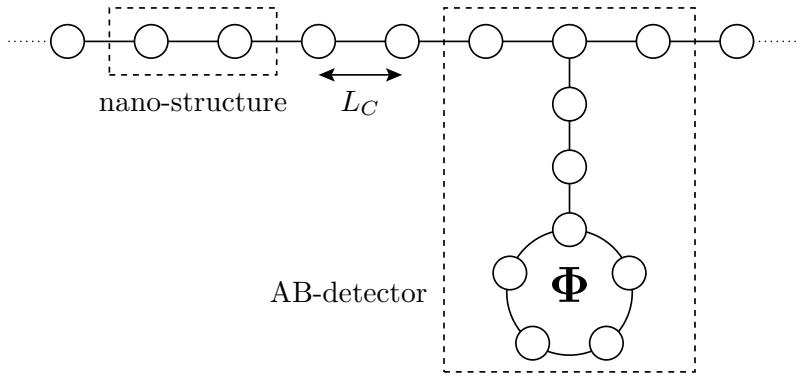

Figure 1.11: An interacting nano-system in series with an Aharonov-Bohm scatterer. The Aharonov-Bohm scatterer is modelled by an attached ring of L_R sites, which is threaded by a magnetic flux Φ. The length of the vertical lead used to connect the ring is given by L'_C.

L_C, the conduction of the two nano-system in series exhibits oscillations of period π/k_F, which decay as $1/L_C$. The analytical results obtained by the Hartree-Fock approximation are compared to exact numerical results given by the embedding method and the DMRG algorithm. The Hartree-Fock approximation qualitatively reproduces the exact DMRG results: When the interaction strength U is increased, the non-local effect grows first, before it decreases down to zero when U is further increased. For small interaction strengths U, the Hartree-Fock theory reproduces even quantitatively the DMRG results.

To observe non-local interaction effects in conductance measurement, a single interacting nano-system in series with a non-interacting scatterer is sufficient. We study such a setup in chapter 4, where the second nano-system is replaced by an attached ring, which can be threaded by a magnetic flux Φ. This attached ring acts as an Aharonov-Bohm scatterer, inducing flux-dependent oscillations in the model. Due to the local electron-electron interactions U inside the nano-system, the scattering matrix S_{sys} describing the nano-system depends upon the magnetic flux Φ threading the ring. This interaction-induced effect results in flux-dependent oscillations of the transmission coefficient t_{sys} through the nano-system. In addition, this effect increases the sensitivity of the total conductance g_{tot} through the complete setup (nano-system and attached ring) upon the magnetic flux Φ. For some specific geometries (parameters L'_C and L_R of the attached ring) a particular interesting situation can appear: it is possible that the Aharonov-Bohm scatterer becomes independent of the magnetic flux Φ at the Fermi energy E_F. Because of this, the total conductance g_{tot} through the complete setup is flux-independent when the electron-electron interaction U inside the nano-system can be ignored. However, when the interaction U becomes important, the effective scattering properties of the

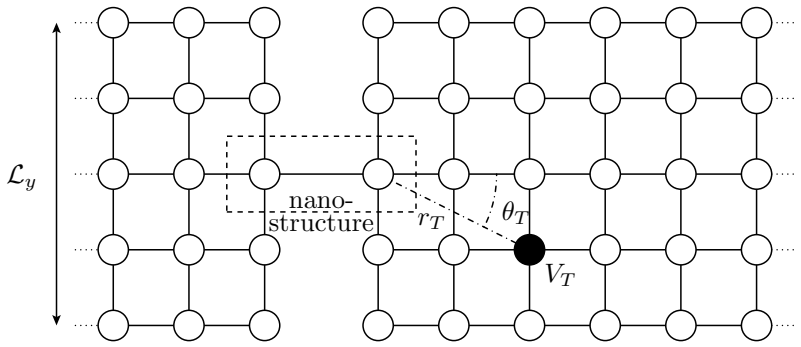

Figure 1.12: The two-dimensional "Scanning Gate Microscopy" - setup: The interacting nano-system is coupled to two semi-infinite two-dimensional leads, whose transverse size is given by $\mathcal{L}_y$. The conductance is measured between the left and the right lead.

nano-system depend on the magnetic flux through the ring. This non-local effect induces flux-dependent oscillations of the total conductance g_{tot}, which is a pure many-body effect in this limit.

After the study of purely one-dimensional systems in chapters 2 to 4, we study in chapter 5 an interacting nano-structure which is coupled to two-dimensional leads. Again, the interacting nano-structure is modelled by the nano-system shown in Fig. 1.9. A movable local potential V_T is added at a distance r_T from the nano-system. The complete model is shown in Fig. 1.12. This setup is motivated by the "Scanning Gate Microscopy" (SGM), which was introduced in section 1.2, the potential V_T being used to model the charged tip. SGM images are obtained by scanning the charged tip around the nano-system and measuring the conductance between the left and the right lead.

We study the influence of the interaction-induced non-local effect upon the quantum conductance of this setup. The oscillations of period π/k_F which can be seen in the SGM images are enhanced by presence of the local interactions U inside the nano-system. This interaction-induced contribution decays as $1/r_T^2$ with the tip position, while in the case without interaction the oscillations decay as $1/r_T$ as a function of the tip position r_T. Using these different decays, it is possible to deduce the importance of the local interaction by analyzing the conductance oscillations in the SGM images.

2 The interacting nano-system

In this chapter, we describe the interacting nano-system which is used to model the nano-structure within this thesis. Connecting the nano-system to two one-dimensional leads, we derive analytical formulas for the Hartree-Fock equations describing the system. It is possible to identify two different parameter regimes: In one regime no interesting non-local effects appear. In the other regime the effective one-body Hamiltonian derived within the Hartree-Fock approximation depends largely upon external scatterers in the leads and the nano-system becomes non-local. Eventually, we discuss the validity of the Hartree-Fock approximation for this model.

2.1 Microscopic Model

We consider a one-dimensional tight-binding model of spin polarized electrons (spinless fermions), in which the electrons do not interact outside a small region, which we call the nano-system. The nano-system consists of two sites ($x = 0$ and $x = 1$). In order to study transport properties, the nano-system is coupled to two semi-infinite perfect leads. The complete model is shown in Fig. 2.1, the dashed box indicating the nano-system: The nearest-neighbour interaction acting between these two sites is described by a repulsion energy U when both sites are occupied. We add two local potentials V_0 and V_1 acting on these two sites to model an applied external gate voltage. The two sites of the nano-system are coupled by an hopping term t_d. The nano-system is coupled by two coupling terms t_c to two perfect leads with hopping terms t_h. Inside the leads, the electron-electron interaction is neglected.

The Hamiltonian describing the nano-system reads

$$H_{\text{sys}} = -t_d(c_0^\dagger c_1 + \text{H.c.}) + V_0 n_0 + V_1 n_1 + U n_1 n_0 \,, \tag{2.1}$$

where $c_x^\dagger$ (c_x) describe the usual creation (annihilation) operator for the site x, and $n_x = c_x^\dagger c_x$ measures the local density.

The left (L) and the right (R) semi-infinite leads are given by the two Hamiltonians

$$H_{\text{lead}}^{L,R} = -\sum_x t_{\text{h}}(c_{x-1}^\dagger c_x + \text{H.c.}), \tag{2.2}$$

where x runs from $-\infty$ to -1 for the left and from 3 to ∞ for the right lead respectively. The hopping amplitude in the leads is set to $t_{\text{h}} = 1$, defining the

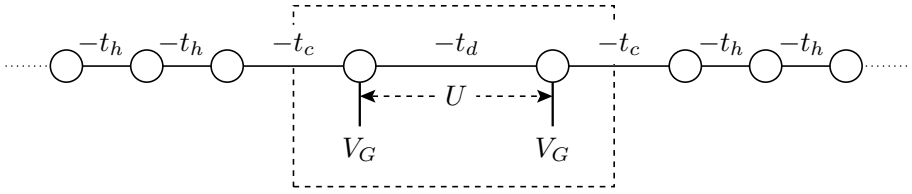

Figure 2.1: The nano-system with two semi-infinite one-dimensional leads: Spin polarized electrons interact only inside the nano-system (sites $x = 0$ and $x = 1$) with inter-site repulsion U and local gate-potentials V_0 and V_1 on the sites $x = 0$ and $x = 1$. The hopping terms are given by t_d inside the nano-system, by t_c for the coupling between the nano-system and the leads, and by $\mathrm{h} = 1$ in the leads.

energy scale. The conduction band corresponds to energies $-2 < E = -2\cos k < 2$, where k denotes the wave-vector of the state.

The two leads and the nano-system are coupled by the two coupling Hamiltonians

$$H^L_{\mathrm{coupling}} = -t_\mathrm{c}(c^\dagger_{-1}c_0 + \mathrm{H.c.}) \tag{2.3}$$

$$H^R_{\mathrm{coupling}} = -t_\mathrm{c}(c^\dagger_1 c_2 + \mathrm{H.c.}), \tag{2.4}$$

which give the coupling to the left and right lead respectively. The complete model is described by the Hamiltonian

$$H = H_{\mathrm{sys}} + \sum_{l=L,R}(H^l_{\mathrm{lead}} + H^l_{\mathrm{coupling}}), \tag{2.5}$$

defining the interacting nano-system coupled to two non interacting one-dimensional semi-infinite leads.

2.2 Hartree-Fock approximation of the nano-system

Using the Hartree-Fock approximation, the many-body Hamiltonian H_{sys} describing the nano-system (Eq. (2.1)) is replaced by an effective one-body Hamiltonian

$$H^{\mathrm{HF}}_{\mathrm{sys}} = -v(c^\dagger_0 c_1 + \mathrm{H.c.}) + V^{\mathrm{HF}}_0 n_0 + V^{\mathrm{HF}}_1 n_1\,, \tag{2.6}$$

which gives the single-particle Hartree-Fock wave-functions. H^{HF}_{sys} does not contain the interacting two particle term Un_1n_0 of H_{sys}, but instead a renormalized hopping term v (instead of t_d) and two renormalized gate potentials V^{HF}_0 and V^{HF}_1 (instead of V_0 and V_1). These three renormalized parameters have to be determined self-consistently. As the nearest-neighbour repulsion U acts only between the sites 0 and 1, the exchange correction modifies only the strength of the hopping term t_d coupling

those two sites, while the Hartree correction contributes to the site-potentials on the sites $x = 0$ and $x = 1$ only. The part of the Hamiltonian which describes the two leads and the couplings between the nano-system and the leads is unchanged by the interaction in the Hartree-Fock approximation.

The Hartree-Fock calculations can be separated into three distinct steps. First, the wave-functions $\psi_k(x)$ of energy E_k are calculated for all energies $E_k \leq E_F$, either numerically for some arbitrary starting values of v, V_0^{HF} and V_0^{HF} or analytically as functions of the parameters v, V_0^{HF} and V_1^{HF}. Then, the expectation values

$$\left\langle c_0^\dagger c_1(v, V_0^{\mathrm{HF}}, V_1^{\mathrm{HF}}) \right\rangle = \sum_{E_k<E_F} \psi_k^*(0)\psi_k(1) \tag{2.7}$$

$$\left\langle c_0^\dagger c_0(v, V_0^{\mathrm{HF}}, V_1^{\mathrm{HF}}) \right\rangle = \sum_{E_k<E_F} \psi_k^*(0)\psi_k(0) \tag{2.8}$$

$$\left\langle c_1^\dagger c_1(v, V_0^{\mathrm{HF}}, V_1^{\mathrm{HF}}) \right\rangle = \sum_{E_k<E_F} \psi_k^*(1)\psi_k(1), \tag{2.9}$$

are evaluated.

In the third step, the values of the three Hartree-Fock parameters v, V_0^{HF} and V_1^{HF} are adjusted until they converge towards the three self-consistent values which satisfy the three coupled integral equations (the Hartree-Fock equations):

$$v = t_d + U \left\langle c_0^\dagger c_1(v, V_0^{\mathrm{HF}}, V_1^{\mathrm{HF}}) \right\rangle \tag{2.10}$$

$$V_0^{\mathrm{HF}} = V_0 + U \left\langle c_0^\dagger c_0(v, V_0^{\mathrm{HF}}, V_1^{\mathrm{HF}}) \right\rangle \tag{2.11}$$

$$V_1^{\mathrm{HF}} = V_1 + U \left\langle c_0^\dagger c_0(v, V_0^{\mathrm{HF}}, V_1^{\mathrm{HF}}) \right\rangle \tag{2.12}$$

Once the self-consistent values of v, V_0^{HF} and V_1^{HF} are determined as solution of the Hartree-Fock equations (2.10)-(2.12), the effective one-body Hamiltonian which defines the single-particle wave-functions $\psi_k(x)$ forming the many-body ground state is given by Eq. (2.5), H_{sys} being replaced by $H_{\mathrm{sys}}^{\mathrm{HF}}$. The single-particle wave-functions $\psi_k(x)$ can be divided into two classes: First, there are scattering states of energies $E_k = -2\cos k$, which are situated inside the conduction band ($-2 \leq E_k \leq 2$) of the leads. These states contribute to the quantum conductance through the nano-system. Second, bound states below ($E_k < -2$) or above ($E_k > 2$) the conduction band can exist. For the Hamiltonian given in Eq. (2.5) (with H_{sys} replaced by $H_{\mathrm{sys}}^{\mathrm{HF}}$), between zero and four bound states exist, depending on the model parameters. As these bound states are centered inside the nano-system and decay exponentially in the leads, their contribution to the expectations values $\langle c_0^\dagger c_1\rangle$, $\langle c_0^\dagger c_0\rangle$ and $\langle c_1^\dagger c_1\rangle$ and hence to the Hartree-Fock parameters is important.

For the nano-system coupled to two ideal leads, it is possible to give analytical formulas for all these eigenstates. We write the wave functions inside the conduction

band in the usual form for scattering states as

$$\psi_{k,+}(x) = \frac{1}{\sqrt{2\pi}} \begin{cases} e^{ikx} + r_{k,+}e^{-ikx} & \text{if} \quad x \leq -1 \\ \psi_{k,+,0} & \text{if} \quad x = 0 \\ \psi_{k,+,1} & \text{if} \quad x = 1 \\ t_{k,+}e^{ikx} & \text{if} \quad x \geq 2 \end{cases} \tag{2.13}$$

$$\psi_{k,-}(x) = \frac{1}{\sqrt{2\pi}} \begin{cases} e^{-ikx} + r_{k,-}e^{ikx} & \text{if} \quad x \geq 2 \\ \psi_{k,-,1} & \text{if} \quad x = 1 \\ \psi_{k,-,0} & \text{if} \quad x = 0 \\ t_{k,-}e^{-ikx} & \text{if} \quad x \leq -1, \end{cases} \tag{2.14}$$

for incoming waves coming from the left (Eq. (2.13)) or the right (Eq. (2.14)) lead, which are scattered by the nano-system and partly reflected and transmitted. The reflection ($r_{k,\pm}$) and transmission ($t_{k,\pm}$) amplitudes of the nano-system can be obtained by solving the Schrödinger equation for these scattering states. One obtains:

$$t_{k,\pm} = -\frac{2\mathrm{i}\mathrm{e}^{-\mathrm{i}k}\sin k}{G(k) - 2(F(k) + 2t_c^2\mathrm{e}^{\mathrm{i}k})\cos k} \tag{2.15}$$

$$r_{k,\pm} = \frac{(t_c^2\mathrm{e}^{\mp\mathrm{i}k} + V_0^{\mathrm{HF}})(t_c^2\mathrm{e}^{\pm\mathrm{i}k} + V_1^{\mathrm{HF}}) - v^2 - 2(F(k) + 2t_c^2\cos k)\cos k}{G(k) - 2(F(k) + 2t_c^2\mathrm{e}^{\mathrm{i}k})\cos k}. \tag{2.16}$$

with

$$F(k) = V_0^{\mathrm{HF}} + V_1^{\mathrm{HF}} - 2\cos k \tag{2.17}$$

$$G(k) = (t_c^2\mathrm{e}^{\mathrm{i}k} + V_0^{\mathrm{HF}})(t_c^2\mathrm{e}^{\mathrm{i}k} + V_1^{\mathrm{HF}}) - v^2\,. \tag{2.18}$$

We see that $t_{k,-} = t_{k,+}$, while the two reflection coefficients ($r_{k,\pm}$) differ if $V_0 \neq V_1$.

The states inside the nano-system (on the sites $x = 0$ and $x = 1$) are given by

$$\psi_{k,+,0} = \frac{1 + r_{k,+}}{\sqrt{2\pi}t_c} \tag{2.19}$$

$$\psi_{k,-,0} = \frac{t_{k,-}}{\sqrt{2\pi}t_c} \tag{2.20}$$

$$\psi_{k,+,1} = \frac{t_{k,+}}{\sqrt{2\pi}t_c}\mathrm{e}^{\mathrm{i}k} \tag{2.21}$$

$$\psi_{k,-,1} = \frac{\mathrm{e}^{-\mathrm{i}k} + r_{k,-}\mathrm{e}^{\mathrm{i}k}}{\sqrt{2\pi}t_c} \tag{2.22}$$

$$\tag{2.23}$$

In addition to these states in the conductance band, there can be up to four bound states centered at the nano-system. These bound states decay exponentially in the

leads, as their energies are outside the conduction band. Assuming $V_0 = V_1 = V$ and $t_c = 1$, their wave functions can be written in the general form:

$$\psi_{bs}^{\alpha,\beta}(x) = A_{\alpha,\beta}(-1)^{x\alpha}\text{sign}(x - \frac{1}{2})^{\beta} e^{-K_{\alpha,\beta}|x-\frac{1}{2}|}, \tag{2.24}$$

where the different four possible bound states are labeled by $\alpha, \beta \in (0, 1)$. The eigenenergies $E_{\alpha,\beta}$ and the corresponding wave vectors $K_{\alpha,\beta}$ describing the exponential decay are given by

$$E_{\alpha,\beta} = -2(-1)^{\alpha}\cosh(K_{\alpha,\beta}) \tag{2.25}$$

$$K_{\alpha,\beta} = \ln\left((-1)^{\beta}v - (-1)^{\alpha}V\right) \tag{2.26}$$

for all four possible bound states $(\alpha, \beta) = (0, 0), (0, 1), (1, 0)$ and $(1, 1)$. The bound state (α, β) exists if and only if its wave vector $K_{\alpha,\beta}$ is a real number.

The normalization constants $A_{\alpha,\beta}$ appearing in the bound states are given by

$$A_{\alpha,\beta} = \sqrt{\frac{-1 + v^2 + V^2 - (-1)^{\alpha+\beta}2vV}{2((-1)^{\alpha}v - (-1)^{\beta}V)}}. \tag{2.27}$$

Two of these bound states (with $\alpha = 1$) oscillate between even and odd sites. These two states have energies above the conduction band. The other two states (with $\alpha = 0$) do not oscillate and are situated below the conduction band. At zero temperature and a Fermi energy inside the conductance band ($-2 < E_F < 2$), the two states above the conduction band ($\alpha = 1$) are empty and can be ignored, while the two bound states below the conduction band ($\alpha = 0$) are always occupied.

2.2.1 Analytical form of the Hartree-Fock equations

For the nano-system connected to two one-dimensional semi-infinite leads, the expectation values $\langle c_0^{\dagger}c_1\rangle$, $\langle c_0^{\dagger}c_0\rangle$ and $\langle c_1^{\dagger}c_1\rangle$ needed in the Hartree-Fock equations (2.10)-(2.12) can be given analytically and only the self-consistent solution of the three coupled equations (2.10)-(2.12) has to be done numerically. For simplicity, we assume $t_c = 1$ and $V_0 = V_1 = V_G$, such that the model obeys inversion symmetry around $x = 1/2$ ($x \leftrightarrow -x + 1$). This symmetry reduces the three coupled equations (2.10)-(2.12) to two equations only, as the effective site potentials $V = V_0^{\text{HF}} = V_0^{\text{HF}}$ are identical.

Using the expressions for the eigenstates given in Eqs. (2.13), (2.14) and (2.24) the expectation values of $\langle c_0^{\dagger}c_1\rangle$ and $\langle c_0^{\dagger}c_0\rangle = \langle c_1^{\dagger}c_1\rangle$ can be explicitly calculated as sum of the contributions of the conduction band and the contributions of the bound states as

$$\begin{aligned}\left\langle c_0^{\dagger}c_1\right\rangle &= \left\langle c_0^{\dagger}c_1\right\rangle_{\text{cb}} + \left\langle c_0^{\dagger}c_1\right\rangle_{\text{bs}} \\ \left\langle c_0^{\dagger}c_0\right\rangle &= \left\langle c_0^{\dagger}c_0\right\rangle_{\text{cb}} + \left\langle c_0^{\dagger}c_0\right\rangle_{\text{bs}} .\end{aligned} \tag{2.28}$$

The contributions of the conduction band read

$$\begin{aligned}\left\langle c_0^\dagger c_1 \right\rangle_{\text{cb}} =& \sum_{q=\pm} \int_0^{k_F} \mathrm{d}k \psi_{k,q}(0)^* \psi_{k,q}(1) \\ =& \frac{f_+ - f_- + 2v(k_F V + \Delta \sin k_F)}{2\pi\Delta^2} \\ \left\langle c_0^\dagger c_0 \right\rangle_{\text{cb}} =& \sum_{q=\pm} \int_0^{k_F} |\psi_{k,q}(0)|^2 dk \\ =& \frac{f_+ + f_- + k_F(v^2 + V^2 + \Delta^2) + 2V\Delta \sin k_F}{2\pi\Delta^2}\end{aligned} \tag{2.29}$$

respectively, where we have introduced different auxiliary functions to simplify the expression:

$$\begin{aligned}\Delta =& v^2 - V^2 \\ f_0(\pm) =& \arctan\left(\frac{v \pm (V-1)}{v \pm (V+1)} \tan\frac{k_F}{2}\right), \\ f_\pm =& f_0(\pm)\left(\Delta^2 - (v \mp V)^2\right).\end{aligned} \tag{2.30}$$

The contributions of the bound states to the expectation values are given by

$$\begin{aligned}\left\langle c_0^\dagger c_1 \right\rangle_{bs} =& \left(\frac{1}{2} - \frac{1}{2(v-V)^2}\right)\Theta(v - V - 1) \\ &+ \left(-\frac{1}{2} + \frac{1}{2(v+V)^2}\right)\Theta(-v - V - 1) \\ \left\langle c_0^\dagger c_0 \right\rangle_{bs} =& \left(\frac{1}{2} - \frac{1}{2(v-V)^2}\right)\Theta(v - V - 1) \\ &+ \left(\frac{1}{2} - \frac{1}{2(v+V)^2}\right)\Theta(-v - V - 1),\end{aligned} \tag{2.31}$$

where the Heaviside step-function

$$\Theta(x) = \begin{cases} 0 & \text{if } x <= 0 \\ 1 & \text{if } x > 0\,. \end{cases} \tag{2.32}$$

is used to describe the parameter ranges in which the respective bound state exists.

Using these analytical expressions for the expectation values, we can solve numerically the two coupled Hartree-Fock equations (2.10) and (2.11) to obtain the self-consistent values v and V in the Hartree-Fock approximation.

2.3 Two limits for the Hartree-Fock approximation

Looking more closely at the Hartree-Fock equations for the interacting nano-system, one can realize that two fundamentally different regimes exist, depending on the

value of the hopping term t_d inside the nano-system. Again we study the inversion symmetric nano-system with the gate potential $V_G = V_0 = V_1$.

- If the hopping term t_d is small compared to the other relevant energy scales, the nano-system transmission becomes highly sensitive to external scatterers. In the next chapters, we will consider the effect of three different external scatterers upon the nano-system transmission.

- If the hopping term t_d is large, the Hartree-Fock equations can be solved analytically, the Hartree-Fock parameters which describe the interacting nano-system and thus its effective quantum transmission become independent of external scatterers. The non-local effects are suppressed.

2.3.1 Simple limit with large hopping t_d

In the limit where the hopping t_d inside the nano-system is large, there is a large interval of values of V_G and E_F where the HF parameters are given by:

$$\begin{aligned} v \approx & t_d + \frac{U}{2} \\ V \approx & V_G + \frac{U}{2} \end{aligned} \tag{2.33}$$

To derive this result, we have to study the model without interaction ($U = 0$). For finite leads of length N_L and N_R for the left and the right lead respectively, the resulting one-body Hamiltonian $H_0 = H_{\text{sys}}(U = 0) + \sum_{l=L,R}(H^l_{\text{lead}} + H^l_{\text{coupling}})$ can be written in real space as a $N \times N$ matrix

$$\mathcal{H}_0 = \begin{pmatrix} \mathcal{H}^L_{lead} & \mathcal{H}_L & 0 \\ \mathcal{H}^T_L & \mathcal{H}_4 & \mathcal{H}_R \\ 0 & \mathcal{H}^T_R & \mathcal{H}^R_{lead} \end{pmatrix}, \tag{2.34}$$

where $N = N_L + N_R + 2$ is the total number of sites in the model. $\mathcal{H}^{L,R}_{\text{lead}}$, $\mathcal{H}_{L,R}$ and $\mathcal{H}_4$ are sub-matrices defining the different parts of the complete model: $\mathcal{H}_4$ is the 4×4 matrix

$$\mathcal{H}_4 = \begin{pmatrix} 0 & -t_c & 0 & 0 \\ -t_c & V_G & -t_d & 0 \\ 0 & -t_d & V_G & -t_c \\ 0 & 0 & -t_c & 0 \end{pmatrix} \tag{2.35}$$

describing the nano-system and the sites of the leads, which are directly coupled to the nano-system. The Hamiltonians of the leads except these two sites are described

by

$$\mathcal{H}_{\text{lead}}^{R,L} = \begin{pmatrix} 0 & -t_h & 0 & \dots \\ -t_h & 0 & \ddots & \ddots \\ 0 & \ddots & \ddots & -t_h \\ \vdots & \ddots & -t_h & 0 \end{pmatrix} \tag{2.36}$$

$\mathcal{H}_L$ and $\mathcal{H}_R$ are matrices of size $(N_L - 1) \times 4$ and $4 \times N_R - 1)$, which contain just one non-zero matrix element in their lower left corner.

The $N \times N$ matrix

$$\mathcal{O} = \begin{pmatrix} \mathbf{1}^L & 0 & 0 \\ 0 & \mathcal{O}_4 & 0 \\ 0 & 0 & \mathbf{1}^R \end{pmatrix} \tag{2.37}$$

describes an orthogonal transformation of the complete model, which projects the nano-system upon the symmetric and anti-symmetric state in the nano-system. $\mathcal{O}$ is described by the identity matrices $\mathbf{1}^L$ and $\mathbf{1}^R$ of dimension N_L and N_R, acting upon the left and right lead respectively, and

$$\mathcal{O}_4 = \begin{pmatrix} 1 & 0 & 0 & 0 \\ 0 & \frac{1}{\sqrt{2}} & \frac{1}{\sqrt{2}} & 0 \\ 0 & \frac{1}{\sqrt{2}} & -\frac{1}{\sqrt{2}} & 0 \\ 0 & 0 & 0 & 1 \end{pmatrix} . \tag{2.38}$$

One gets

$$\mathcal{O}_4^T \mathcal{H}_4 \mathcal{O}_4 = \frac{1}{\sqrt{2}} \begin{pmatrix} 0 & -t_c & -t_c & 0 \\ -t_c & \sqrt{2}V_S^0 & 0 & -t_c \\ -t_c & 0 & \sqrt{2}V_A^0 & +t_c \\ 0 & t_c & +t_c & 0 \end{pmatrix} , \tag{2.39}$$

where the symmetric and antisymmetric potentials are given by $V_S^0 = V_G - t_d$ and $V_A^0 = V_G + t_d$ respectively.

The annihilation operators of the transformed states inside the nano-system are given by $d_S = (c_0 + c_1)/\sqrt{2}$ and $d_A = (c_0 - c_1)/\sqrt{2}$, corresponding to the symmetric and antisymmetric combination of the two nano-system sites respectively. The occupation numbers of these two states in the transformed model are given by $n_S = d_S^\dagger d_S$ and $n_A = d_A^\dagger d_A$. The three Hartree-Fock equations (2.10) - (2.12) are reduced to two equations only, as $V_0 = V_1$ are identical. Since $n_1 n_0 = n_A n_S$, we can write the two remaining Hartree-Fock equations in the transformed basis as

$$\begin{aligned} V_A &= V_A^0 + U \left\langle d_S^\dagger d_S \right\rangle \\ V_S &= V_S^0 + U \left\langle d_A^\dagger d_A \right\rangle \\ v_{AS} &= U \left\langle d_A^\dagger d_S \right\rangle . \end{aligned} \tag{2.40}$$

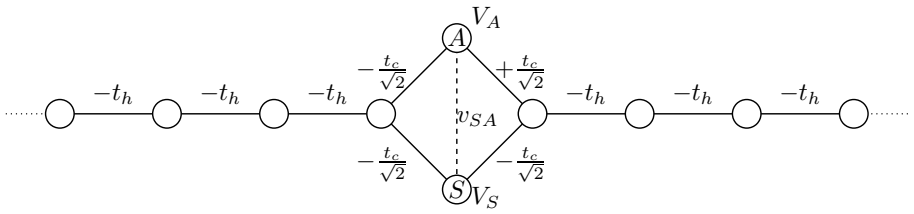

Figure 2.2: Set-up obtained by the orthogonal transformation $\mathcal{O}$ (Eq. (2.37)) from the original setup drawn in Fig. 2.1. The equivalent nano-system is made of two sites in parallel, each connected to both leads by modified hopping terms $\pm t_c/\sqrt{2}$. The site corresponding to the symmetric (anti-symmetric) state has an energy $V_S = V_G$ (V_A) which are given by Eqs. (2.33) in the HF approximation. The exchange contribution v_{AS} is zero in the presence of reflection symmetry.

In the presence of inversion symmetry, the hopping term between the symmetric and the antisymmetric state of the nano-system is given by $v_{AS} = 0$, since the expectation value

$$\left\langle d_A^\dagger d_S \right\rangle = \frac{1}{2}\left(\langle n_0\rangle - \langle n_1\rangle + \left\langle c_0^\dagger c_1\right\rangle - \left\langle c_1^\dagger c_0\right\rangle\right) = 0\,. \tag{2.41}$$

The model resulting from the application of the orthogonal transformation $\mathcal{O}$ on the original Hamiltonian $\mathcal{H}$ is sketched in Fig. 2.2. The transformed nano-system consists of two parallel sites, which are both coupled to each lead. The coupling between these two sites v_{AS} is equal to zero, even in the presence of interaction. Three different limits for this Hamiltonian can be distinguished as a function of the Fermi energies E_F:

- For a small Fermi energy $E_F \ll V_S, V_A$, the nano-system is completely empty, $\langle n_S\rangle \approx \langle n_A\rangle \approx 0$. This effectively decouples the two leads and the transmission $|t_{\rm sys}(E_F)|^2 \approx 0$.
- For a large Fermi energy $E_F \gg V_A, V_S$, the nano-system is completely occupied, $\langle n_S\rangle \approx \langle n_A\rangle \approx 1$. The two leads are again decoupled, and $|t_{\rm sys}(E_F)|^2 \approx 0$.
- The interesting case is obtained for intermediate Fermi energies, for which the energies of the symmetric and antisymmetric eigenstates of the nano-system fulfill the conditions $V_S = V_G - t_d \ll E_F$ and $V_A = V_G + t_d \gg E_F$. In this parameter range, only the symmetric state is occupied ($\langle n_S\rangle \approx 1$), while the antisymmetric state is empty ($\langle n_A\rangle \approx 0$).

We are interested here in the third limit where $|t_{\rm sys}(E_F)|^2 \neq 0$. For a given Fermi energy E_F, the range of values V_G which corresponds to this limit grows linearly

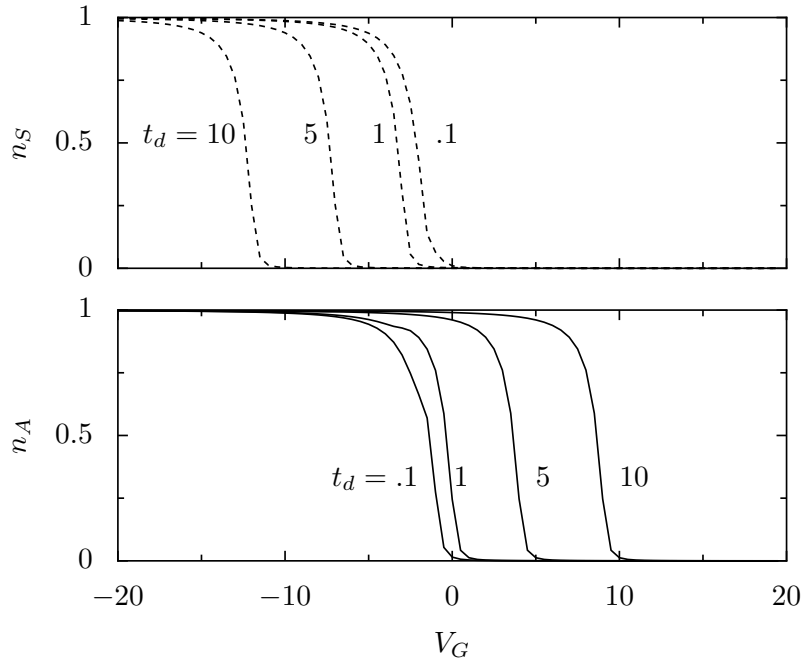

Figure 2.3: The occupation numbers $\langle n_S \rangle$ (lower part, solid lines) and $\langle n_A \rangle$ (upper part, dashed lines) as a function of the gate potential V_G for a filling factor $\nu = 1/8$ ($k_F = \pi/8$) and different values of $t_d = 0.1, 1, 5, 10$ given in the figure. The other parameters are selected as $U = 1$ and $t_c = t_h = 1$. The picture is calculated using the exact Hartree-Fock algorithm.

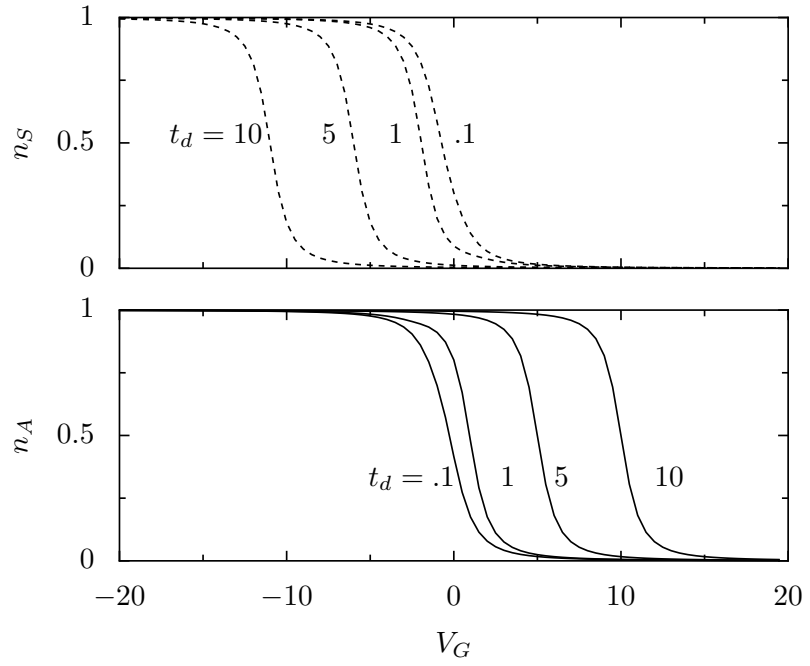

Figure 2.4: The occupation numbers $\langle n_S \rangle$ (lower part, solid lines) and $\langle n_A \rangle$ (upper part, dashed lines) as a function of the gate potential V_G for a half-filled chain $\nu = 1/2$ ($k_F = \pi/2$) and different values of $t_d = 0.1, 1, 5, 10$ given in the figure. The other parameters are selected as $U = 1$ and $t_c = t_h = 1$. The picture is calculated using the exact Hartree-Fock algorithm.

with t_d. Using $\langle n_S \rangle \approx 1$ and $\langle n_A \rangle \approx 0$, the Hartree-Fock equations (2.40) can be solved as

$$\begin{aligned} V_A \approx & V_G + t_d + U \\ V_S \approx & V_G - t_d. \end{aligned} \tag{2.42}$$

The approximated Hartree-Fock Hamiltonian, defined on the basis of the symmetric and antisymmetric nano-system states, is given by Eq. (2.39), where the values V_S^0 and V_A^0 are replaced by the approximated Hartree-Fock values V_S and V_A (Eq. (2.42)). Eqs. (2.33) are obtained by applying the inverse transformation $\mathcal{O}^{\text{inv}} = \mathcal{O}^\dagger$ upon the approximated Hartree-Fock Hamiltonian.

Using the analytical form of Hartree-Fock equations given in subsection 2.2.1, we have calculated the two occupation numbers $\langle n_S \rangle$ and $\langle n_A \rangle$ as a function of the gate potential V_G for different values of the Fermi energy $E_F = -2 \cos k_F$ and the hopping term t_d inside the nano-system. For these calculations, we used a coupling term $t_c = 1$. Fig. 2.3 shows the result for $E_F = -1.84776$, which corresponds to a Fermi wave length of $k_F = \pi/8$. The two occupation numbers n_S and n_A at half filling ($E_F = 0$, $k_F = \pi/2$) are shown in Fig. 2.4. One can see that for large values of $t_d \gg 1$ there is a large interval in which the occupation of the states inside the nano-system is well described by $\langle n_S \rangle \approx 0$ and $\langle n_A \rangle \approx 1$. In this interval, the approximated Hartree-Fock theory provides the correct results, and the Hartree-Fock parameters v and V are given by Eqs. (2.33). Using these values, the nano-system transmission $|t_{\text{sys}}|^2$ at the Fermi energy can be obtained directly from the transmission coefficient $t_{k,\pm}$ given in Eq. (2.15). For the symmetric model ($V_0^{\text{HF}} = V_1^{\text{HF}}$), the effective transmission can be written as

$$|t_{\text{sys}}|^2 = \frac{v}{x} \left(\frac{\Gamma^2}{(v-x)^2 + \Gamma^2} - \frac{\Gamma^2}{(v+x)^2 + \Gamma^2} \right), \tag{2.43}$$

where

$$\begin{aligned} \Gamma = & t_c^2 \sin k_F \\ x = & V + (2 - t_c^2) \cos k_F. \end{aligned} \tag{2.44}$$

When the Hartree-Fock parameters v and V are given by Eqs. (2.33), the transmission in terms of the nano-system parameters and the interaction strength can be written as:

$$|t_{\text{sys}}|^2 \approx \Delta \left(\frac{\Gamma^2}{(V_G - V_+)^2 + \Gamma^2} - \frac{\Gamma^2}{(V_G - V_-)^2 + \Gamma^2} \right), \tag{2.45}$$

where

$$\begin{aligned} \Delta = & \frac{2t_d + U}{2V_G + U + 2(2 - t_c^2) \cos k_F} \\ V_+ = & (t_c^2 - 2) \cos k_F + t_d \\ V_- = & (t_c^2 - 2) \cos k_F - t_d - U. \end{aligned} \tag{2.46}$$

As a function of the gate voltage V_G, Eq. (2.45) gives two peaks in the transmission $|t_{\text{sys}}|^2$, located at $V_G = V_+ = (t_c^2 - 2) \cos k_F + t_d$ and $V_G = V_- = (t_c^2 - 2) \cos k_F - t_d - U$.

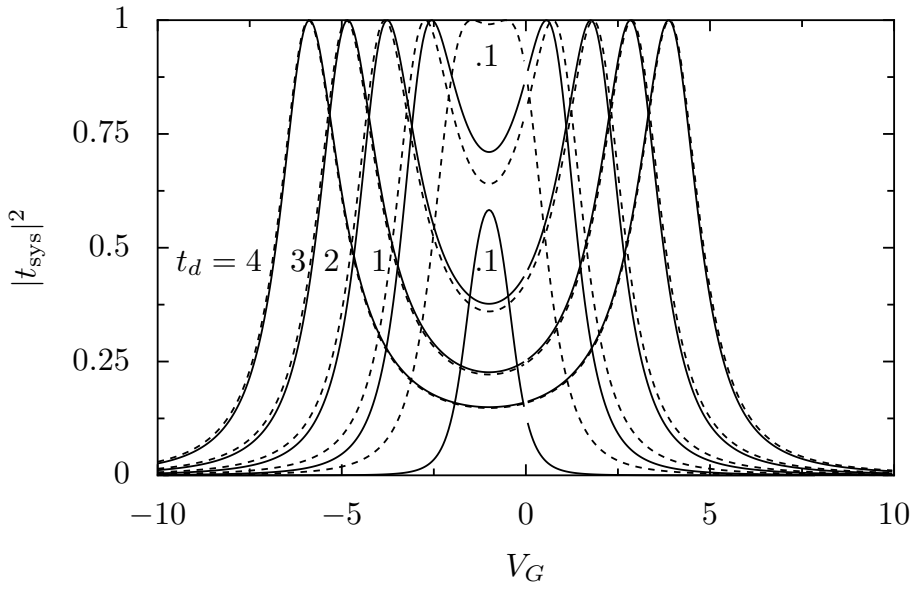

Figure 2.5: Effective nano-system transmission $|t_S|^2$ as a function of V_G for half-filling ($k_F = \pi/2$) and values of $t_d = 0.1, 1, 2, 3, 4$ given in the figure. The other parameters are selected as $U = 2$ and $t_c = t_h = 1$. The solid lines give the transmission probability $|t_s|^2$ calculated using Eq. (2.43) with the HF parameters v and V calculated exactly. The dashed lines give $|t_s|^2$ calculated using Eq. (2.45), v and V being given by Eqs. (2.33). When t_d is increased even further, the differences between the approximated and exact values vanish completely.

They are separated by an interval $2t_d+U$ for large t_d. The position of the first peak at V_+ is independent of the interaction strength U, the second one moves proportional with U. The width of both transmission peaks is given by $\Gamma = t_c^2 \sin k_F$. When the nano-system is only weakly coupled to the leads ($t_c \ll 1$), $\Gamma \ll 1$ induces two sharp peaks at $V_G \approx E_F + t_d$ and $V_G \approx -t_d - U$. This is the usual Coulomb blockade when the nano-system is transparent ($|t_{\rm sys}|^2 = 1$) only when it has one state at the Fermi energy. For a nano-system with $N = 2$ sites, we obtain two peaks in the transmission. When the coupling t_c between the nano-system and the leads is increased ($t_c \to 1$), the peak width Γ is wider and the two values of V_G for which the transmission is large are shifted by an amount equal to $E_F/2$ to larger values of V_G.

In Fig. (2.5), the transmission is shown as a function of the gate potential V_G for a well coupled nano-system ($t_c = 1$) at half filling ($E_F = 0$): for large values of t_d, the double peak structure predicted by Eq. (2.45) evolves and the agreement between the results of the approximation and the exact Hartree-Fock calculations is very good for all values of V_G. On the other hand, for small values of t_d the double peak

structure is still given by Eq. (2.45), while in the exact Hartree-Fock transmission the two peaks merge to form a single peak, whose transmission is much smaller, as shown in Figs. (2.5) and (2.6).

When t_d is large, the potential of the symmetric state $V_S = V_G - t_d$ is much smaller than the potential of the anti-symmetric state $V_A = V_G + t_d$. For intermediate Fermi energies, both potentials V_A and V_S are far from the Fermi energy E_F and the occupation numbers of the two states are given by $\langle n_A \rangle \approx 0$ and $\langle n_S \rangle \approx 1$. In this limit, only huge Friedel oscillations induced by external scatterers can enter inside the nano-system and modify its internal state, thus changing $|t_{\text{sys}}|^2$. Thus the sensitivity of the nano-system transmission for external scatterers is limited for large t_d.

The limit where the solution of Hartree-Fock equations is straightforward is also the limit where the nano-system transmission is almost independent of external scatterers. Only when $V_A^{\text{HF}} \approx V_S^{\text{HF}} \approx E_F$ it is possible to induce large changes of $|t_{\text{sys}}|^2$ by the Friedel oscillations induced by an external scatterer.

2.3.2 Non-local limit with small hopping t_d

When the hopping term t_d inside the nano-system is small, the condition $V_S \ll E_F \ll V_A$ cannot be fulfilled.

- For a small Fermi energy $E_F \ll V_S, V_A$, the nano-system is completely empty. As in the case with large t_d, the leads are effectively decoupled and the transmission is given by $|t_{\text{sys}}(E_F)|^2 \approx 0$.

- For a large Fermi energy $E_F \gg V_S, V_A$, the nano-system is completely occupied. As in the case with large t_d, the leads are effectively decoupled and the transmission is given by $|t_{\text{sys}}(E_F)|^2 \approx 0$ in this limit.

- However for small t_d it is possible to adjust the Fermi energy E_F such that both the potential of the symmetric state $V_S = V_G - t_d$ and of the anti-symmetric state $V_A = V_G + t_d$ are near the Fermi energy. For these values of E_F, the simple approximation given in 2.3.1 is no longer possible.

We are interested here in the third situation, when both the symmetric state and the anti-symmetric state are in the vicinity of the Fermi energy. By choosing a suitable gate potential V_G, this is possible for all Fermi energies E_F. For a small hopping term t_d, the two transmission peaks merge into a single one, as shown in Figs. 2.5 and 2.6 for $t_d = 0.1$. In Fig. 2.6, both the effective transmission probability $|t_{\text{sys}}|^2$ and the particle number $\langle n_S + n_A \rangle$ inside the nano-system are shown as function of the gate potential V_G for different interaction strengths U. Around the transmission peak, the states inside the nano-system are approximately half filled. At the peak,

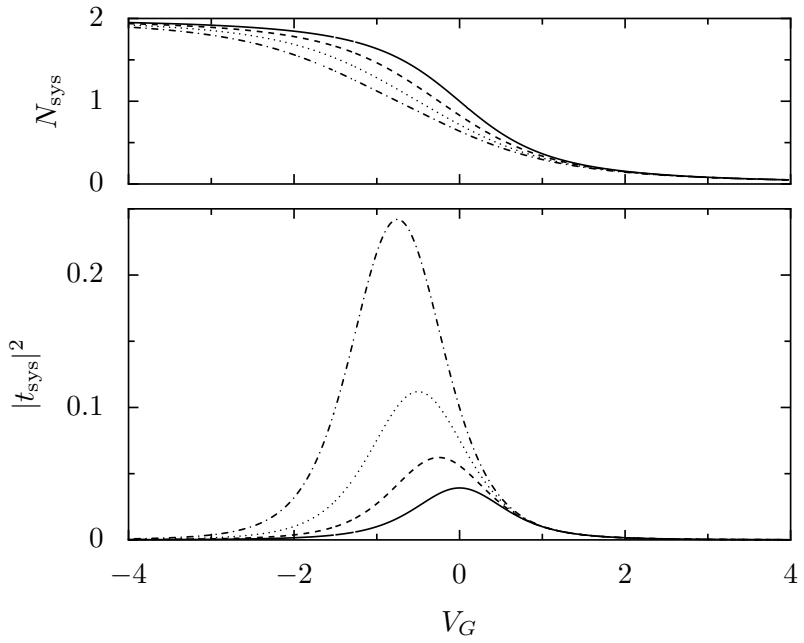

Figure 2.6: The occupation number $N_{\rm sys} = \langle n_S \rangle + \langle n_A \rangle = \langle n_0 \rangle + \langle n_1 \rangle$ (upper part) and the corresponding effective transmission $|t_s|^2$ (lower part) as a function of V_G for different interaction strengths $U = 0$ (solid line), $U = 0.5$ (dashed line), $U = 1$ (dotted line), $U = 1.5$ (dashed-dotted line). The calculations are done for a half-filled chain ($k_F = \pi/2$). The hopping parameter in the nano-system is small ($t_d = 0.1$), and the nano-system is well coupled to the leads ($t_c = t_h = 1$).

$\langle n_S + n_A \rangle = 1$ precisely. The occupation numbers $\langle n_S \rangle$ and $\langle n_A \rangle$ differ when $t_d \neq 0$, as shown in Figs. 2.3 and 2.4.

This is the interesting non-local limit where the nano-system occupation numbers $\langle n_A \rangle$ and $\langle n_S \rangle$ can be strongly varied by the introduction of external scatterers in the semi-infinite leads. In this regime, the Friedel oscillations induced by external scatterers can significantly enter into the nano-system. This yields large variations of the Hartree-Fock parameters, which depend on the external scatterers. This dependency of the effective one-body Hamiltonian describing the nano-system upon external scatterers can give large changes of the effective transmission $|t_s|^2$, when a scatterer in one of the leads is modified. In this limit, it is not possible to derive a simple approximation like it was done in the limit $t_d \gg 1$, but it is necessary to solve the Hartree-Fock equations numerically.

Another condition for having big non-local effects is that the nano-system and the leads are well coupled: if the coupling term t_c is small, the states of the nano-system are separated from the leads, and the Hartree-Fock parameters are independent of the leads. In that case, non-local effects will also be largely suppressed. To allow Friedel oscillations from the leads to enter into the nano-system, a good coupling $t_c \approx 1$ and a small hopping t_d are necessary.

2.4 Validity of Hartree-Fock

The Hartree-Fock theory approximates the ground state of the interacting model by the slater determinant of single-particle wave-function which minimizes the ground-state energy. In this section we want to study the validity of Hartree-Fock for our specific model. In some parameter ranges, Hartree-Fock reproduces the results of exact theories, but there are also parameter ranges, where Hartree-Fock fails to describe the physics correctly: For example for small hopping terms t_c and t_d, an orbital Kondo effect due to the inversion symmetry can arise in our spinless model.

2.4.1 DMRG calculations and the embedding method

"Density Matrix Renormalization Group" (DMRG) [56, 78, 79] is a numerical technique which allows to obtain the ground state energy of an one-dimensional interacting system at zero temperature with very high precision. In addition, it is possible to calculate ground state expectation values like the local electron density using DMRG. A possible way to obtain the effective one-body transmission of a nano-system with the DMRG-technique is given by the embedding method [49–52, 67], which determines the transmission coefficient of a nano-system from the persistent current of a large non-interacting ring which embeds the nano-system. In the embedding method, the nano-system is included into a non-interacting ring of length L. Using DMRG, the ground state energy of this setup is calculated both for pe-

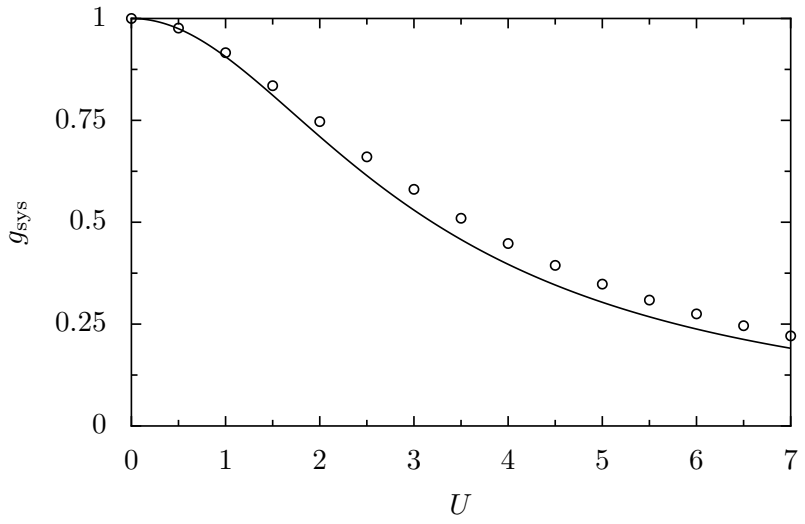

Figure 2.7: Conductance g^{k_F} of the interacting nano-system as a function of the interaction strength U for a half-filled chain $k_F = \pi/2$, $t_d = 1$ and $V_G = -U/2$. The Hartree-Fock transmission obtained from Eq. 3.1 is given by the solid line. The circles show the exact results for the conductance, obtained with the embedding method and the DMRG algorithm [49–52]. The DMRG results are taken from reference [52].

riodic and anti-periodic boundary conditions. This is equivalent to the study of a ring threaded by a magnetic flux $\Phi = 0$ and $\Phi = \pi$ for periodic and anti-periodic boundary conditions, respectively. Taking the limit of infinite ring size $L \to \infty$, the effective transmission probability through the nano-system can be calculated as

$$|t_{\rm DMRG}|^2 = \left|\sin\left(\frac{\pi}{2}\frac{D}{D^0}\right)\right|^2 , \tag{2.47}$$

where D and D^0 are the charge stiffness of the model including the nano-system (D) and of the clean ring without the nano-system (D^0). The charge stiffness can be determined from the two ground-state energies obtained by DMRG as

$$D = (-1)^N \frac{L}{2}(E(\Phi = 0) - E(\Phi = \pi)) . \tag{2.48}$$

D is proportional to the difference of the two ground-state energies obtained by DMRG. L denotes the total length of the ring, N the particle number of the model [49].

In Fig. 2.7, we compare the Hartree-Fock results (solid line) with the exact DMRG-values (circles) for the conductance through the nano-system. The calculations are done at half-filling with compensated interaction ($V_G = -U/2$), resulting in a uniform density $\nu = 1/2$ of the model. The Hartree terms being cancelled by

$V_G = -U/2$, the Hartree-Fock equations (2.10)-(2.12) reduce to a single equation. Only the Fock term has to be calculated from Eq. (2.10). For this small interacting region the Hartree-Fock theory works quite well. Even for strong interactions up to $U = 7$, the Hartree-Fock and the exact DMRG results for the conductance agree qualitatively, the Hartree-Fock theory underestimating the conductance by $\approx 10\%$.

In section 3.3 we will see that the Hartree-Fock approximation becomes less accurate when calculating the total conductance through to interacting nano-systems in series: The exact DMRG results are reproduced only in the weak interaction limit.

2.4.2 The Kondo effect

In the inversion symmetric case ($V_0 = V_1 = V_G$), the physical properties of the model (Eq. (2.5)) are equivalent to those of the Anderson Hamiltonian [3, 38, 39], with an additional local magnetic field applied to the impurity spin. The Anderson model consists of a local impurity which is coupled to a bath of non-interacting electrons, including the spin degree of freedom:

$$\begin{aligned} H_{\mathrm{A}} = &\sum_{\sigma,k} \epsilon_k c^\dagger_{k,\sigma} c_{k,\sigma} + \sum_{k,\sigma} V_k (c^\dagger_{k,\sigma} a_{d,\sigma} + c_{k,\sigma} a^\dagger_{d,\sigma}) \\ &+ \sum_{\sigma} \epsilon_d a^\dagger_{d,\sigma} a_{d,\sigma} + U n_{d,\downarrow} n_{d,\uparrow} \,, \end{aligned} \tag{2.49}$$

where $c_{k,\sigma}$ is the annihilation operator for a state of energy ϵ_k in the bath, $\sigma = \uparrow, \downarrow$ being the spin index. $a_{d,\sigma}$ is the annihilation operator for the impurity state with spin σ, and $n_{d,\sigma} = a^\dagger_{d,\sigma} a_{d,\sigma}$. In our model, an additional term $\vec{S_d}.\vec{B}$ appears for finite t_d, which can be understood as a local magnetic field, which is coupled to the impurity spin. $\vec{S_d}$ is given by $\vec{S_d} = (\sigma_x, \sigma_y, \sigma_z)$, σ_i being the three Pauli matrices

$$\sigma_x = \begin{pmatrix} 0 & 1 \\ 1 & 0 \end{pmatrix} \tag{2.50}$$

$$\sigma_y = \begin{pmatrix} 0 & -\mathrm{i} \\ \mathrm{i} & 0 \end{pmatrix} \tag{2.51}$$

$$\sigma_z = \begin{pmatrix} 1 & 0 \\ 0 & -1 \end{pmatrix} . \tag{2.52}$$

In our spinless model Eq. (2.5), a pseudo-spin exists due to inversion symmetry of our model. Using the symmetric and antisymmetric states given by

$$c_{x,s} = \frac{1}{\sqrt{2}} (c_{-x+1} + c_x) \tag{2.53}$$

$$c_{x,a} = \frac{1}{\sqrt{2}} (c_{-x+1} - c_x) \,, \tag{2.54}$$

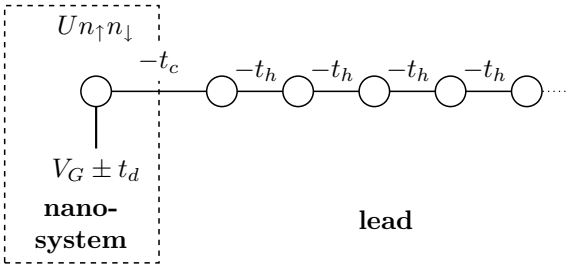

Figure 2.8: The transformed model: $\sigma = \uparrow, \downarrow$ describes a pseudo-spin due to inversion symmetry of the model. Inside the nano-system, the two sites interact as $Un_\uparrow n_\downarrow$. The spin-dependence of the potential inside the nano-system can be understood as magnetic field $\vec{S}..\vec{B}$.

our model-Hamiltonian (Eq. (2.5), with $V_0 = V_1 = V_G$) can be written as

$$\begin{aligned} H = &-t_d(n_{1,s} - n_{1,a}^\dagger) + Un_{1,s}n_{1,a} \\ &+ \sum_{\sigma=s,a} \left(-t_c(c_{1,\sigma}^\dagger c_{2,\sigma} + \text{H.c.}) + \sum_{x=2}^{\infty}(c_{x+1,\sigma}^\dagger c_x + \text{H.c.}) + V_G n_{1,\sigma} \right) , \end{aligned} \tag{2.55}$$

where $n_{x,\sigma} = c_{x,\sigma}^\dagger c_x$. This transformed model is sketched in Fig. 2.8.

To obtain a form similar to the Anderson-Hamiltonian Eq. (2.49), some additional steps are necessary.

The potential difference for the two sites $1, \uparrow$ and $1, \downarrow$ inside the nano-system can be written as a magnetic field $\vec{B} = (0, 0, t_d)$ which couples to the pseudo-spin $\vec{S}$ inside the nano-system.

In addition, for the Anderson Hamiltonian the bath is given in the basis of its eigenstates $c_{k,\sigma}$. By diagonalizing the Hamiltonian describing semi-infinite lead ($\sum_{x=2}^{\infty}(c_{x+1,\sigma}^\dagger c_{x,\sigma} + \text{H.c.})$), we obtain eigenstates of the bath in our model as

$$f_{k,\sigma} = \frac{1}{\sqrt{2\pi}} \sum_{x=2}^{\infty} \sin(k(x-1)) c_{x,\sigma} \tag{2.56}$$

with the eigen-energies $\epsilon_k = -2\cos k$. In this basis, the lead Hamiltonian H_{lead} (Eq. (2.2)) is diagonal. It can be written as

$$H_{\text{lead}} = \sum_\sigma \int_{-\pi}^{\pi} \epsilon_k f_{k,\sigma}^\dagger f_{k,\sigma} \mathrm{d}k \, . \tag{2.57}$$

This transformation of the lead states changes also the form of the coupling term $t_c(c_{2,\sigma}^\dagger c_{1,\sigma} + \text{H.c.})$. Replacing $c_{1,\sigma}$ by its value in the diagonal basis (2.56) we obtain

the new coupling term

$$c^{\dagger}_{1,\sigma} c_{2,\sigma} = \frac{1}{\sqrt{2\pi}} \int_{-\pi}^{\pi} \sin(k) f^{\dagger}_{k,\sigma} c_{d,\sigma} \,. \tag{2.58}$$

If we discretize the integrals, replace $\sigma = s, a$ by a pseudo-spin $\sigma = \uparrow, \downarrow$ and rename $c_{1,\sigma} \to a_{d,\sigma}$, $V_G \to \epsilon_d$, $f_{k,\sigma} \to c_{k,\sigma}$ and $-t_c \sin(k)/\sqrt{2\pi} \to V_k$, this model is identical to the Anderson Hamiltonian (2.49) in the limit $t_d \to 0$. For finite values t_d, a local magnetic field $\vec{B} = (0, 0, t_d)$ couples to the impurity spin $\vec{S}$.

The Anderson model was extensively studied by Krishna-murthy *et al.* [38, 39], using the Numerical Renormalization Group (NRG) technique [14]. The Numerical Renormalization Group was introduced by Wilson [80] to explain the Kondo problem [28]. In the presence of inversion symmetry the Kondo effect appears in the Anderson model only for strong interactions U.

However, as a local magnetic field on the impurity site destroys the Kondo effect, the Kondo effect will appear only for small hopping terms t_d, when the left and the right leads are only weakly coupled and the conductance is very small. For larger hopping terms t_d, the Kondo effect disappears. Thus the importance of the Kondo effect upon the conductance through the nano-system given by Eq. (2.1) at zero-temperature remains to be studied. A detailed analysis of the orbital Kondo effect resulting from the inversion symmetry of the nano-system given in Eq. (2.1) is in progress and will be published in a separate work.

3 Exchange corrections for two nano-systems in series

In this chapter, we analyze the non-local effect upon the transmission through an interacting nano-system in series with another identical nano-system. Although it is possible at zero temperature to describe the transmission properties of an interacting nano-system coupled to non-interacting leads by an effective one-body transmission matrix [49], this transmission matrix becomes non-local in the presence of interactions: When another scatterer is introduced into the leads in the vicinity of the nano-system, the effective transmission matrix of the nano-system is changed by the presence of the second scatterer. This effect has been studied previously using exact density matrix renormalization group calculations and the "embedding method" [52]. In this chapter, we use the Hartree-Fock theory to give an easy explanation for the non-locality: The second scatterer induces Friedel oscillations of the density $\langle n_x \rangle$ and similar oscillations of the correlation term $\langle c_x^\dagger x_{x+1} \rangle$ in the first scatterer, which influence its Hartree-Fock corrections.

For our study, we use the nano-system discussed in chapter 2, consisting of two sites with nearest-neighbour repulsion U. First, we look at a single nano-system and study the oscillation of the density $\langle c_x^\dagger c_x \rangle$ and the correlation function $\langle c_x^\dagger x_{x+1} \rangle$ in the leads. After that, we include a second (identical) nano-system into the model, and study its effect upon the effective transmission of the first scatterer.

We show that the non-local effect is suppressed when the length L_C between the two interacting nano-systems exceeds the thermal length L_T for non-zero temperature T.

We conclude the chapter by a comparison of the Hartree-Fock results with exact DMRG-results: While the Hartree-Fock approximation reproduces qualitatively the DMRG result, it strongly underestimates the non-local effects.

3.1 Microscopic model

In order to reduce all equations to a simpler form, we use $t_c = 1$ as coupling between the nano-system and the leads. As discussed in section 2.3.2, the non-local effects are increased by using a good coupling between nano-system and leads.

In this chapter we focus on the exchange correction. In order to detect the effect of the exchange correction only, we apply a positive background potential $V_0 = V_1$

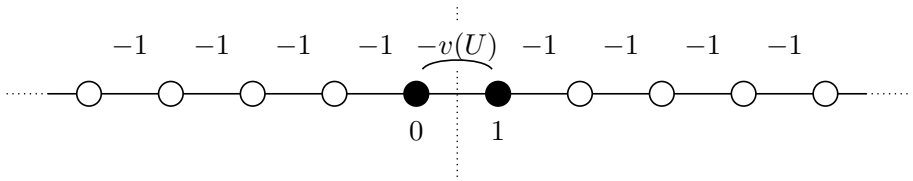

Figure 3.1: Effective one-body model obtained from the Hartree-Fock approximation for a single many-body nano-system (Hamiltonian (2.6) with compensated Hartree terms $V_0^{\mathrm{HF}} = V_1^{\mathrm{HF}} = 0$): The interaction U acts between the sites $x = 0$ and $x = 1$, giving rise to an effective hopping term $v(U, E_F)$ between these two sites.

in the nano-system, which cancels exactly the Hartree corrections appearing in the model. At half filling, this background potential is given by $V_0 = V_1 = -U/2$ and introduces particle-hole symmetry in the model Hamiltonian. In this case we obtain a uniform filling factor of $\nu = 1/2$ and no Friedel oscillations of the density can occur. The three Hartree-Fock equations (2.10)-(2.12) simplify to a single equation: The two Hartree terms being cancelled by the background potential, it is sufficient to consider the exchange term

$$v = t_d + U \left\langle c_1^\dagger c_0 \right\rangle . \tag{3.1}$$

The effective one-body model described by this equation is sketched in Fig. 3.1.

3.1.1 Eigenstates of the effective Hamiltonian

With the selected coupling $t_c = 1$ and the compensated Hartree terms ($V_0^{\mathrm{HF}} = V_1^{\mathrm{HF}} = 0$), the formulas for the eigenstates given in chapter 2 simplify considerably: Using the reflection symmetry $x \to -x+1$ of the model, the even and odd eigenstates of the model can now be written separately as $\psi_k^{\mathrm{e}}(x)$ and $\psi_k^{\mathrm{o}}(x)$

$$\begin{aligned} \psi_k^{\mathrm{e}}(x) &= \frac{1}{\sqrt{2\pi}} \cos\left(k\left(x - \frac{1}{2}\right) \pm \delta_e(k)\right) \quad \text{for} \quad x \gtrless \frac{1}{2} \\ \psi_k^{\mathrm{o}}(x) &= \frac{1}{\sqrt{2\pi}} \sin\left(k\left(x - \frac{1}{2}\right) \pm \delta_o(k)\right) \quad \text{for} \quad x \gtrless \frac{1}{2}\,, \end{aligned} \tag{3.2}$$

The corresponding energies are given by $E(k) = -2\cos(k)$, the wave vector k can take all values in the range $[0, \pi]$.

To determine the even and odd phase shifts $\delta_e(k)$ and $\delta_o(k)$, we write the Schrödinger equation on the two central sites for both the even and odd solutions:

$$\begin{aligned} -2\psi_k^{\mathrm{e/o}}(0)\cos k &= -\psi_k^{\mathrm{e/o}}(-1) - v\psi_k^{\mathrm{e/o}}(1) \\ -2\psi_k^{\mathrm{e/o}}(1)\cos k &= -v\psi_k^{\mathrm{e/o}}(0) - \psi_k^{\mathrm{e/o}}(2). \end{aligned} \tag{3.3}$$

Using the eigenstates given in Eq. (3.2), we obtain:

$$\tan\delta_e(k) = \frac{v-1}{v+1}\cot\left(\frac{k}{2}\right) \tag{3.4}$$

$$\tan\delta_o(k) = -\frac{v-1}{v+1}\tan\left(\frac{k}{2}\right)\,. \tag{3.5}$$

Beside these solutions inside the conduction band, two bound state exists when the hopping term inside the nano-system exceeds 1 ($v > 1$), instead of the four possible bound states for a general gate potentials V_G given in Eq. (2.24). The bound state with an energy below the conduction band, the even state, is given by

$$\psi_{\mathrm{bs,e}} = \left(\sqrt{\frac{v-v^{-1}}{2}}\right) v^{-|x-1/2|}, \tag{3.6}$$

with an corresponding energy

$$E_{bs,e} = -(v+v^{-1})\,, \tag{3.7}$$

while bound state with an energy above the conduction band, the odd state, is given by

$$\psi_{\mathrm{bs,o}} = (-1)^x\left(\sqrt{\frac{v-v^{-1}}{2}}\right) v^{-|x-1/2|}, \tag{3.8}$$

with an corresponding energy

$$E_{bs,o} = v+v^{-1}\,. \tag{3.9}$$

As discussed in section 2.2.1, the energy of the odd bound state is always above the Fermi energy and thus it can be neglected at zero temperature.

In order to obtain an analytical expression for the Hartree-Fock equation (3.1), we need to calculate $\langle c_1^\dagger c_0\rangle$ which is the sum of the contribution of the occupied bound state $A_{\mathrm{bs}}^{1,0}$ and the contribution from the occupied states in the conductance band $A_{\mathrm{cb}}^{1,0}$.

$$\langle c_1^\dagger c_0\rangle = A_{\mathrm{bs}}^{1,0} + A_{\mathrm{cb}}^{1,0} \tag{3.10}$$

The contribution of the even bound state is given by

$$A_{\mathrm{bs}}^{1,0} = \psi^*_{\mathrm{bs,e}}(1)\psi^*_{\mathrm{bs,e}}(0) = \frac{1-v^{-2}}{2} \tag{3.11}$$

The contribution of the conduction band can be calculated as

$$\begin{aligned} A_{\mathrm{cb}^{1,0}} &= \frac{L}{2\pi}\int_0^{k_F}\mathrm{d}k\,(\psi_k^{e,*}(1)\psi_k^{o,*}(0)) \\ &= \frac{1}{\pi}\int_0^{k_F}\mathrm{d}k\left(\frac{4v\cos(k)\sin(k)^2}{1+v^4-2v^2\cos(2k)}\right) \\ &= \frac{v^-2}{2\pi}\arctan\left(\frac{2v\sin(k_F)}{v^2-1}\right)+\frac{\sin(k_F)}{\pi v} \end{aligned} \tag{3.12}$$

Using these two expressions, one can determine v as a function of the interaction strength U and the Fermi momentum k_F by solving the equation (3.1) self-consistently. Only this last step has to be done numerically.

Also the expressions for the transmission and reflection coefficients t_{sys} and r_{sys} can be rewritten in a compact form, which depends only on the Hartree-Fock hopping term v and the Fermi vector k_F. Using the Landauer-Büttiker formula [17], the dimensionless conductance g_{sys} of the effective one-particle system is given by the effective transmission probability $|t_{\text{sys}}(v)|^2$ through the nano-system. We obtain

$$\begin{aligned} t_{\text{sys}}(v) =& \frac{v(\mathrm{e}^{2\mathrm{i}k_F}-1)}{v^2-\mathrm{e}^{-2\mathrm{i}k_F}} \\ r_{\text{sys}}(v) =& -\frac{(v^2-1)\mathrm{e}^{-\mathrm{i}k}}{v^2-\mathrm{e}^{-2\mathrm{i}k}} \\ g_{\text{sys}}(v) =& |t_{\text{sys}}(v)|^2 = \frac{4v^2\sin^2(k_F)}{v^4-2v^2\cos(2k_F)+1}. \end{aligned} \tag{3.13}$$

The reflection amplitude $r_{\text{sys}}(v)$ is given here for later reference. At half filling ($E_F = 0$, $k_F = \pi/2$), the behavior of g_{sys} is shown in Fig. 2.7 as a function of the interaction strength U. In addition to the Hartree-Fock values, also exact results obtained using the embedding method [49, 50] and the "Density matrix renormalization group" (DMRG) - algorithm [78, 79] are presented in Fig. 2.7, confirming the validity of the Hartree-Fock approximation for this model.

3.1.2 Oscillations of $\langle c_x^\dagger c_x\rangle$ and $\langle c_{x+1}^\dagger c_x\rangle$ in the leads

As already mentioned in section 1.1.2, the non-local effect upon the quantum transmission of an interacting nano-system can be explained in terms of the Friedel oscillations of $\langle c_x^\dagger c_x\rangle$ and $\langle c_{x+1}^\dagger c_x\rangle$. In this section we study these oscillations created by a single nano-system.

For a compensated interaction, the Hamiltonian obeys particle-hole symmetry at half filling. This results in a uniform density $n_x = \langle c_x^\dagger c_x\rangle = 1/2$ on all sites. As shown in the upper half of Fig. 3.2, this is due to the fact that the decrease of the density inside the conduction band (dashed line), which results from the local repulsion $U = 0.4$ inside the nano-system, is exactly compensated by the emergence of a bound state which is introduced through the interaction (not shown in Fig. 3.2). Outside of half-filling, Friedel-oscillations of the density n_x can emerge. As the positive gate potential $V_0 = V_1$ is adjusted to exactly cancel the Hartree terms, the oscillations resulting from the exchange energy persist and induce Friedel oscillation around the nano-system. This situation is shown in the lower part of Fig. 3.2: For a filling factor $\nu = 1/32$, the contribution of the conduction band n_{cb}^x (dash-dotted line) and the contribution of the even bound state n_{bs}^x (dotted line) do not result in a uniform density, but induce Friedel oscillations of the density.

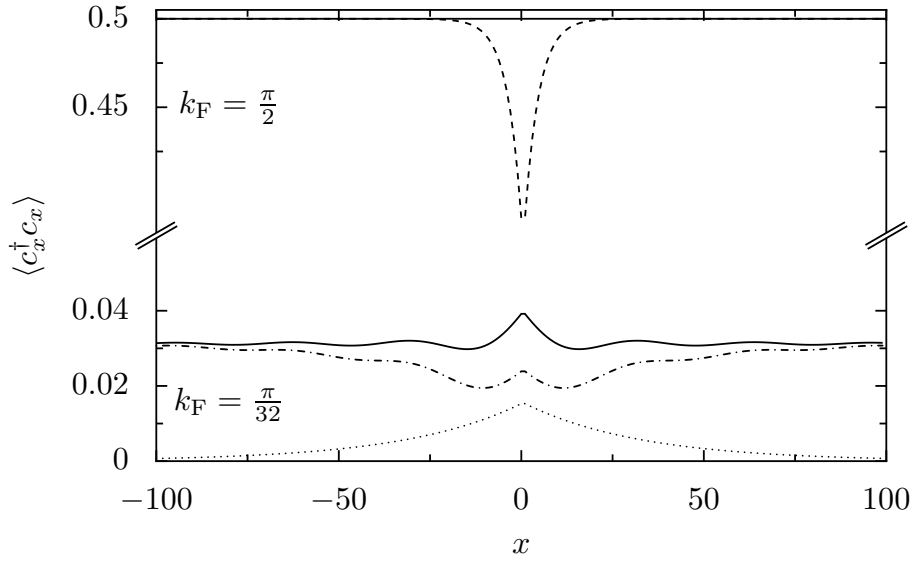

Figure 3.2: Particle density $n_x = \langle c_x^\dagger c_x \rangle$ around the nano-system with interaction strength $U = 0.4$: At half filling ($k_F = \pi/2$, upper part), the contributions of the conducting states (dashed line) and the even bound state (not indicated) compensate exactly, resulting in a uniform density $n_x = 1/2$. At low filling ($k_F = 1/32$, lower part), the contributions of the conducting states (dot-dashed line) and the even bound state (dotted line) result in Friedel oscillations around the nano-system (solid line). The hopping term inside the nano-system is set to $t_d = 1$.

The second important quantity which has to be studied is the correlation term $\langle c_{x+1}^\dagger c_x \rangle$, since it will influence the exchange correction of another interacting nano-system when it is located at the position x and $x+1$. We will give an analytical expression for this term. For $x \geq 1$ and $E_F < 2$ (the odd bound state being empty), $\langle c_{x+1}^\dagger c_x \rangle$ reads:

$$\langle c_{x+1}^\dagger c_x \rangle = A_{\mathrm{cb}}^{x+1,x} + A_{\mathrm{bs}}^{x+1,x}\,, \tag{3.14}$$

where

$$A_{\mathrm{bs}}^{x+1,x} = \frac{v^2-1}{2} v^{-2x-1} \tag{3.15}$$

and

$$\begin{aligned} A_{\mathrm{cb}}^{x+1,x} &= \frac{L}{2\pi} \int_0^{k_F} \mathrm{d}k \left(\psi_k^{e*}(x+1)\psi_k^e(x) + \psi_k^{o*}(x+1)\psi_k^o(x)\right) \\ &= \frac{1}{\pi} \int_0^{k_F} \mathrm{d}k (\cos(k) - G(v,k))\,. \end{aligned} \tag{3.16}$$

The function $G(v,k)$ is defined by

$$G(v,k) = (v^2-1)\frac{v^2\cos(k(2x-1)) - \cos(k(2k+1))}{1+v^4-2v^2\cos(2k)}. \tag{3.17}$$

This integral can be evaluated analytically, resulting in

$$\langle c_{x+1}^\dagger c_x \rangle = \frac{\sin k_F}{\pi} + \frac{v^2-1}{\pi(2x+1)} X(k_F, x, v), \tag{3.18}$$

the function $X(k_F, x, v)$ is defined as the imaginary part of the Gauss hypergeometric function:

$$X(k_F, x, v) = \Im\left({}_2F_1(1, \frac{1}{2}+x, \frac{3}{2}+x, v^2\mathrm{e}^{2\mathrm{i}k_F})\mathrm{e}^{\mathrm{i}k_F}(2x+1)\right)\,, \tag{3.19}$$

${}_2F_1(\alpha,\beta,\gamma,z)$ denoting the Gauss hypergeometric function

$${}_2F_1(\alpha,\beta,\gamma,z) = \sum_{n=0}^{\infty} \frac{(\alpha)_n(\beta)_n}{(\gamma)_n n!} z^n. \tag{3.20}$$

The expression $(x)_n$ is defined as $(x)_n = \prod_{m=0}^{n}(x+m)$. Far away from the nano-system, we can expand the Gauss Hypergeometric function in order to describe the asymptotic behavior of $\langle c_{x+1}^\dagger c_x \rangle$ with the expansion

$${}_2F_1(1, \frac{1}{2}+x, \frac{3}{2}+x, v^2\mathrm{e}^{2\mathrm{i}k_F}) \to \frac{1}{1-v^2\mathrm{e}^{2\mathrm{i}k_F}} \tag{3.21}$$

of the Gauss hypergeometric function ${}_2F_1$, which is valid in the limit $x \to \infty$. One obtains the simpler expression

$$\langle c_{x+1}^\dagger c_x \rangle \to \frac{1}{\pi}\left(\sin k_F + \frac{H_{k_F,v}(x)}{2x+1}\right), \tag{3.22}$$

where $H_{k_F,v}(x)$ is an oscillatory function given by

$$H_{k_F,v}(x) = \frac{(v^2-1)(-v^2\sin(k_F(2x-1)) + \sin(k_F(2x+1)))}{1+v^4-2v^2\cos(2k_F)}. \tag{3.23}$$

3.2 Two interacting nano-systems in series coupled by a non-interacting lead

After the study of the effect of a single interacting nano-system upon the leads, we now consider two nano-systems in series, coupled by a non-interacting lead of length L_C. To simplify the formulas, we will again use a coupling term $t_c = 1$. The resulting model is sketched in Fig. 3.3. The Hartree term is compensated by the two potentials V_{1+} and V_{2+}, which will be different as the model is inversion symmetric around $x = 1/2$, but not around the nano-systems ($x = -(L_C+1)/2$ and $x = (L_C+3)/2$). The Hamiltonian describing this model reads

$$\begin{aligned} H = &- \sum_{x=-\infty}^{\infty} (c_x^\dagger c_{x+1} + \text{H.c.}) \\ &+ U(n_{\frac{L_C}{2}+2} - V_{1+})(n_{\frac{L_C}{2}+1} - V_{2+}) + U(n_{-\frac{L_C}{2}} - V_{1+})(n_{-\frac{L_C}{2}-1} - V_{2+}) \\ &- (t_d - 1)\left(c^\dagger_{\frac{L_C}{2}+1} c_{\frac{L_C}{2}+2} + c^\dagger_{-\frac{L_C}{2}-1} c_{-\frac{L_C}{2}} + \text{H.c.}\right) \end{aligned} \tag{3.24}$$

At half-filling, the model obeys particle-hole symmetry for $V_{1+} = V_{2+} = 1/2$, resulting in uniform density along the chain. As in the case with only one nano-system, the exchange term will modify the local hopping terms t_d inside the system in the Hartree-Fock approximation. However, as soon as there are two scatterers, the value v characterizing each scatterer is different to the value of v for a single scatterer in the complete chain. This is due to a kind of indirect exchange interaction, which is induced between the two scatterers by the conduction electrons. Because of the inversion symmetry $x - 1/2 \leftrightarrow -x + 1/2$, this modification is identical for the two scatterers, resulting in a single Hartree-Fock equation

$$v = t_d + U\left\langle c^\dagger_{\frac{L_C}{2}+2} c_{\frac{L_C}{2}+1}\right\rangle, \tag{3.25}$$

or equivalently

$$v = t_d + U\left\langle c^\dagger_{-\frac{L_C}{2}} c_{-\frac{L_C}{2}-1}\right\rangle. \tag{3.26}$$

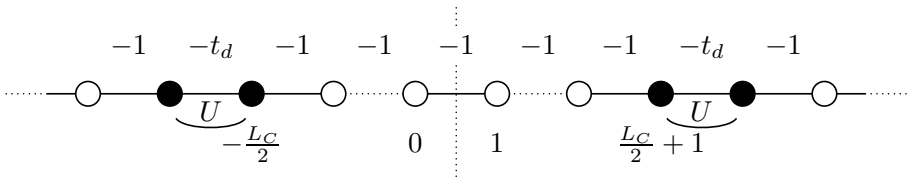

Figure 3.3: The model with two interacting nano-systems in series. Both systems are connected by a chain of L_C sites, on which the electrons do not interact. The left nano-system occupies the sites $-L_C/2-1$ and $-L_C/2$, the right one the sites $L_C/2+1$ and $L_C/2+2$. Inside the nano-systems, there acts a nearest-neighbor repulsion U.

First, we want to study this non local correction in the limit of a small interaction strength, $U \to 0$. In this limit it is possible to give the hopping term $v(U)$ for the effective one-body model describing one interacting nano-system in the presence of the second one analytically. Only the results for even distances L_C between the two nano-systems are studied. The generalization of this calculation for odd length L_C is straightforward. Moreover at half filling ($k_F = \pi/2$) and for odd lengths L_C, the transmission of the two nano-systems in series is exactly unity $g_{\mathrm{tot}} = 1$, independent of the interaction strength U and the distance L_C (see e. g. [51]).

3.2.1 The weak interaction limit

The effective hopping term $v = 1 + U \left\langle c^\dagger_{L_C/2+2} c_{L_C/2+1}(v,v) \right\rangle_2$ of the right scatterer has to be evaluated in the presence of the left scatterer located on the two sites $-L_C/2-1$ and $-L_C/2$, as this expectation value depends upon the presence of the left scatterer. The two parameters v, v appearing in the expectation value refer to the effective hopping terms characterizing the left and the right scatterer. Because of the inversion symmetry of the model, both effective hopping terms are identical. For a hopping term $t_d = 1$, it is possible to expand the Hartree-Fock equations in $v - 1$ and give an analytical perturbative result for $v(U, L_C)$.

As the Hartree-Fock parameter v will be close to 1 in the limit of a weak interaction strength $U \ll 1$, we can develop the expectation value $\left\langle c^\dagger_{L_C/2+2} c_{L_C/2+1}(v,v) \right\rangle_2$ in orders of $(v-1)$:

$$\begin{aligned} \left\langle c^\dagger_{\frac{L_C}{2}+2} c_{\frac{L_C}{2}+1}(v,v) \right\rangle_2 &= \left\langle c^\dagger_{\frac{L_C}{2}+2} c_{\frac{L_C}{2}+1}(1,1) \right\rangle_2 \\ &\quad + (v-1)\left(\frac{\partial}{\partial v} F_1(L_C, v)\right) + O((v-1)^2), \end{aligned} \tag{3.27}$$

where the first-order term of $F_1(L_C, v)$ is given by

$$F_1(L_C, v) = \left\langle c^\dagger_{\frac{L_C}{2}+2} c_{\frac{L_C}{2}+1}(v, 1) \right\rangle_2 + \left\langle c^\dagger_{\frac{L_C}{2}+2} c_{\frac{L_C}{2}+1}(1, v) \right\rangle_2 . \tag{3.28}$$

Up to first order in $(v-1)$, only expectation values where at least one of the hopping terms $v = 1$ appear in this expansion. Therefore the results for a single scatterer, which have been calculated in section 3.1.2, can be used. It is only necessary to shift the index x such that the scatterer with $v \neq 1$ is positioned on the sites 0 and 1, as in section 3.1.2. Doing this one obtains the relations:

$$\left\langle c^\dagger_{\frac{L_C}{2}+2} c_{\frac{L_C}{2}+1}(1, 1) \right\rangle_2 = \left\langle c^\dagger_1 c_0(1) \right\rangle \tag{3.29}$$

$$\left\langle c^\dagger_{\frac{L_C}{2}+2} c_{\frac{L_C}{2}+1}(1, v) \right\rangle_2 = \left\langle c^\dagger_1 c_0(v) \right\rangle \tag{3.30}$$

$$\left\langle c^\dagger_{\frac{L_C}{2}+2} c_{\frac{L_C}{2}+1}(v, 1) \right\rangle_2 = \left\langle c^\dagger_{L_C+3} c_{L_C+2}(v) \right\rangle . \tag{3.31}$$

Using the expressions given in Eq. (3.10) and (3.18) for these expectation values in the presence of only a single nano-system, we obtain for $v \to 1$:

$$\begin{aligned} \frac{\partial}{\partial v} \langle c^\dagger_1 c_0(v) \rangle &\to \frac{1}{2} - \frac{\sin k_F}{\pi} \\ \frac{\partial}{\partial v} \langle c^\dagger_{L_C+3} c_{L_C+2}(v) \rangle &\to \frac{2X(k_F, L_C+2, 1)}{\pi(2L_C+5)}, \end{aligned} \tag{3.32}$$

the function $X(k_F, x, 1)$ being defined in Eq. (3.19).

With these results, the self-consistent equation giving the effective hopping term v for each of the two nano-systems in series can be written as:

$$v \approx 1 + U \left(\frac{\sin k_F}{\pi} + (v-1) \frac{\partial}{\partial v} C_2(L_C, v) \right)_{v \to 1^+} , \tag{3.33}$$

where the function $C_2(L_C, v)$ is given as $C_2(L_C, v) = \langle c^\dagger_1 c_0(v) \rangle + \langle c^\dagger_{L_C+3} c_{L_C+2}(v) \rangle$. Solving this equation for v, one obtains

$$v \approx 1 + \left(\frac{\pi(2-U)}{2U} - \frac{2X(k_F, L_C+2, 1)}{2L_C+5} + \sin k_F \right)^{-1} . \tag{3.34}$$

One can see that the indirect exchange interaction between the two nano-systems gives rise to a correction for the effective hopping term v, which decays with a power law in the coupling length L_C. In the limit of infinite coupling length ($L_C \to \infty$), the exchange correction disappears and the two nano-systems become independent one-body scatterers. In this limit, the two nano-systems are independent and no non-local effects contribute to the conductance. The total transmission g_{tot} through both nano-systems in series can be obtained by the usual combination law for non interacting scatterers.

3.2.2 Exact solution of the Hartree-Fock equations

After the expansion in the weak interaction limit, we will now solve the self consistent Hartree-Fock equation for v at general interaction strengths U. As already done in the case with just one interacting nano-system, we will give analytical expressions for the expectation values appearing in the Hartree-Fock equation (3.25), which has to be resolved numerically. Again, we have to distinguish between the states in the conduction band and the bound states with energies below or above the conduction band. In the conduction band, the even and odd standing waves can be written separately for the left lead ($x \leq -\frac{L_C}{2} - 1$), the right lead ($x \geq \frac{L_C}{2} + 2$) and the central region between both scatterers ($-\frac{L_C}{2} \leq x \leq \frac{L_C}{2} + 1$). The even solution $\psi_k^e(x)$ is given by

$$\psi_k^e(x) = \sqrt{\frac{2}{L}} \begin{cases} \cos\left(k(x-\frac{1}{2}) - \delta_e(k)\right) & \text{if } x \leq -\frac{L_C}{2} - 1 \\ a_e \cos\left(k(x-\frac{1}{2})\right) & \text{if } -\frac{L_C}{2} \leq x \leq \frac{L_C}{2} + 1 \\ \cos\left(k(x-\frac{1}{2}) + \delta_e(k)\right) & \text{if } x \geq \frac{L_C}{2} + 2\,, \end{cases} \tag{3.35}$$

the odd solution $\psi_k^o(x)$ by:

$$\psi_k^e(x) = \sqrt{\frac{2}{L}} \begin{cases} \sin\left(k(x-\frac{1}{2}) - \delta_o(k)\right) & \text{if } x \leq -\frac{L_C}{2} - 1 \\ a_o \sin\left(k(x-\frac{1}{2})\right) & \text{if } -\frac{L_C}{2} \leq x \leq \frac{L_C}{2} + 1 \\ \sin\left(k(x-\frac{1}{2}) + \delta_o(k)\right) & \text{if } x \geq \frac{L_C}{2} + 2 \end{cases} \tag{3.36}$$

The factors a_e and a_o for the even and odd functions between the two scatterers, as well as the scattering phases can be obtained by solving the Schrödinger equation inside the scatterers, using the standing waves given in Eqs. (3.35) and (3.36) as basis structure for the solutions

$$\begin{aligned} a_e =& v|\sin k| \Bigg[\left((v^2-1)\cos\left(\frac{k}{2}(L_C+1)\right)\right)^2 \\ &+ \sin k \left(v^2 \sin k + (v^2-1)\sin(k(L_C+2))\right) \Bigg]^{-\frac{1}{2}}, \\ a_o =& v|\sin k| \Bigg[\left((v^2-1)\sin\left(\frac{k}{2}(L_C+1)\right)\right)^2 \\ &+ \sin k \left(v^2 \sin k - (v^2-1)\sin(k(L_C+2))\right) \Bigg]^{-\frac{1}{2}}. \end{aligned} \tag{3.37}$$

The scattering phase shifts $\delta_e(k)$ and $\delta_o(k)$ are given by

$$\tan\delta_e(k) = \frac{(v^2-1)\left(\cos(k(L_C+2)) + \cos k\right)}{(v^2-1)\sin(k(L_C+2)) + (v^2+1)\sin k} \tag{3.38}$$

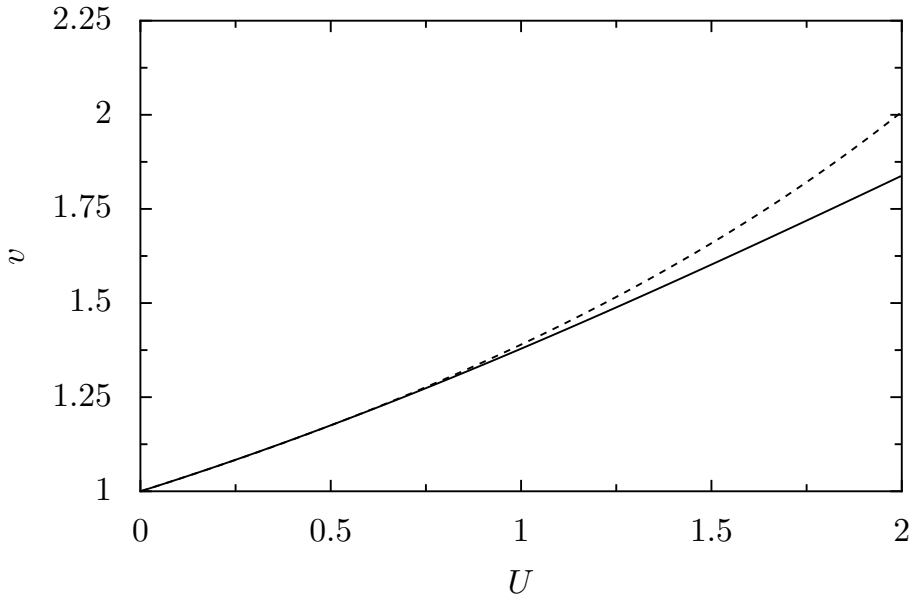

Figure 3.4: Validity of the approximated Hartree-Fock theory: For two scatterers in series, separated by $L_C = 4$ sites without interaction, the effective hopping term v has been calculated as a function of U for half-filled chains ($k_F = \pi/2$). The solid line gives the exact results, using the exact expression for $\langle c^\dagger_{x+1} c_x \rangle$ (Eq. (3.46)). The dashed line shows the approximate results, $\langle c^\dagger_{x+1} c_x \rangle$ being given by Eq. (3.27).

and

$$\tan \delta_o(k) = \frac{(1-v^2)\,(-\cos(k(L_C+2)) + \cos k)}{(v^2-1)\sin(k(L_C+2)) - (v^2+1)\sin k} \tag{3.39}$$

for the even and odd subspaces, respectively.

For $v > 1$, up to four additional bound states can exist. The bound states are localized around the two scatterers and decay exponentially. They have energies outside the conduction band. All four bound states can be given by the general formula

$$\psi_{\rm bs}^{\alpha,\beta} = A_{\alpha,\beta}(-1)^{\beta x} \begin{cases} (-1)^\alpha \mathrm{e}^{+K_{\alpha,\beta}(x-\frac{1}{2})} & \text{if } x \le -\frac{L_C}{2} - 1 \\ b_{\alpha,\beta}(\mathrm{e}^{+K_{\alpha,\beta}(x-\frac{1}{2})} + (-1)^\alpha \mathrm{e}^{-K_{\alpha,\beta}(x-\frac{1}{2})}) & \text{if } -\frac{L_C}{2} \le x \le \frac{L_C}{2} + 1 \\ \mathrm{e}^{-K_{\alpha,\beta}(x+\frac{1}{2})} & \text{if } x \ge \frac{L_C}{2} + 2, \end{cases} \tag{3.40}$$

where α and β are used to indicate the different states. α and β can take all combinations from 0 and 1, defining the four possible bound states. Two of the states ($\psi_{\rm bs}^{0,0}$ and $\psi_{\rm bs}^{1,1}$) are of even symmetry, while the other two ($\psi_{\rm bs}^{0,1}$ and $\psi_{\rm bs}^{1,0}$) are of odd symmetry. The energy of the bound states is given by

$$E_{\rm bs}^{\alpha,\beta} = -(-1)^\beta 2 \cosh K_{\alpha,\beta}, \tag{3.41}$$

the factor $b_{\alpha,\beta}$ is given as

$$b_{\alpha,\beta} = \frac{2v}{(-1)^\alpha + \mathrm{e}^{K_{\alpha,\beta}(L_C+3)}}. \tag{3.42}$$

The wave numbers $K_{\alpha,\beta}$ are the solutions of

$$1 + (-1)^\alpha \mathrm{e}^{K_{\alpha,\beta}(L_C+3)} = (1 + (-1)^\alpha \mathrm{e}^{K_{\alpha,\beta}(L_C+1)})v^2. \tag{3.43}$$

As a function of $\mathrm{e}^{K_{\alpha,\beta}}$, this equation is a polynomial of order $L_C + 3$, making it very difficult to obtain an analytical formula which gives $\mathrm{e}^{K_{\alpha,\beta}}$ (and thus $K_{\alpha,\beta}$) as a function of v and L_C. Instead it is necessary to solve Eq. (3.43) numerically.

However, it is important to notice that not all of these four bound states exist for all parameter ranges: Only, if the equation for the wave-number has a real solution, the corresponding bound states exist. The bound states $\psi_{\mathrm{bs}}^{0,0}$ and $\psi_{\mathrm{bs}}^{0,1}$ have a real solution for all values of L_C and $v > 1$ (see Eq. (3.43)). The other two bound states $\psi_{\mathrm{bs}}^{1,0}$ and $\psi_{\mathrm{bs}}^{1,1}$ exist only for sufficiently large L_C (compare Eq. (3.43)). For calculations at zero temperature and $E_F < 2$, it is sufficient to consider the states below the conduction band ($\psi_{\mathrm{bs}}^{0,0}$ and $\psi_{\mathrm{bs}}^{1,0}$).

Eventually, the factors $A_{\alpha,\beta}$ are given by the normalization condition

$$\sum_{x=-\infty}^{\infty} |\psi_{\mathrm{bs}}^{\alpha,\beta}(x)|^2 = 1. \tag{3.44}$$

Solving this equation, one obtains the normalization factors

$$A_{\alpha,\beta} = \left(\frac{\mathrm{e}^{-K_{\alpha,\beta}(L_C+2)}}{\mathrm{sech}(K_{\alpha,\beta})} + \frac{2v^2[(L_C+2)(-1)^{\alpha+\beta L_C} + \frac{\sinh(k(L_C+2))}{\mathrm{sech}(k)}]}{((-1)^\alpha + \mathrm{e}^{K_{\alpha,\beta}(L_C+3)})^2} \right)^{-\frac{1}{2}} \tag{3.45}$$

for the different combinations of α and β.

One can calculate the exchange term

$$\begin{aligned} \left\langle c_{x+1}^\dagger c_x \right\rangle_2 =& \frac{L}{2\pi} \int_0^{k_F} \mathrm{d}k \, [\psi_k^{\mathrm{e}*}(x+1)\psi_k^{\mathrm{e}}(x) + \psi_k^{\mathrm{o}*}(x+1)\psi_k^{\mathrm{o}}(x)] \\ &+ \sum_{\mathrm{bs}} \psi_{\mathrm{bs}}^*(x+1)\psi_{\mathrm{bs}}(x) \end{aligned} \tag{3.46}$$

inside the scatterers ($x = \frac{L_C}{2} + 1$) to obtain the self-consistent Hartree-Fock equation (Eq. (3.25)) giving v for two scatterers in series. The above integrals also have to be calculated numerically, which can be done easily.

The two figures 3.4 and 3.5 show a comparison of the weak interaction expansion derived in section 3.2.1 (Equation (3.34)) and the exact solution given by Eqs. (3.1) and (3.46). In Fig. 3.4, we show $v(U)$ as a function of the interaction strength,

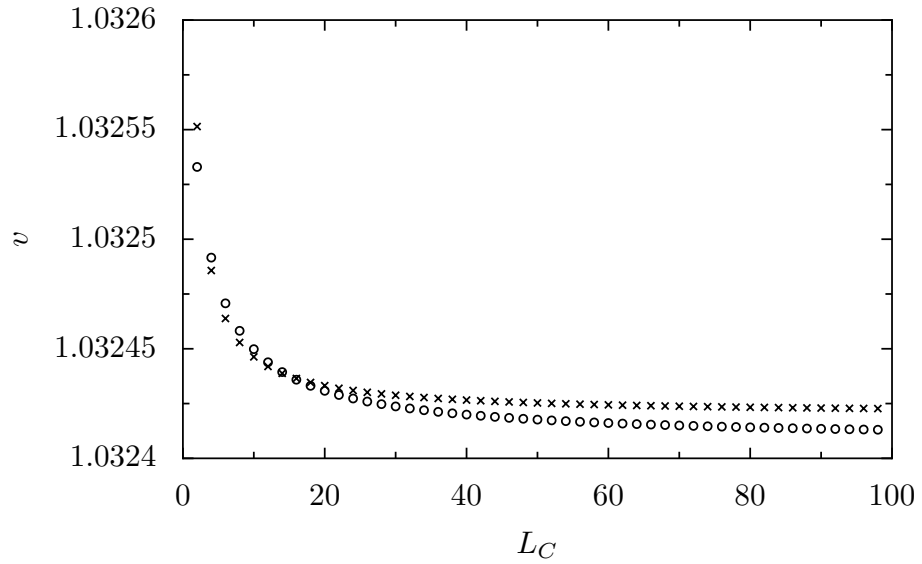

Figure 3.5: Validity of the approximated Hartree-Fock theory: As a function of the distance L_C between the two nano-systems in series, the effective hopping term v has been calculated for a weak interaction strength of $U = 0.1$. The points are calculated at half-filling. In order to simplify the picture, the even-odd oscillations characteristic for $k_F = \pi/2$ are not shown, v is only plotted for even values of L_C. The circles give the exact values, the crosses are calculated using the approximated Hartree-Fock theory ($\langle c^\dagger_{x+1} c_x \rangle$ given by Eq. (3.27)).

both nano-systems separated by $L_C = 4$ sites. For small interaction strength up to $U \approx 1$, the two theories agree very well. On the chosen scale, it is almost impossible to see the difference. For larger interactions, the difference between the approximation and the exact result increases, the approximation overestimating the value $v(U)$. Nevertheless, the qualitative behavior $v(U)$ is described correctly by the approximation even for stronger interactions.

In Fig. 3.5, the Hartree-Fock parameter $v(L_C)$ is shown as a function of the distance L_C between the two scatterers, always restricted to even lengths L_C. The figure shows the disappearance of the non-local effect for $L_C \to \infty$. In these images, we have used a weak interaction $U = 0.1$, which explains the small scale of the effects upon the Hartree-Fock parameter v. For small length until $L_C \approx 20$, the approximation Eq. (3.34) agrees very well with the exact result. For larger distances, Eq. (3.34) overestimates the value of v.

3.2.3 Density oscillations and quantum conductance outside half-filling

Outside half filling, our model exhibits Friedel oscillations of the density $n_x = \langle c_x^\dagger x_c \rangle$ around the two scatterers, as soon as the interaction strength $U \neq 0$: Though we can adjust the two potentials V_{1+} and V_{2+} to compensate the Hartree terms, the influence of the exchange correction upon the density remains. In Fig. 3.6 the oscillations of the density n_x are shown for a low Fermi energy with $k_F = \pi/32$. This results in a mean density of $\nu = 1/32$ in the model. Setting the distance between the two nano-systems to $L_C = 100$ sites, the nano-systems are located at the sites $x = -51, -50$ and $x = 51, 52$. At these positions, the particle density is strongly increased. In the semi-infinite chains at $x < -51$ or $x > 52$, one can see the expected Friedel-oscillations for an one-dimensional system, decaying as $\frac{\cos(2k_F \delta x)}{\delta x}$, δx being the distance from the left or right scatterer respectively. In the central part, $-50 < x < 51$, the image becomes a bit more difficult: in this region, the Friedel-oscillations induced from the both scatterers interfere, the density oscillations being given approximately by $\propto (\frac{\cos(2k_F(x+50)+\delta)}{x+50} + \frac{\cos(2k_F(x-51)-\delta)}{x-51})$ for large L_C and small values of $|x|$.

In order to obtain the Landauer-Büttiker conductance [17] of the two scatterers in series, we use the transmission and reflection coefficients $t_{\text{sys}}(v)$ and $r_{\text{sys}}(v)$ of a single scatterer given in equation (3.13). With these, we can write the transfer matrix $M_{\text{sys}}(v)$ describing a single nano-system as

$$M_{\text{sys}}(v) = \begin{pmatrix} (1/t_{\text{sys}})^* & r_{\text{sys}}/t_{\text{sys}} \\ (r_{\text{sys}}/t_{\text{sys}})^* & 1/t_{\text{sys}} \end{pmatrix}. \tag{3.47}$$

The non-interacting lead of length L_C between the two nano-systems is described

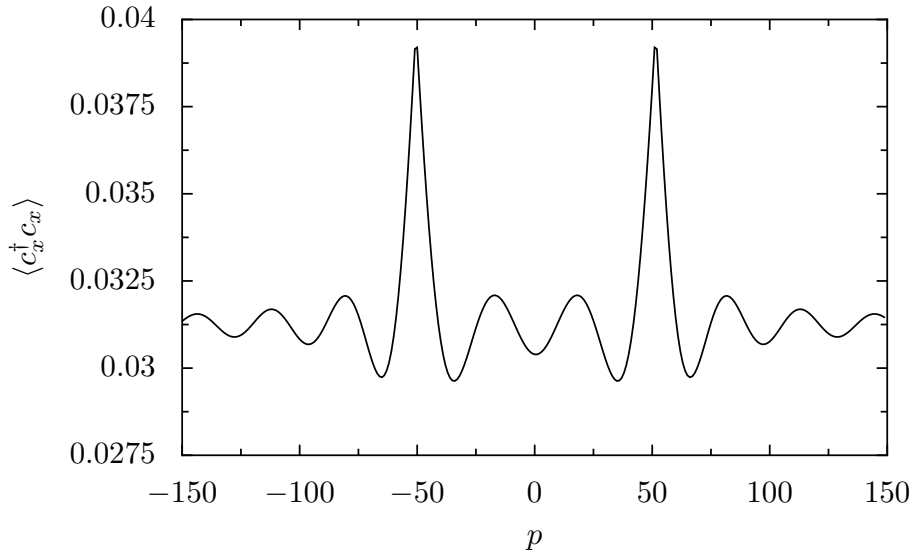

Figure 3.6: Two nano-systems in series: The Friedel oscillations of the density $n_x = \langle c_x^\dagger c_x \rangle$ created by each nano-system are superposed. With $L_C = 100$, the nano-systems are located at $x = 51, 52$ and $x = -51, -50$, at the two peaks. The values shown are obtained for interaction $U = 0.4$, hopping $t_d = 1$ inside the nano-system and a low Fermi energy with $k_F = \pi/32$.

by the transfer matrix

$$M_{L_C}^{k_F} = \begin{pmatrix} \mathrm{e}^{\mathrm{i}k_F L_C} & 0 \\ 0 & \mathrm{e}^{-\mathrm{i}k_F L_C} \end{pmatrix}. \tag{3.48}$$

The total transfer matrix describing both systems in series, separated by the non-interacting lead of length L_C, can be obtained by the multiplication of the three transfer matrices:

$$M_{\mathrm{tot}}^{k_F} = M_{\mathrm{sys}} M_{L_C}^{k_F} M_{\mathrm{sys}} \tag{3.49}$$

This combination law, giving the total transfer matrix as a product of transfer matrices describing the different parts of the complete problem, is exact for non-interacting problems. As the Hartree-Fock theory reduces the many-body Hamiltonian to an effective one-body problem, Eq. (3.49) gives the exact Hartree-Fock result for the transfer matrix $M_{\mathrm{tot}}^{k_F}$ describing both scatterers in series, separated by a perfect lead of length L_C. The important point is, that during the Hartree-Fock calculations done to obtain the parameter v, one has to take into account the influence of the second nano-system. Because of this, also the transfer matrix M_{sys} describing a single nano-system depends on the second nano-system and on L_C.

The transmission coefficient $t_{\mathrm{tot}}^{k_F}$ and the dimensionless conductance g_{tot} describing

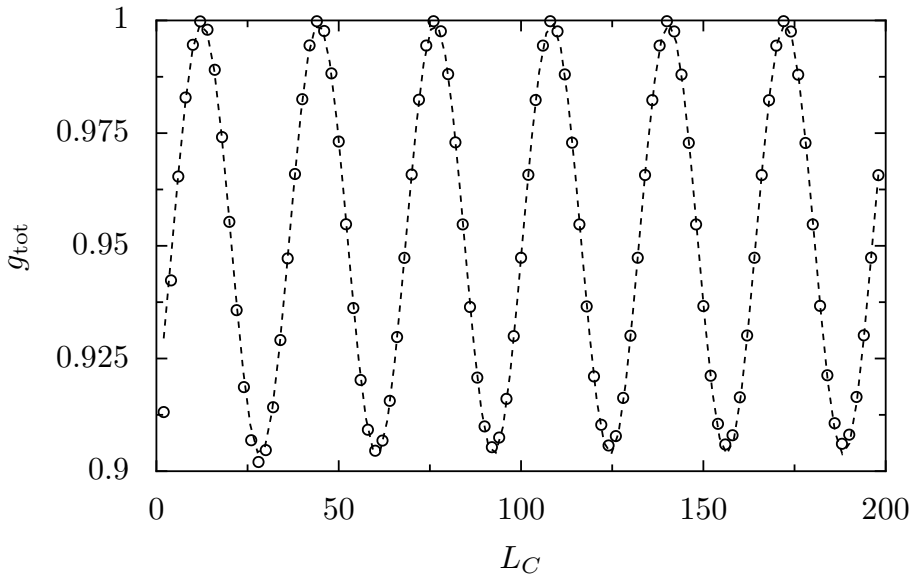

Figure 3.7: The total conductance for two nano-systems in series. For an effective hopping term $v(L_C, U)$, the total conductance $g^{k_{\rm F}}_{\rm tot}(L_C, U)$ is given by Eq (3.50) as a function of $L_C c$ for $U = 0.4$ and $k_F = \pi/32$. The circles are the results using the exact Hartree-Fock theory. Only the values for even L_C are plotted, for odd L_C one obtains a similar image. The dashed line is a fit with $g(L_C) = 0.952 - 0.04777 \sin(2k_F L_C + 2.269)$, as expected for Fabry-Pérot-oscillations. This fit is correct for large L_C, when the non-local correction can be neglected. For small values of L_C, corrections to the fit can be seen around $L_C \approx 25$.

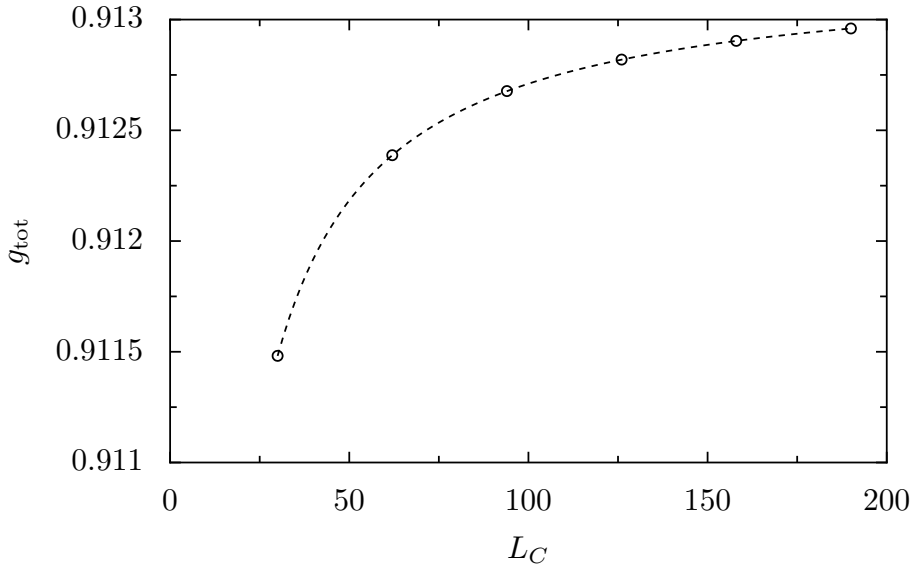

Figure 3.8: The minimum values of the conductance $g_{\rm tot}(L_c, U)$ for the successive conductance oscillations are shown to underline the power law decay of the corrections to the simple Fabry-Pérot-fit in Fig. 3.7 as a function of L_C. For $k_F = \pi/16$, the values with minimal conductance for the different oscillations are shown (at $L_C = 30, 62, 94, 126, 158$ and 190). Again, is set to $U = 0.4$. The dashed line a fit giving the decay $g_{\rm min}(L_C) = 0.91324 - 0.05267/L_C$.

the two scatterers in series, are then given by

$$\begin{aligned} t_{\mathrm{tot}}^{k_F}(v) =& -\frac{2\mathrm{i}v^2\mathrm{e}^{2\mathrm{i}k_F}\sin^2 k_F}{d^{k_F}(v)} \\ g_{\mathrm{tot}}(v) =& \frac{4v^4\sin^4 k_F}{\left|d^{k_F}(v)\right|^2}, \end{aligned} \tag{3.50}$$

where

$$\begin{aligned} d^{k_F}(v) =& \mathrm{e}^{-\mathrm{i}k_F}\sin(k_F(L_c+3)) - 2v^2\sin(k_F(L_c+2)) \\ &+ v^4\mathrm{e}^{\mathrm{i}k_F}\sin(k_F(L_c+1)). \end{aligned} \tag{3.51}$$

The presence of L_C dependent corrections to v shown in Figs. 3.4 and 3.5 indicates that the effective transmission coefficient t_{sys} describing one nano-system is influenced by the presence of the second nano-system. As g_{tot} depends on v, this non-local effect will also influence the total conductance g_{tot} of two interacting nano-systems in series.

We show this effect in Figs. 3.7 and 3.8. The total conductance g_{tot} of the two nano-systems in series is plotted as a function of the distance L_C for a low filling factor ($k_F = \pi/32$). The results are obtained by the exact solution of the Hartree-Fock equation (3.25). One can see conductance oscillations as a function of L_C, described by $\sin(2\pi k_F L_C + \delta)$ for even values of L_C. The values for odd L_C are not included in the figure. For large values of L_C, these are the usual Fabry-Pérot oscillations, resulting from the interference of the reflected and transmitted states. When L_C is small, the amplitude of the conductance oscillations is increased, due to the non local effect upon the exchange correction v. For the selected parameters, this effect is hardly visible on the scale used in Fig. 3.7. It can be better observed in Fig. 3.8, where only the minimal values of each conductance oscillation are plotted (for $L_C = 30$, 62, 94, 126, 158 and 190), together with the fit underlining the $1/L_C$-decay of the exchange-contribution to the conductance oscillations and the decrease of the oscillations towards the asymptotic L_c-independent value for a larger filling factor with $k_F = \pi/16$.

3.2.4 Suppression of the non-local effect above the thermal wave length L_T

We have shown that the effective transmission through a nano-system in which the electrons interact depends on the presence of another scatterers at the distance L_C. This dependence decays as $1/L_C$ at zero temperature.

At finite temperatures T, this effect is suppressed when L_C exceeds the thermal length L_T. Since our Hartree-Fock approach is essentially valid in the limit of weak interactions U, it is sufficient to consider the weak interaction limit discussed in subsection 3.2.1 for zero temperature. In this limit, the non-local effect is given by

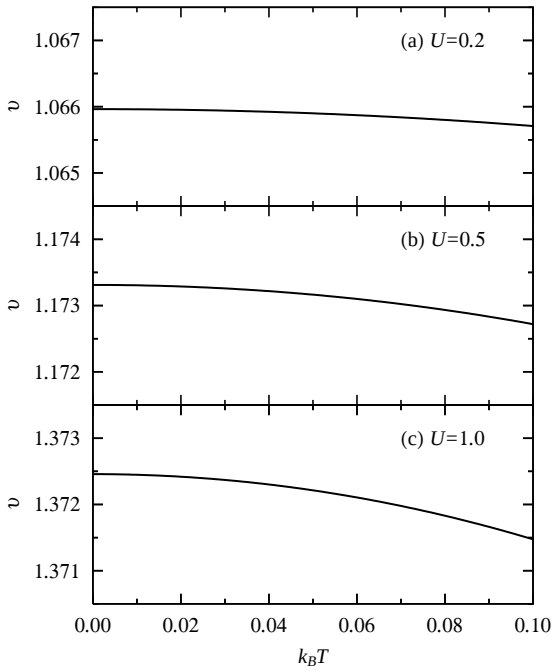

Figure 3.9: Hopping term v given by Eq. (3.56) as a function of the temperature $k_BT = \beta^{-1}$ for different values of U and $\mu_{\rm F} = 0$.

the deviation of $\langle c^\dagger_{x+1} c_x \rangle$ from its asymptotic value $\sin(k_F/\pi)$. To show that this non-local effect vanishes when $L_C > L_T$, it is sufficient to show that this deviation is exponentially suppressed for $L_C > L_T$.

At a finite temperature $k_BT = \beta^{-1}$, the Fermi-Dirac function $f(E, \mu_F)$, giving the occupation number of a state with energy E at a chemical potential μ, reads

$$f_\beta(E, \mu_F) = \frac{1}{\mathrm{e}^{\beta(E-\mu_F)} + 1} \,. \tag{3.52}$$

When a single scatterer is connected to two perfect leads, the temperature modifies the value of $\langle c^\dagger_1 c_0 \rangle$ inside the scatterer [26], and Eq. (2.28) is changed to:

$$\langle c^\dagger_1 c_0 \rangle_\beta = \langle c^\dagger_1 c_0 \rangle_{cb}(\beta, \mu_{\rm F}) + \langle c^\dagger_1 c_0 \rangle_{\rm bs}(\beta, \mu_{\rm F}) \,, \tag{3.53}$$

where the contribution of the conduction band is given by:

$$\begin{aligned} \langle c^\dagger_1 c_0 \rangle_{\rm cb}(\beta, \mu_{\rm F}) =& \frac{1}{2\pi} \sum_{q=\pm} \int_0^\pi dk f_\beta(E_k, \mu_{\rm F}) \left(\psi^*_{k,q}(1) \psi_{k,q}(0) \right) \\ =& \int_0^\pi \frac{dk}{\pi} f_\beta(E_k, \mu_{\rm F}) \left(\frac{4v \cos k \sin^2 k}{1 + v^4 - 2v^2 \cos(2k)} \right) , \end{aligned} \tag{3.54}$$

and the contribution of the two bound states (given in Eqs. (3.6) and (3.8)) reads:

$$\begin{aligned}\langle c_1^\dagger c_0\rangle_{\mathrm{bs}}(\beta,\mu_\mathrm{F}) &= \sum_{i=e,o} f_\beta(E_{bs,i},\mu_\mathrm{F})\psi^*_{\mathrm{bs,i}}(1)\psi_{\mathrm{bs,i}}(0) \\ &= \{f_\beta(E_{\mathrm{bs,e}},\mu_\mathrm{F}) - f_\beta(E_{\mathrm{bs,o}},\mu_\mathrm{F})\}\,\frac{1-v^{-2}}{2}\,.\end{aligned} \tag{3.55}$$

The effective hopping term v is given by the implicit equation

$$v = 1 + U\langle c_1^\dagger c_0(v)\rangle_\beta, \tag{3.56}$$

and depends on the temperature T and the chemical potential μ_F.

In Fig. 3.9 we show the temperature-dependence of v for different small values of the interaction strength U. One can see that the T-dependence of v remains small when $k_BT \leq 0.1$ and U is small.

To calculate the correlation function $\langle c_{x+1}^\dagger x_x\rangle$ in the leads, we have to generalize Eq. (3.14) to finite temperature. This yields:

$$\begin{aligned}\left\langle c_{x+1}^\dagger c_x\right\rangle_\beta =& \frac{1}{2\pi}\int_0^\pi \mathrm{d}k f_\beta(E_k,\mu_\mathrm{F})\left(\sum_{q=\pm}\psi^*_{k,q}(x+1)\psi_{k,q}(x)\right) \\ &+ \sum_{i=e,o} f_\beta(E_{\mathrm{bs,i}},\mu_\mathrm{F})\psi_{\mathrm{bs,i}}(x+1)\psi_{\mathrm{bs,i}}(x) \\ =& \frac{1}{\pi}\int_0^\pi dk f_\beta(E_k,\mu_\mathrm{F})(\cos k - G(v,k)) \\ &+ (f_\beta(E_{\mathrm{bs,e}},\mu_\mathrm{F}) - f_\beta(E_{\mathrm{bs,o}},\mu_\mathrm{F}))\,\frac{v^2-1}{2}v^{-2p-1}\end{aligned} \tag{3.57}$$

where the function $G(v,k)$ is given by Eq. (3.17).

By numerical integration we have calculated $\langle c_{x+1}^\dagger c_x\rangle_\beta$ as a function of x for different temperatures T and $\mu_\mathrm{F} = 0$. $\langle c_{x+1}^\dagger c_x\rangle_\beta$ exhibits oscillations, which decay faster when the temperature increases. In Fig. 3.10, we show the decay of the absolute difference between $\langle c_{x+1}^\dagger c_x\rangle_\beta$ and its asymptotic value A. One can see that for large x this decay becomes exponential:

$$\left|\left\langle c_{x+1}^\dagger c_x\right\rangle_\beta - A\right| \propto \mathrm{e}^{-\frac{x}{L_\mathrm{T}}}\,, \tag{3.58}$$

characterized by a decay length L_T.

In Fig. 3.11, L_T is shown as a function of T, showing a temperature dependence of

$$L_\mathrm{T} = \frac{1}{\pi k_B T}. \tag{3.59}$$

Ignoring a multiplicative factor of $1/(2\pi)$, one can identify L_T with the usual thermal length for free fermions in one dimension.

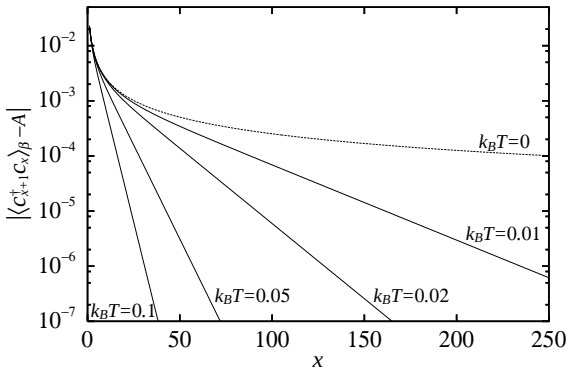

Figure 3.10: $\left|\left\langle c^\dagger_{x+1}c_x\right\rangle - A\right|$ as a function of x for $U = 0.5$ at half-filling ($\mu_{\rm F} = 0$). A is the asymptotic value when $x \to \infty$.

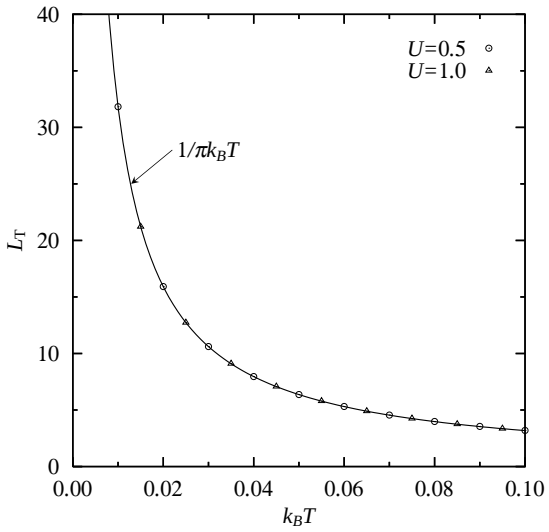

Figure 3.11: Thermal length $L_{\rm T}$ as a function of the temperature T obtained from the exponential decays of $\langle c^\dagger_{x+1}c_x\rangle_\beta$ shown in Fig. 3.10. The points obtained for different values of T and $U = 0.5$ and $U = 1$ can be fitted with a single curve $L_{\rm T} = 1/(\pi k_B T)$.

3.3 Comparison with exact DMRG results

We have compared in Fig. 2.7 the self-consistent Hartree-Fock approximation and the exact DMRG results for a single nano-system. The difference was negligible for small values of U up to the order of $U \approx 1$. Nevertheless, the Hartree-Fock results differ [5] more and more from the exact values when the length of the nano-system in which the electrons interact is increased. We will show that for two nano-systems in series the difference between the Hartree-Fock and the DMRG results becomes more important than in the case of a single nano-system only.

Here we study the validity of the Hartree-Fock approximation to describe the non-local correction to the total conductance $g_{\rm tot}$ for two interacting nano-systems in series. We assume a half filled chain ($k_F = \pi/2$), the Hamiltonian obeying particle-hole symmetry. In order to extract this information from the conductance data, we compare the conductance obtained when the non-local correction is taken into account with the one obtained when the non-local correction is ignored.

At half filling, the conductance $g_{\rm tot}(k_F = \pi/2) = 1$ for two one-body scatterers in series, when the length L_C of the coupling lead is odd. When L_C is even, the conductance is given by [52]

$$g_{\rm tot}(k_F = \pi/2) = \left(\frac{g_{\rm sys}}{g_{\rm sys} - 2} \right)^2 , \tag{3.60}$$

where $g_{\rm sys}$ refers to the conductance of a single nano-system.

Let us define two procedures for calculating the total conductance $g_{\rm tot}(k_F = \pi/2)$ (including the non-local effect) and $g_{\rm tot}(k_F = \pi/2)^*$ (neglecting the non-local effect):

- One can calculate the conductance of a single nano-system $g^*_{\rm sys}$, neglecting completely the effect of the other scatterer, by doing the same calculation as in chapter 2. The total conductance $g^*_{\rm tot}$ can then be obtained from Eq. (3.60). This procedure **neglects** the non-local effect and gives an error when $U \neq 0$ and L_C is not very large.

- One can calculate directly the total conductance $g_{\rm tot}$ through both nano-systems in series. In DMRG this is done with the embedding method upon the complete model consisting of two nano-systems separated by L_C non-interacting sites. In Hartree-Fock this is done by calculating the effective hopping parameter v using Eq. (3.25), where the second scatterer is taken into account when evaluating the expectation value $\langle c^\dagger_{L_C/2+2} c_{L_C/2+1} \rangle$. This procedure **includes** the non-local effect.

The comparison of $g^*_{\rm tot}$ and $g_{\rm tot}$ gives the importance of the non-local effect upon the total conductance $g_{\rm tot}$.

This was done in Ref. [52] by Molina *et al.* , using the embedding method and the DMRG algorithm. For odd length L_C, both procedures give a perfect conductance

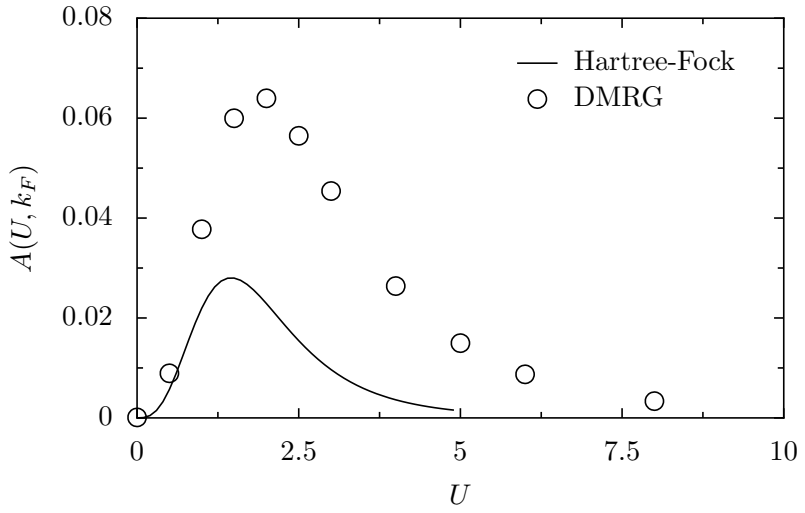

Figure 3.12: Function $A(U, k_F)$ (Eq. equation (3.61)) characterizing the correction $\delta g_{\rm tot}(L_C) = g_{\rm tot}(k_F) - g_{\rm tot}(k_F)^*$ of two nano-systems in series, which is induced by the non-local effect. The data shown in this image are calculated at half filling ($k_F = \pi/2$). The exact values obtained from the embedding method and the DMRG algorithm are shown by circles, the values obtained from the Hartree-Fock theory by a solid line. [The DMRG results are taken from [52]]

$g_{\rm tot} = 1$. For even length L_C, both procedures give different results, the two values $g^*_{\rm tot}$ and $g_{\rm tot}$ converging towards the same value in the limit $L_C \to \infty$. For short lengths L_C, the non-local effect decreases the total conductance by $\delta g_{\rm tot}(L_C) = g^*_{\rm tot} - g_{\rm tot}$. One can obtain a general fit describing the difference $\delta g_{\rm tot}$ as a function of L_C:

$$\delta g_{\rm tot}(L_C) = \frac{A(U, k_F)}{L_C}\,, \tag{3.61}$$

which is characterized by the function $A(U, k_F)$.

Also within Hartree-Fock theory, odd L_C implies $g_{\rm tot} = 1$ and for even L_C, $\delta g_{\rm tot}(L_C)$ can be described by the same fit (Eq. (3.61)). However, another function $A(U, k_F)$ is obtained in the Hartree-Fock approximation.

In Fig. 3.12 we show the function $A(U, k_F)$ for a half-filled chain ($k_F = \pi/2$) as a function of U, comparing the Hartree-Fock and the DMRG result. One can see that the Hartree-Fock approximation reproduces qualitatively the exact DMRG results even up to very strong interaction strengths: For increasing interaction U, the function $A(U, k_F)$ grows first, before it goes down to zero again. For strong interactions both theories give $A(U, k_F) \to 0$. For weak interactions up to $U \approx 0.75$ the Hartree-Fock theory reproduces even quantitatively the exact DMRG results. For intermediate interactions, the Hartree-Fock approximation fails, making the use

of powerful numerical methods (like NRG [14, 28, 30, 54, 80] or DMRG) necessary to obtain a correct description of the physics.

4 Influence of an attached Aharonov-Bohm scatterer

After the study of two identical interacting nano-systems in series in chapter 3, we study in this chapter an attached ring, threaded by a magnetic field, as second scatterer. The non-local effects result from the flux-dependent Friedel oscillations of the density $\langle c_x^\dagger c_x \rangle$ and from the equivalent oscillations of the correlation term $\langle c_x^\dagger c_{x+1} \rangle$ induced by the ring. The magnetic field threading the ring can be varied very easily in a possible experiment. We will see that the effective transmission through the interacting nano-system can depend strongly on the magnetic flux threading the ring, when the electrons interact inside the nano-system: The attached ring (an Aharonov-Bohm scatterer [2]) can influence the effective transmission of the nano-system. This effect exists only in the presence of local interactions, without interaction the effective transmission of the nano-system is completely independent of the flux. Because of this, our model describes a nice possibility to detect the non-local effects upon the effective transmission through an interacting nano-system.

4.1 The Aharonov-Bohm scatterer

4.1.1 A three-lead contact

In order to be able to model the Aharonov-Bohm ring, it is necessary to model a contact connecting three leads. There are many propositions for such three-lead contacts in the literature (see e. g. [16]) by assuming scattering matrices which fulfill a given symmetry. However, in order to be able to solve the Hartree-Fock equations, it is not sufficient to describe the scattering properties of this three-lead contact at the Fermi energy E_F only, but it has to be done for all energies below E_F. We use the microscopic model sketched in Fig. 4.1 to describe the three lead contact. For this specific model, we can determine the scattering matrix as a function of the energy E by direct calculation. The local Hamiltonian of the three lead contact shown in Fig. 4.1 is given by

$$H_{3\mathrm{LC}} = -\sum_{p=1}^{3} t_p (c_P^\dagger c_p + \mathrm{H.c.}), \tag{4.1}$$

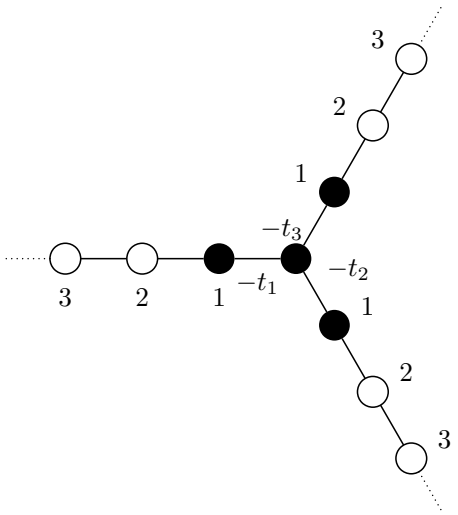

Figure 4.1: The microscopic model for three-lead contact . The Hamiltonian for the 4 central sites (indicated in black) is given in Eq. (4.1). The connections between these central sites and the four leads are given by the hopping terms $-t_p$.

P denoting the central site of the three-lead contact, the sum p being taken over its three neighbors. t_p gives the coupling of the lead p to the central site. We will use a symmetric contact with the hopping terms t_p set to $t_p = t_h = 1$ in the following.

The scattering matrix which describes the three lead contact can be obtained in the usual way: A incoming wave in lead p can be written as

$$\psi_k^p(x, p') = \frac{1}{\sqrt{2\pi}} \begin{cases} \mathrm{e}^{-\mathrm{i}kx} + r_k \mathrm{e}^{+\mathrm{i}kx} & \text{if } p' = p \\ t_k \mathrm{e}^{+\mathrm{i}kx} & \text{if } p' \neq p, \end{cases} \tag{4.2}$$

where $p = 1, 2, 3$ indicates the lead on which the wave arrives, and (x, p') refers to the point x on lead $p' = 1, 2, 3$. Using the Hamiltonian (4.1), we can determine the 3×3 scattering matrix $S_{3\mathrm{LC}}(k)$, which describes the scattering by the three lead contact at an energy $E(k) = -2\cos k$:

$$\mathsf{S}_{3\mathrm{LC}}(k) = \begin{pmatrix} s_d & s_o & s_o \\ s_o & s_d & s_o \\ s_o & s_o & s_d \end{pmatrix} \tag{4.3}$$

where the rotational symmetry of the three lead contact can be seen: The scattering matrix $S_{3\mathrm{LC}}(k)$ is invariant under exchange of the three leads. The diagonal and

off-diagonal elements of $S_{3\mathrm{LC}}(k)$ are given by the expressions

$$\begin{aligned} s_d =& \frac{-e^{ik}}{3e^{ik} - 2\cos k} \\ s_o =& \frac{2i\sin k}{3e^{ik} - 2\cos k}. \end{aligned} \tag{4.4}$$

4.1.2 Using an attached ring as Aharonov-Bohm scatterer

Using the three-lead contact from Eq. (4.1), we can define the Aharonov-Bohm scatterer which is used to create the flux-dependent Aharonov-Bohm fluctuations in the lead. It consists of an attached ring, which is threaded by a magnetic field. Varying the magnetic field will change the reflection properties of the Aharonov-Bohm scatterer.

The complete model we want to study is shown in Fig. 4.2. In order to model the attached ring, we use two three lead contacts: Starting with a nano-system described by Eq. 2.1, which is coupled to two semi-infinite leads, a first three lead contact is integrated into the right lead, at a distance of L_C sites from the nano-system. It allows to connect an additional lead of L'_C sites to the semi-infinite chain. At the end of this additional lead, the second three lead contact is attached, allowing to couple the ring with L_R sites to the model. This adds four new parameters to the model: the lengths L_C, L'_C and L_R, which are all defined excluding the eight sites belonging to the two three lead contacts (indicated in black in Fig. 4.2), and the magnetic flux φ, which threads the ring. The flux is given by $\varphi = 2\pi\Phi/\Phi_0$, $\Phi_0 = h/e$ being the flux quantum.

Varying the distance L_C between the nano-system and the three lead contact in the chain, we will study the influence of the Aharonov-Bohm scatterer upon the effective transmission $|t_{\mathrm{sys}}|^2$ of the nano-system.

The reflection amplitude $r_R(\varphi)$ of an incoming electron in the vertical lead by the ring threaded by a flux φ can be obtained by solving the system of linear equations, which results from the scattering matrix describing the three lead contact and the transfer matrix describing the L_R sites of the ring, including the magnetic flux:

$$\begin{pmatrix} d \\ c \end{pmatrix} = \mathsf{M}_{L_R}(\varphi) \begin{pmatrix} b \\ a \end{pmatrix} \tag{4.5}$$

$$\begin{pmatrix} r_R(\varphi) \\ a \\ d \end{pmatrix} = \mathsf{S}_{3\mathrm{LC}} \begin{pmatrix} 1 \\ b \\ c \end{pmatrix}, \tag{4.6}$$

where the coefficients a, b, c and d describe the state in the lead (see Fig. 4.3), and $\mathsf{M}_{L_R}(\varphi)$ denotes the transfer matrix of a lead with L_R sites and the magnetic flux φ:

$$\mathsf{M}_{L_R}(\varphi) = \begin{pmatrix} \mathrm{e}^{I(kL_R+\varphi)} & 0 \\ 0 & \mathrm{e}^{-I(kL_R-\varphi)} \end{pmatrix}. \tag{4.7}$$

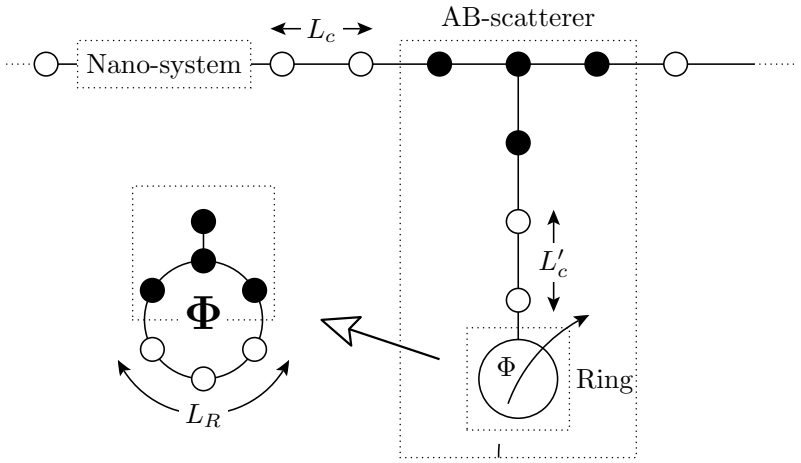

Figure 4.2: The microscopic model of the considered setup: at a distance L_C from the nano-system (see chapter 2), a three-lead contact is used to connect an Aharonov-Bohm scatterer, consisting of a ring of $L_R + 3$ sites, which is attached by an lead of $L'_C + 2$ sites. The ring is threaded by a magnetic flux Φ. For the nano-system, an internal hopping term t_d and a inter-site interaction U is used. In addition, to site potential V_G can be applied to the two sites of the nano-system (see Fig. 2.1).

Solving Eqs. (4.5) and (4.6) for $r_R(\varphi)$, one obtains the reflection amplitude of the ring

$$r_R(\varphi) = \frac{2e^{ik}\sin k(\cos(kL_R) - \cos\varphi) - \sin(kL_R)}{-2e^{ik}\sin k(\cos(kL_R) - \cos\varphi) + e^{2ik}\sin(kL_R)}. \tag{4.8}$$

To obtain the reflection and transmission amplitudes describing the scattering by the complete Aharonov-Bohm scatterer, we have have to solve the equations

$$\begin{pmatrix} \beta \\ \gamma \\ \epsilon \end{pmatrix} = \mathsf{S}_{3\mathrm{LC}} \begin{pmatrix} \alpha \\ \delta \\ \eta \end{pmatrix} \tag{4.9}$$

$$\eta = \mathrm{e}^{2\mathrm{i}kL'_C} r_R(\varphi)\epsilon, \tag{4.10}$$

where α, β, γ and δ are used to describe the state in the chain, while ϵ and η describe the state in the transverse lead between the two three lead contacts (see Fig. 4.3).

Solving these equations, one obtains the reflection and transmission amplitudes of the complete Aharonov-Bohm scatterer for an electron moving in the horizontal lead. In terms of the flux-dependent reflection amplitude $r_R(\varphi)$ of the ring, they

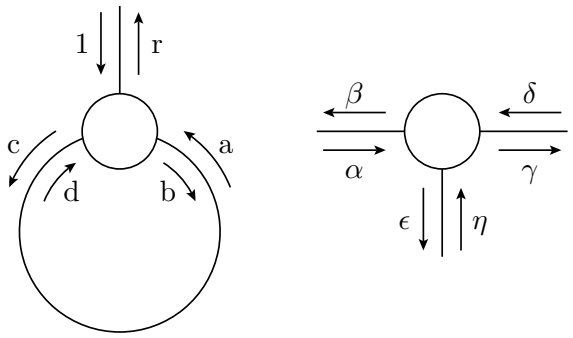

Figure 4.3: The states in the ideal leads can be written as scattering waves $\psi(x) = ae^{ikx} + be^{-ikx}$. The image shows the definition of the variables used in Eqs. (4.5), (4.6) and (4.10). The circles indicate the three-lead contacts given in Eq. (4.1).

can be written as:

$$r_{AB}(k) = \frac{-e^{2ik} - e^{2ikL'_c} r_R(\varphi)}{2e^{2ik} - 1 + r_R(\varphi) e^{2ik(L'_c+1)}} \tag{4.11}$$

$$t_{AB}(k) = \frac{2i \sin k e^{ik}(1 + e^{2ikL'_c} r_R(\varphi))}{2e^{2ik} - 1 + r_R(\varphi) e^{2ik(L'_c+1)}}. \tag{4.12}$$

4.2 Friedel oscillations and particle-hole symmetry

In this section, we illustrate separately the effect of the nano-system and of the Aharonov-Bohm scatterer onto the attached leads. For the special case of half-filling and with $V_0 = V_1 = -U/2$, the model fulfills particle-hole symmetry resulting in a uniform density $\langle c_x^\dagger c_x \rangle = 1/2$ everywhere in the system and the attached leads. In this case, no Friedel-oscillations of the density exist. Nevertheless, both the nano-system and the Aharonov-Bohm scatterer induce oscillations of the correlation function $\langle c_L^\dagger c_{L+1} \rangle$ in the leads. Although the exact form of $\langle c_L^\dagger c_{L+1} \rangle$ differ between the oscillations induced by the nano-system and the ones induced by the Aharonov-Bohm scatterer, the asymptotic behavior of $\langle c_L^\dagger c_{L+1} \rangle$ can be given for both scatterers by

$$\left\langle c_L^\dagger c_{L+1} \right\rangle \approx \frac{\sin(k_F)}{\pi} + b \frac{\cos(2k_F L + \delta)}{L} \tag{4.13}$$

where the parameter b and the phase shift δ depend on the scatterer.

For the nano-system only, Fig. 4.4 shows the correlation term $\langle c_L^\dagger c_{L+1} \rangle$ at a distance L from the nano-system. $\langle c_L^\dagger c_{L+1} \rangle$ decays as $1/L$ towards $\sin k_F/\pi = 1/\pi$. The figure was calculated for two different hopping terms $t_d = 0.1$ and $t_d = 1$ inside

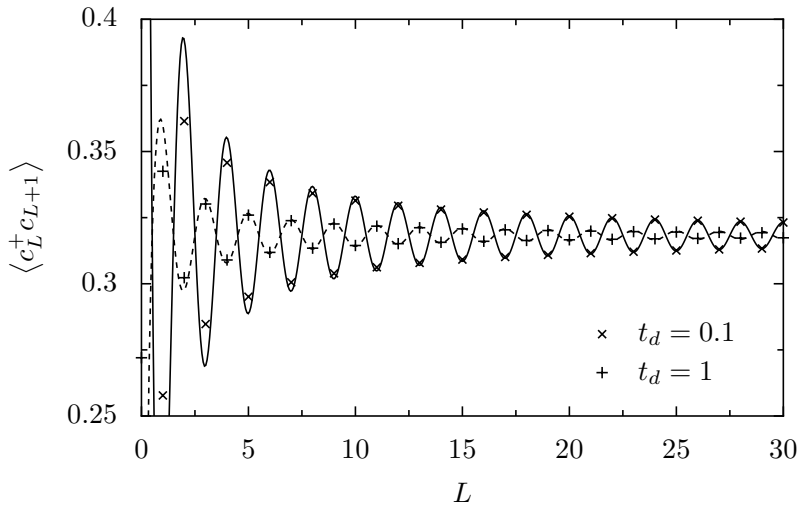

Figure 4.4: Friedel-like oscillations of the correlation function $\langle c_L^\dagger c_{L+1} \rangle$ induced by the nano-system. At half filling ($k_F = 1/2$), this are even-odd oscillations. The oscillations decay towards $1/\pi$ with a $1/L$ decay. The image is calculated for $U = 1$, $V_G = -U/2$ (compensating the Hartree term and creating particle-hole symmetry) and $t_c = t_h = 1$. The solid and the dashed line show the two asymptotic fits $1/\pi + b(t_d)\cos(\pi x + c(t_d))/x$ with $b(1) = 0.04151$, $b(0.1) = 0.14776$, $c(0) = \pi$ and $c(0.1) = 0$, respectively. The data in this figure are calculated without the Aharonov-Bohm scatterer, L indicates the distance from the nano-system.

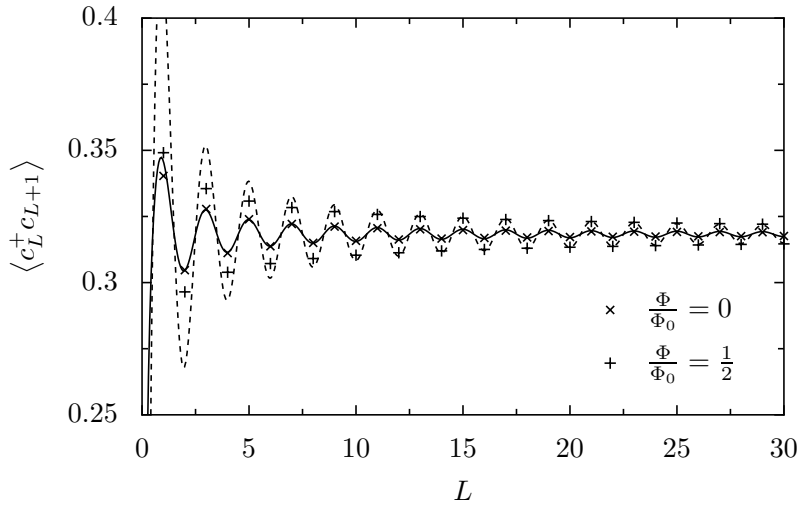

Figure 4.5: The Aharonov-Bohm scatterer induces Friedel-like oscillations of the correlation function $\langle c_L^\dagger c_{L+1} \rangle$ in the leads. At half filling ($k_F = 1/2$), these are even-odd oscillations. The oscillations decay towards the asymptotic value $1/\pi$ with a $1/L$ decay. The length of the ring is set to $L_R = 6$, the distance $L'_C = 4$. The values are calculated for the two flux values $\Phi = \Phi_0/2$ (++) and $\Phi = 0$ (×). The solid and dashed lines show the two asymptotic fits $1/\pi + b(\Phi)\cos(\pi L + c(\Phi))/L$ with $b(\frac{\Phi_0}{2}) = 0.09983$, $b(0) = 0.02746$, $c(\frac{\Phi_0}{2}) = \pi$ and $c(0) = \pi$ respectively.

the nano-system, with $U = 1$. As expected, $t_d = 0.1$ leads to much larger oscillations, as the scattering with $t_d = 0.1$ is more important than for $t_d = 1$. The Friedel-oscillations of the density, which emerge inside the leads if the particle-hole symmetry is broken, have the same asymptotic decay as given in equation 4.13, but with the asymptotic value $\langle c_L^\dagger c_L \rangle = k_F/\pi = 1/\nu$.

The attached ring without the nano-system always fulfills particle-hole symmetry, thus no oscillations of the density $\langle c_L^\dagger c_L \rangle$ are created by the Aharonov-Bohm scatterer. Nevertheless, it induces oscillations of the correlation term $\langle c_L^\dagger c_{L+1} \rangle$ in the leads, L denoting the distance from the Aharonov-Bohm scatterer. These oscillations will change the exchange correction in the Hartree-Fock equations describing the nano-system, leading to the non-local contribution to the effective transmission t_{sys} through the nano-system.

For half-filling, these oscillations are shown in Figs 4.5 and 4.6 for rings of size $L_R = 6$ and $L_R = 7$, respectively. We use both even and odd length L_R for the study at half-filling, because the scattering matrix describing the complete Aharonov-Bohm scatterer behaves very differently for even and odd lengths L_R at $k_F = \pi/2$, as implied by Eqs. (4.11) and (4.12): For an even length L_R, the Aharonov-Bohm scatterer is independent of the flux φ at $k_F = \pi/2$. For an odd length L_R, the

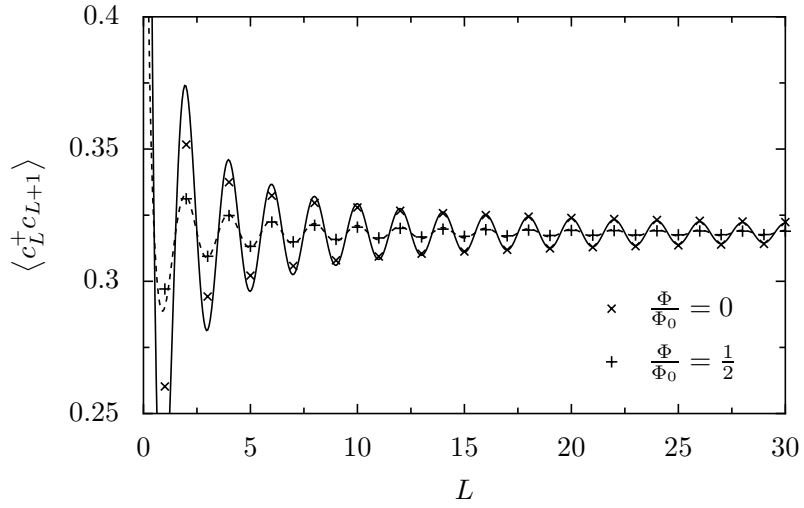

Figure 4.6: The Aharonov-Bohm scatterer induces Friedel-like oscillations of the correlation function $\langle c_L^\dagger c_{L+1} \rangle$ in the leads. At half filling ($k_F = 1/2$), these are even-odd oscillations. The oscillations decay towards the asymptotic value $1/\pi$ with a $1/L$ decay. The length of the ring is set to $L_R = 7$, the distance $L'_C = 4$. The values are calculated for the two flux values $\Phi = \Phi_0/2$ (+) and $\Phi = 0$ (×). The solid and dashed lines show the two asymptotic fits $1/\pi + b(\Phi)\cos(\pi L + c(\Phi))/L$ with $b(\frac{\Phi_0}{2}) = 0.027997$, $b(0) = 0.11029$, $c(\frac{\Phi_0}{2}) = 0$ and $c(0) = \pi$ respectively.

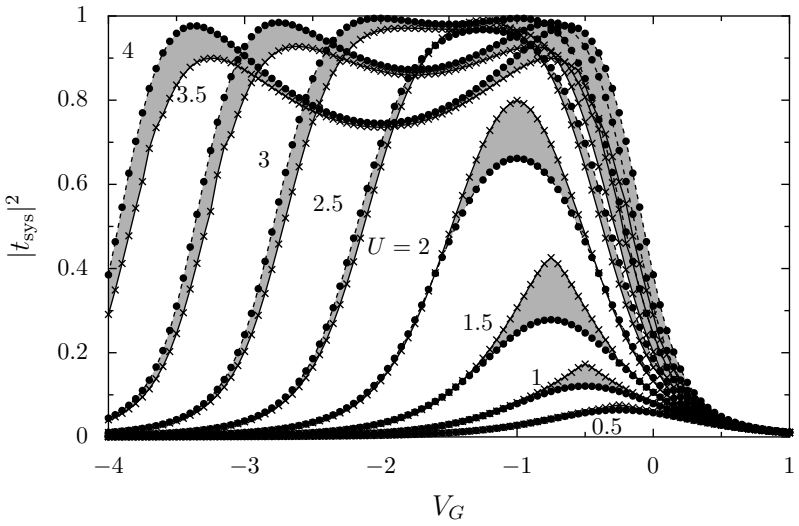

Figure 4.7: The effective transmission $|t_{\rm sys}|^2$ of the nano-system as a function of the gate voltage V_G for half-filled chains (Fermi momentum $k_F = \pi/2$) and a hopping term $t_d = 0.1$ inside the nano-system. The AB-scatterer with its attached ring is given by $L'_C = 4$ and $L_R = 7$. It is attached $L_C = 2$ sites from the nano-system. The curves are calculated for different interaction strengths U as indicated in the figure. As flux threading the ring, the two values $\Phi = 0$ (×) and $\Phi = \Phi_0/2$ (•) are used. The grey areas underline the effect of Φ upon $|t_{\rm sys}|^2$.

Aharonov-Bohm scatterer depends on the flux φ at $k_F = \pi/2$. Nevertheless, the correlation function $\langle c_L^\dagger c_{L+1}\rangle$ being the sum over all states below the Fermi energy $E_F = 0$, exhibits always flux-dependent oscillations, both for even and odd values of L_R. Figures 4.5 and 4.6 show $\langle c_{L+1}^\dagger c_L\rangle$ for the two cases without magnetic flux trough the ring ($\Phi = 0$) and with half a flux quantum threading the ring ($\Phi = \frac{1}{2}\Phi_0$). For all other flux values Φ, the results are situated between these two curves.

4.3 Influence of the magnetic flux upon the nano-system transmission $t_{\rm sys}$

In this section, we will use a non-compensated interaction U, but with $V_0 = V_1 = V_G$. This gives rise to Hartree corrections in addition to the Fock correction studied so far. Consequently, we will have to solve the three coupled Hartree-Fock equations (2.10)-(2.12). For the numerical calculations, this makes it necessary to search the solution in a three-dimensional parameter space consisting of v, $V_0^{\rm HF}$ and $V_1^{\rm HF}$..

When the nano-system and the Aharonov-Bohm scatterer are put in series, the oscillations of both interfere with each other, resulting in a more complex expres-

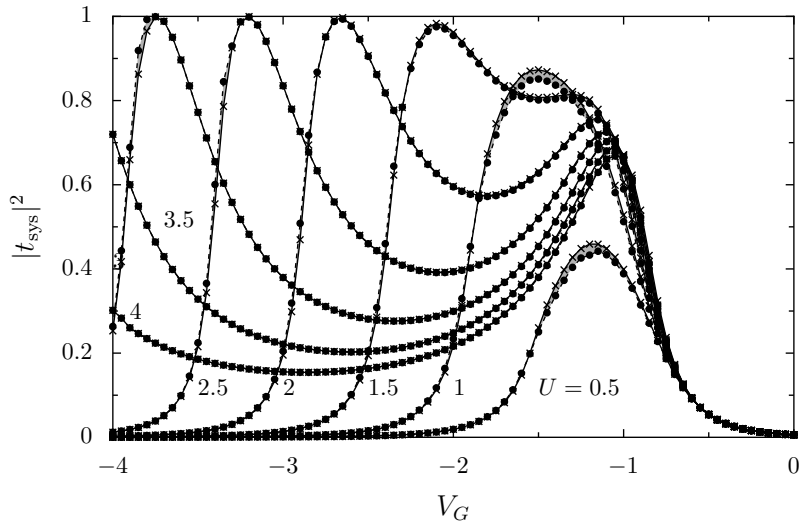

Figure 4.8: The effective transmission $|t_{\rm sys}|^2$ of the nano-system as a function of the gate voltage V_G, for a filling factor 1/8 in the chains (Fermi momentum $k_F = \pi/8$) and a hopping term term $t_d = 0.1$ inside the nano-system. The AB-scatterer with its attached ring is given by $L'_C = 4$ and $L_R = 7$. It is attached $L_C = 2$ sites from the nano-system. The curves are calculated for different interaction strengths U as indicated in the figure. As flux threading the ring, the two values $\Phi = 0$ (x) and $\Phi = \Phi_0/2$ (•) are used. The grey areas underline the effect of Φ upon $|t_{\rm sys}|^2$.

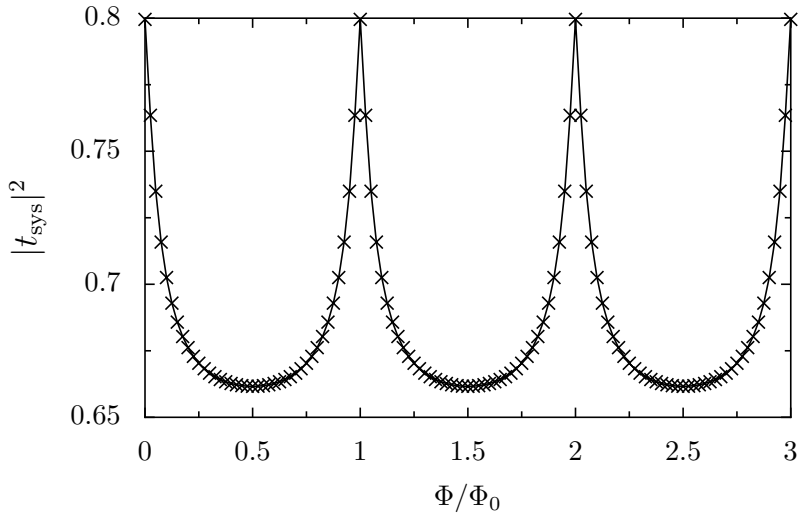

Figure 4.9: The effective nano-system transmission $|t_{\rm sys}|^2$ as a function of the magnetic flux Φ/Φ_0, at half filling ($k_F = \pi/2$), interaction $U = 2$ and gate potential $V_G = -U/2$. For these parameters, particle-hole symmetry is fulfilled, resulting in $V_0 = V_1 = 0$. The other parameters defining the model are $L_C = 2$, $L'_C = 4$, $L_R = 7$ and $t_d = 0.1$.

sion for $\langle c^\dagger_{x+1} c_x \rangle$ and $\langle c^\dagger_x c_x \rangle$. In addition, as the Hartree-Fock parameters depend on the Aharonov-Bohm scatterer, the Hartree-Fock equations (2.10)-(2.12) have to be solved self-consistently for each flux value Φ. The analytic calculation of the expectation values $\langle c^\dagger_0 c_1 \rangle$, $\langle c^\dagger_0 c_0 \rangle$ and $\langle c^\dagger_1 c_1 \rangle$ becomes much more complicated in the presence of the Aharonov-Bohm scatterer. Instead of performing an analytical calculation, we use the numerical method sketched in section A.1 in order to obtain the self-consistent values for v, $V_0^{\rm HF}$ and $V_1^{\rm HF}$. Once the effective one-body model (given by v, $V_0^{\rm HF}$ and $V_1^{\rm HF}$) is known, the effective transmission amplitude $t_{\rm sys}$ of the nano-system at an energy $E = -2\cos k$ is given by Eq. (2.15), for a coupling $t_c = 1$ between the nano-system and the leads.

In order to obtain large effects of the magnetic flux Φ upon the transmission probability $|t_{\rm sys}|^2$ of the nano-system, we have to select a small value $t_d = 0.1$ for the hopping term inside the nano-system, as discussed in section 2.3.2. The resulting transmission probability $|t_{\rm sys}|^2$ is shown in Figs. 4.7 and 4.8 as a function of the gate potential V_G, for two different filling factors $k_F = \pi/2$ and $k_F = \pi/8$ respectively. For both images, the same geometric parameters of the Aharonov-Bohm scatterer ($L_C = 2$, $L'_C = 4$ and $L_R = 7$) were used. For each interaction strength U, we plot the results for two different fluxes Φ threading the ring: The first curve (x in the figures) is calculated when there is no flux Φ threading the ring, the second curve ($\bullet$ in the figures) is calculated for half a flux quantum $\Phi = \Phi_0/2$ threading the ring. These are the two extreme cases, for other values of the flux Φ, the nano-

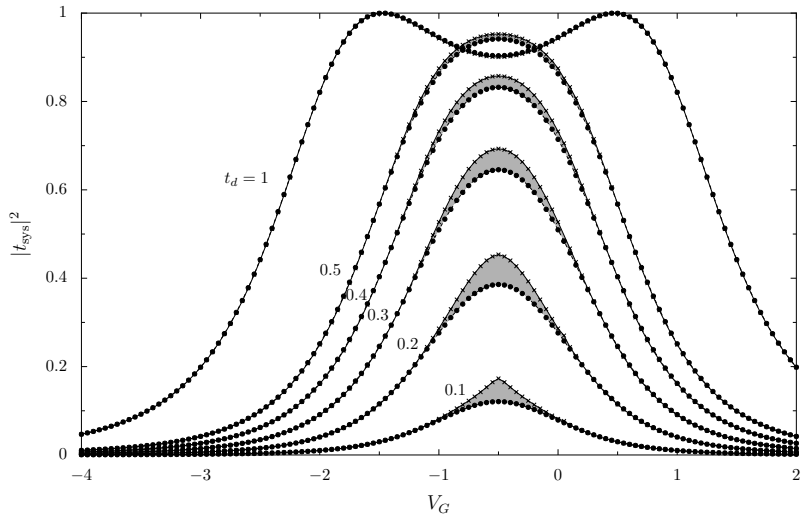

Figure 4.10: The effective transmission $|t_{\rm sys}|^2$ of the nano-system at half-filling as a function of the gate potential V_G for different values of the nano-system hopping term t_d, which are indicated in the figure. The curves are shown for two values of the magnetic flux threading the ring, $\Phi = 0$ (x) and $\Phi = \Phi_0/2$ ($\bullet$). The Aharonov-Bohm scatterer is defined by $L_C = 2$, $L'_C = 4$, $L_R = 7$, the interaction strength is set to $U = 1$. The grey areas underline the effect of Φ upon $|t_{\rm sys}|^2$.

system transmission $|t_{\rm sys}|^2$ is found between these two curves, in the region which is indicated by the grey areas in the figures.

As we consider the transmission through the nano-system only, the grey areas underline a pure many-body effect: Without interaction ($U = 0$), the transmission $|t_{\rm sys}(U = 0)|^2$ of the nano-system would be independent of the flux and the grey areas would vanish.

At half-filling (Fig. 4.7), the effect of Φ upon the nano-system transmission $|t_{\rm sys}|^2$ becomes very important for the chosen set of parameters: Around certain values of U and V_G, the change in the transmission can become as big as 0.2, for a transmission $|t_{\rm sys}|^2 < 1$. If the interaction U is small enough, the two transmission peaks characteristic for a nano-system consisting of two sites merge into a single peak. In this area, the largest effects of Φ upon $|t_{\rm sys}|^2$ are obtained for $V_G = -U/2$, when the Hartree terms are compensated by the gate potential at half filling.

At low filling factors (Fig. 4.8), the non-local interaction effect can be seen but becomes smaller, the effective nano-system transmission exhibiting changes of a few percent only around the transmission peaks. This is due to the difference between the wave-length of the flux-dependent Friedel-oscillations and the size of the nano-system: As the wave length of the Friedel oscillations $\lambda_F/2 = 8$ is much longer than the nano-system, one can expect that larger effects will be observed if the size of the nano-system and the length of the Friedel oscillations are of the same order, as it is the case in Fig. 4.8.

For the particular large effects around $U = 2$ and $V_G = -U/2$ at half-filling, we show the nano-system transmission $|t_{\rm sys}|^2$ as a function of the flux Φ in Fig. 4.9, with $U = 2$ and $V_G = -1$. The transmission oscillates as a function of the flux Φ threading the ring. It reaches its maximum for $\Phi = n\Phi_0$ and its minimum for $\Phi = (n + 1/2)\Phi_0$, n being an integer.

The dependence of the non-local effect on the hopping term t_d is illustrated in Fig. 4.10, where the nano-system transmission $|t_{\rm sys}|^2$ is shown as a function of the gate voltage V_G for a half-filled model and an interaction $U = 1$ inside the nano-system. The V_G-dependence of the transmission is symmetric around $V_G = -U/2$. Again, the biggest effects upon the transmission can be seen around the particle-hole symmetric value $V_G = -U/2$. For $t_d = 1$, the small effect of the flux Φ upon the nano-system transmission $|t_{\rm sys}|^2$ cannot be seen at the used scale.

The flux-dependence of $|t_{\rm sys}|^2$ is underlined by grey areas in Fig. 4.10, as in Fig. 4.8.

4.4 Conductance $g_{\rm tot}$ of the complete model

In the two probe geometry of the model given in Fig. 4.2, the dimensionless quantum conductance $g_{\rm tot}$ of the nano-system and the AB-scatterer in series is given by the

Landauer-Büttiker formula [17, 41] as $g_{\rm tot} = |t_{\rm tot}E_F)|^2$ (in units of e^2/h), where

$$t_{\rm tot}(E_F) = t_{\rm sys}(E_F)\frac{e^{ik_F L_C}}{1 - r'_{\rm sys}(E_F)r_{\rm AB}(E_F)e^{2ik_F L_C}}t_{\rm AB}(E_F)\,. \tag{4.14}$$

The transmission and reflection amplitudes $t_{\rm sys}(E_F)$ and $r'_{\rm sys}(E_F)$ of the nano-system are given by Eqs. (2.15) and (2.16) (with $r'_{\rm sys}(E_F) = r_{k_F,-}$), and $t_{\rm AB}(E_F)$ and $r_{\rm AB}(E_F)$ denoting the transmission and reflection amplitude of the Aharonov-Bohm scatterer as given in Eqs. (4.12) and (4.11) respectively. Because $r_{\rm AB}(E_F)$ and $t_{\rm AB}(E_F)$ depend in general on the flux Φ, the resulting total conductance $g_{\rm tot}(E_F)$ exhibits Aharonov-Bohm oscillations even when $U = 0$, or when $U \neq 0$ and the distance L_C is very large. In these situations $t_{\rm sys}(E_F)$ and $r'_{\rm sys}(E_F)$ are independent of the magnetic flux Φ.

However, when the electrons interact inside the nano-system and if L_C is not to large, the effective nano-systems scattering amplitudes $t_{\rm sys}(E_F)$ and $r'_{\rm sys}(E_F)$ exhibit also Aharonov-Bohm-oscillations which can be important for certain values of V_G. This can strongly influence the AB-oscillations of the total conductance $g_{\rm tot}$. An example for such a situation is shown in Fig. 4.11, where the Aharonov-Bohm oscillations of the total conductance $g_{\rm tot}$ are weak without interaction, and become very important when the electrons interact inside the nano-system. However, since our model depends on many parameters, the conditions under which the non-local many-body effect increases substantially the flux-dependent oscillations of the total conductance $g_{\rm tot}$ become complex. There are also parameter-ranges in which the Aharonov-Bohm-oscillations are large without interaction, contribution of the interaction reducing both the absolute value of $g_{\rm tot}$ and the amplitude of its oscillations.

In our model, there is the special case where $\sin(k_F L_R) = 0$. In this case, Eq. (4.8) giving the reflection amplitude of the ring simplifies to

$$r_R(\varphi) = -1, \tag{4.15}$$

such that the ring is perfectly reflecting at the Fermi energy E_F, independent of the flux Φ threading the ring. For this geometry, also the coefficients $r_{\rm AB}$ and $t_{\rm AB}$ describing the scattering of the complete Aharonov-Bohm scatterer are independent of the flux ϕ. We show such a case in Fig. 4.12, where the Fermi energy $k_F = \pi/2$ and the ring-length $L_R = 6$ lead to $\sin(k_F L_R) = 0$, making the Aharonov-Bohm scatterer independent of the magnetic flux Φ at the Fermi energy. For these parameters, the interaction increases the value of g_T. Because of this, the Aharonov-Bohm oscillations which appear for $U = 1$ in Fig. 4.12 are a pure many body effect.

These oscillations can be understood by looking at the Hartree-Fock equations (2.10)-(2.12): The parameters v, $V_0^{\rm HF}$ and $V_1^{\rm HF}$ which describe the effective one-body model depend on all states with energies $E \leq E_F$. The condition (4.15) is only fulfilled at the Fermi energy E_F, the other states with $E < E_F$ depend on the magnetic flux Φ. Because of this, v, $V_0^{\rm HF}$ and $V_1^{\rm HF}$ depend on the flux, and thus $|t_{\rm sys}|^2$ shows

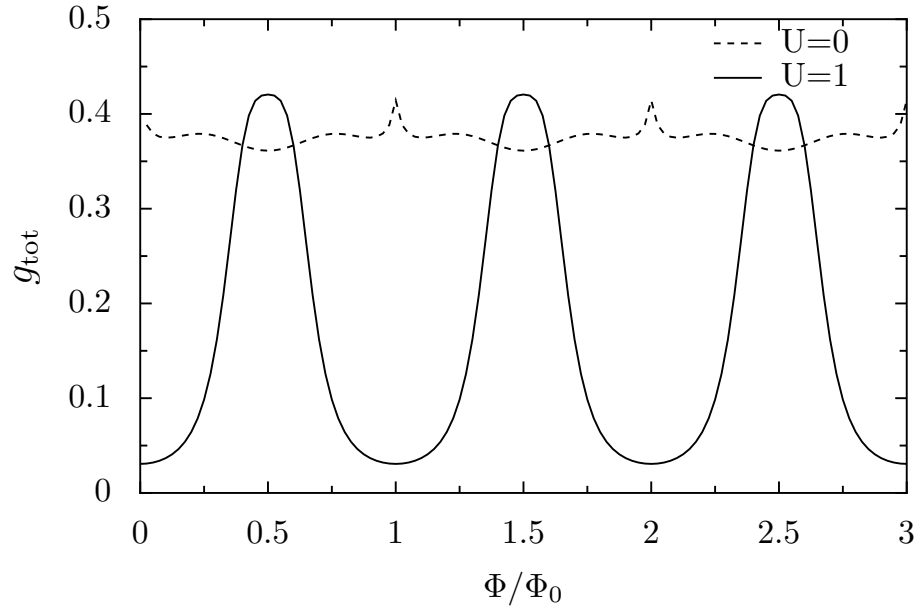

Figure 4.11: The quantum conductance $g_{\rm tot}$ of the nano-system and the attached Aharonov-Bohm scatterer in series as a function of the flux Φ/Φ_0 for half-filling ($k_F = \pi/2$), with and without interaction ($U = 1$: solid line and $U = 0$: dotted line). The geometry is given by $L_C = 4$, $L'_C = 6$ and $L_R = 7$. The gate potential is set to $V_G = -0.5$. The AB-oscillations occurring without interaction ($\sin(k_F L_R) \neq 0$) are strongly increased by the interaction when $U = -2V_G$.

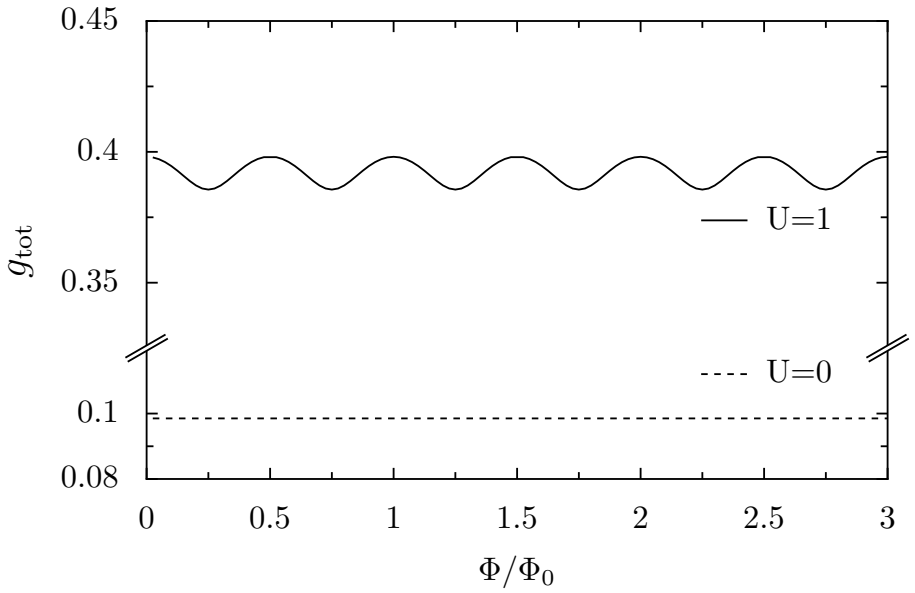

Figure 4.12: Total conductance $g_{\rm tot}$ as a function of Φ/Φ_0 for half-filling ($k_F = \pi/2$), with and without interaction, for $U = 1$ (solid line) and $U = 0$ (dotted line). The geometry is given by $L_C = 4$, $L'_C = 5$ and $L_R = 6$. The gate potential is set to $V_G = -0.5$. Without interaction, there are no AB-oscillations ($\sin(k_F L_R) = 0$). The interaction inside the nano-system increases $g_{\rm tot}$ when $U = -2V_G$ and yields AB-oscillations.

flux-dependent oscillations. With that, also the total conductance $g_{\rm tot}$ given by Eq. (4.14) shows Aharonov-Bohm oscillations, even though $t_{\rm AB}(E_F)$ and $r_{\rm AB}(E_F)$ are independent of Φ for this set of parameters.

4.5 Conclusion

We have shown in this chapter one possibility to detect non-local effects upon the effective transmission $t_{\rm sys}$ of an interacting nano-system: Connecting an attached ring threaded by a magnetic flux Φ at a distance L_C from the nano-system, Aharonov-Bohm oscillations of $t_{\rm sys}$ will appear, when the interaction U inside the nano-system is non-negligible. When measuring the total conductance $g_{\rm tot}$ through both the nano-system and the Aharonov-Bohm scatterer, this non-local interaction effect can largely enhance the oscillations of $g_{\rm tot}$. For some special selection of parameters, the transmission of the Aharonov-Bohm scatterer will be completely independent of the flux Φ at the Fermi energy, such that the conductance oscillations of $g_{\rm tot}$result completely from the non-local contribution.

Another possibility, for detecting the effect of the flux upon the effective transmission $t_{\rm sys}$ is to use of a four-probe setup [22], adding two additional contacts on the two sides of the nano-system, which are weakly coupled to the leads. With this geometry, the potential difference induced by the nano-system can be measured directly, instead of the potential difference of the complete model including the Aharonov-Bohm scatterer only. However, since the non-local effect discussed here makes it mandatory that the Aharonov-Bohm scatterer and the nano-system are in the same quantum coherent region, the conductance obtained by such a four probe measurement is not given by the two-probe formula $g_{\rm sys} = |t_{\rm sys}|^2$, but by the multi-terminal formula derived by Büttiker [15]. This formula adds a dependence of the measured conductance upon Φ, even in the absence of local interactions. This effect was observed in mesoscopic conductors, in which the interaction is too weak to make our non-local many-body effects important, like metallic wires [75] or semiconductor nano-structures [65]. Nevertheless, the non-local effects seen in Refs. [65, 75] will be strongly enhanced if the electron-electron interactions are important in a region included between the two voltage probes.

In the calculations shown in this chapter, the non-local effect of the magnetic flux upon the nano-system was very important at half-filling $\nu = 1/2$ ($k_F = \pi/2$), and became smaller for a filling factor of $\nu = 1/8$ resulting in $\lambda_F/2 = 8$. This decrease of the non-local effect can be probably explained by the difference between the length of the interacting region (2 sites) and the Fermi wave length $\lambda_F/2 = \nu$. At $E_F = 0$, $L_{\rm sys} \approx \lambda_F$ and a large non-local effect is observed.

5 Detecting the local interaction by scanning probe microscopy

After having studied one-dimensional models, we extend the study of the non-local effect on two-dimensional models. This extension is important, because it is much more justified to neglect the electron-electron interactions in two-dimensional leads than in one-dimensional leads, where a Luttinger liquid emerges for interacting fermions.

The model we study in this chapter is a minimalistic model describing a Scanning Gate Microscopy (SGM) - measurement of a quantum point contact. It can be seen that a signature of the non-local effect which we discussed in the last chapters appears in the SGM-images. Particularly, we show that the SGM images should allow to detect the presence of significant electron-electron interaction inside the measured nano-structure.

5.1 Microscopic model

The model we are using is shown in Fig. 5.1, again assuming spin-polarized electrons. The interacting nano-structure at the center is described by the same Hamiltonian (2.1) already discussed in chapter 2. The two 2-dimensional strips are described by a tight-binding lattice with nearest-neighbor hopping terms $t_h = 1$. We assume $V_0 = V_1 = V_G$, V_G playing the role of a gate potential applied to the nano-system.

$$H_{\text{strips}} = -t_h \sum_{x,y} \left(c^\dagger_{x,y} c_{x,y+1} + c^\dagger_{x,y} c_{x+1,y} + \text{H.c.} \right), \tag{5.1}$$

which also includes the coupling to the nano-system. The left strip occupies the sites $-\infty < x \leq 0$ and $-L_y \leq x \leq L_y$, except the right nano-system site $(x, y) = (-1, 0)$. The right strip occupies the sites $1 \leq x < \infty$ and $-L_y \leq x \leq L_y$, except the left nano-system site $(x, y) = (0, 0)$. We assume hard wall boundary conditions in y-direction. Each nano-system site is now coupled to three sites of the particular strip, as shown in Fig. 5.1.

The effect of the charged AFM-tip upon the two-dimensional electron gas (2DEG) in the strip is modelled by a local potential V_T at the tip position (x_T, y_T):

$$H_{\text{tip}} = V_T n_{x_T, y_T}, \tag{5.2}$$

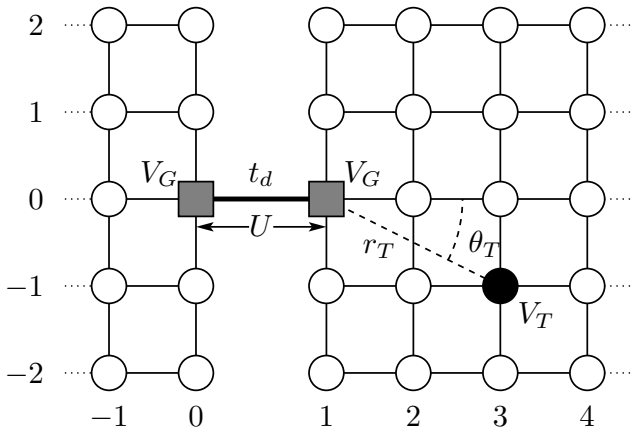

Figure 5.1: The microscopic model we use: The nano-system discussed in chapter 2 is used. The AFM-tip is modelled by a potential V_T at coordinates $(x_T, y_T) = r_T(\cos\theta_T, \sin\theta_T)$. The leads are described by $\mathcal{L}_y = 2L_y + 1$ sites in transverse direction, and stretch to $x \to -\infty$ and $x \to +\infty$.

where the tip coordinates are given by $(x_T, y_T) = r_T(\cos\theta_t, \sin\theta_T)$. Using a positive or a negative potential V_T, we can create a accumulation or depletion region of the electrons in the strip at the tip position.

5.2 The principle in one dimension

In the one-dimensional case it is easy to explain the principle how the importance of the local interaction U can be detected from SGM images: Let us assume a nano-system coupled to two semi-infinite chains with a transverse size of $\mathcal{L}_y = 1$ sites, with the tip potential at a distance r_T from the nano-system. The resulting conductance $g(r_T)$ is shown in Fig. 5.2 as a function of the tip position r_T for a half-filled model, with $U = 1$ (x) and with $U = 0$ (+) as a function of the position r_T of the charged tip.

Without interaction inside the nano-system ($U = 0$), the nano-system and the SGM tip are two independent one-body scatterer: Fabry-Pérot oscillations of period of $\lambda_F/2$ are observed in the conductance by the interference between electrons transmitted through the nano-system interfere and electrons reflected by the tip At zero temperature and in the absence of disorder in the leads, the Fabry-Pérot oscillations do not decay and their amplitude stays constant when $r_T \to \infty$. This motivates the fit-function

$$g(U = 0, r_T) = g(U = 0, \infty) + \alpha \cos(2k_F r_T)\,, \tag{5.3}$$

which is valid when $U = 0$ in one dimension.

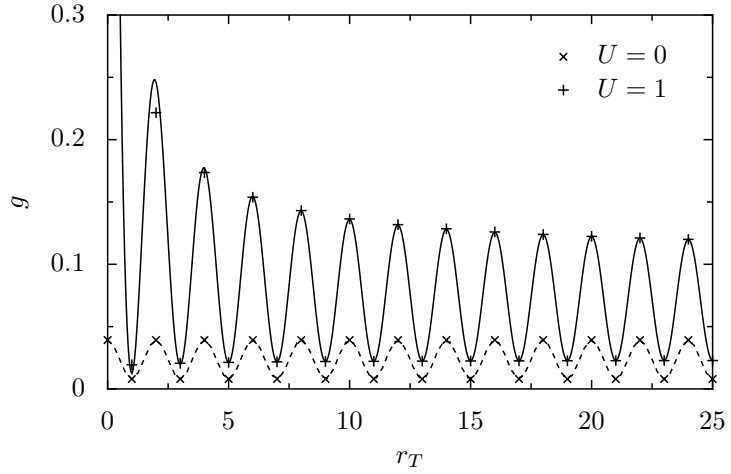

Figure 5.2: Detection of the interaction U in one dimension: For $U = 0$, the conductance g as a function of the tip position r_T shows Fabry-Pérot oscillations with constant amplitude when $r_T \to \infty$ (×). For $U = 1$, an additional contribution to the conductance appears, which decays as $1/r_T$ when $r_T \to \infty$ (+). The solid line shows the fit (5.4) with $g(U = 1, \infty) = 0.0664$, $\beta = 0.0427$ and $\gamma = 0.143$. The parameters are $E_F = 0$, $V_G = -U/2$, $t_d = 0.1$ and $V_T = 2$.

If the interaction inside the nano-system becomes important ($U \neq 0$), the effective one-body Hamiltonian depends on the tip position, via the Friedel-oscillations of $\langle c_x^\dagger c_x \rangle$ and the oscillations of the correlation function $\langle c_x^\dagger c_{x+1} \rangle$ induced by the tip. This non-local effect creates an additional dependence of the total conductance upon the tip position, which decays like the Friedel-oscillations causing it as $1/r_T$ when $r_T \to \infty$. This effect obeys oscillations with period $\lambda_F/2$ too. Thus in the presence of local interactions, we can use the fit-function

$$g(U = 1, r_T) = g(U = 1, \infty) + (\beta + \frac{\gamma}{r_T}) \cos(2k_F r_T) \,, \tag{5.4}$$

in order to describe the total conductance through the model.

In Fig. 5.2 we show both the interacting and the non-interacting situation. The dashed line shows the fit Eq. (5.3) for the case $U = 0$ (x), while the solid line shows the fit Eq. (5.4) for the case $U = 1$ (+). At half-filling, we obtain even-odd oscillations in Fig. 5.2 and the decrease of the interaction-induced contribution can be clearly detected in Fig. 5.2.

A similar one-dimensional setup is studied in more detail in [76], focussing on a special set of parameters, for which the nano-system is perfectly transmitting at the Fermi energy. For these parameters, there are no r_T-dependent oscillations of the conductance in the absence of electron-electron interaction inside the nano-system and $g(U = 0)$ is independent of r_T. In this situation, all oscillations which appear in $g(r_T)$ are pure many-body effects. The calculations in [76] are done using the exact DMRG algorithm and the embedding method [24, 46, 50, 61, 67] to obtain the conductance.

5.3 Hartree-Fock theory and conductance

5.3.1 Hartree-Fock theory

In the one-dimensional case, the Hartree-Fock parameters can be calculated using a simple extrapolation technique described in section A.1. In two dimensions, this approach becomes numerically much more inefficient. For larger transverse directions L_y, it is more efficient to use a Green's function formulation. In this formulation, the effects of the two-dimensional strips can be described by the self-energies $\sigma_L(z)$ for the left strip and $\sigma_R(z, V_T, x_T, y_T)$ for the right strip. σ_R includes the effect of the AFM tip. In this work, the two self-energies σ_L and σ_R are calculated numerically using the recursive Green's function method [63, 64], detailed in appendices A.4 and A.5.

In the Green's function formulation of the Hartree-Fock approximation [26], the Hartree-Fock corrections appear as additional self-energies in the definition of the Green's function. For the nano-system used in this thesis, where interactions are

taken into account between the two central sites only, one has only three Hartree-Fock self-energies $\Sigma^{\mathrm{H}}_{\mathbf{0}}$, $\Sigma^{\mathrm{H}}_{\mathbf{1}}$ and Σ^{F}, which are given by

$$\Sigma^{\mathrm{H}}_{\mathbf{0}} = -\frac{U}{\pi}\int_{-\infty}^{E_F} \mathrm{d}E G_{\mathrm{sys}}(E)_{\mathbf{1},\mathbf{1}} \tag{5.5}$$

$$\Sigma^{\mathrm{H}}_{\mathbf{1}} = -\frac{U}{\pi}\int_{-\infty}^{E_F} \mathrm{d}E G_{\mathrm{sys}}(E)_{\mathbf{0},\mathbf{0}} \tag{5.6}$$

$$\Sigma^{\mathrm{F}} = +\frac{U}{\pi}\int_{-\infty}^{E_F} \mathrm{d}E G_{\mathrm{sys}}(E)_{\mathbf{0},\mathbf{1}}\,. \tag{5.7}$$

As the effect of the strips is described by the self-energies $\sigma_L(z)$ and $\sigma_R(z, V_T, x_T, y_T)$, the retarded ($z = E + \mathrm{i}\eta$) and advanced ($z = E + \mathrm{i}\eta$) nano-system Green's functions $G^{r,a}_{\mathrm{sys}}$ can be given by the 2×2 matrices

$$G_{\mathrm{sys}}(z) = \begin{pmatrix} z - V_G - \Sigma^{\mathrm{H}}_{\mathbf{0}} - \sigma_L(z) & t_d - \Sigma^{\mathrm{F}} \\ t_d - \Sigma^{\mathrm{F}} & z - V_G - \Sigma^{\mathrm{H}}_{\mathbf{1}} - \sigma_R(z, V_T, x_T, y_T) \end{pmatrix}, \tag{5.8}$$

which are defined on the two nano-system sites $\mathbf{0} = (-1, 0)$ and $\mathbf{1} = (0, 0)$.

The integrations in Eqs. (5.5)-(5.7) are done numerically here, the used procedure being described in appendix A.6, using Cauchy theorem to select an integration path in the upper or lower half of the complex plane, depending on whether the retarded or advanced Green's function has to be calculated. In addition, the equations (5.5)-(5.7) have to be solved numerically in order to obtain a self-consistent solution.

5.3.2 Landauer-Büttiker conductance

Once the self-energies Σ^{HF} are obtained as self-consistent solutions of Eqs. (5.5)-(5.7), the interacting model is described by an effective one-body Green's function, which is identical to the one of a non-interacting model with potential $V_G + \Sigma^{\mathrm{H}}_{\mathbf{0}}$ and $V_G + \Sigma^{\mathrm{H}}_{\mathbf{1}}$ instead of V_G, and with a hopping term $t_d + \Sigma^{\mathrm{F}}$ instead of t_d.

Using the Landauer-Büttiker formula, the dimensionless conductance (in units of e^2/h) can be written in the Green's function formalism as [21]

$$g = \mathrm{Tr}\left(\Gamma^L \langle 0|G^a_S|x_T\rangle \Gamma^R \langle x_T|G^r_S|0\rangle\right)_{E_F}, \tag{5.9}$$

where $G^{r,a}_S$ is the Green's function describing the complete model including the tip. $\langle 0|G^{r/a}_S|x_T\rangle$ indicates the submatrix of size $\mathcal{L}_y \times \mathcal{L}_y$ of $G^{r/a}_S(x, y, x', y')$ with $x = 0$ and $x' = x_T$, describing the transport through the system. The $\mathcal{L}_y \times \mathcal{L}_y$ matrices $\Gamma^{L,R}$ describing the transfer of the propagating modes between the system and the leads, are defined in appendix A.3. As the conductance in Eq. 5.9 is calculated for an effective one-body model, it has to be evaluated at the Fermi energy only.

In Eq. (5.9), the Green's functions G^r_S and G^a_S are evaluated between the slices with $x = 0$ and $x = x_T$. These slices include all scatterers in our model, such that it

is sufficient to use these submatrices of the Green's functions in order to determine the conductance. Evaluating the Green's functions over a larger interval does not change the conductance, as the attached leads have a perfect transmission outside this scattering region.

5.4 Results for low filling

In order to obtain results characteristic for the continuum limit and to be able to neglect the lattice effects, we use a low filling factor $\nu \approx 1/25$ in the 2D leads, corresponding to a Fermi energy of $E_F = -3.57$ and a Fermi wave length of approximately $\lambda_F \approx 9.4$. Unless otherwise mentioned, the leads have a transverse width of $\mathcal{L}_y = 301$ sites, which is sufficiently large to obtain an effective 2D behavior in the vicinity of the nano-system. On the other hand, far away from the nano-system one should observe a crossover from the 2D-behavior to the 1D-behavior in the limit $r_T \gg \mathcal{L}_y$. Hereafter, we mainly consider the 2D regime with $r_T < \mathcal{L}_y$.

5.4.1 Conductance profile of the nano-system

First we analyze the conductance of the nano-system coupled to two perfect two-dimensional strips without the SGM tip ($V_T = 0$). For different interaction strengths $U = 0$, 0.5, 1, 1.5 and 2, we show the conductance $g_0(V_G)$ in Fig. 5.3 as function of the gate potential V_G.

The overall behavior of $g_0(V_G)$ is similar to the one with one-dimensional leads ($\mathcal{L}_y = 1$). For big or small gate potentials ($V_G > -1$ or $V_G < -4$), we obtain $g_0(V_G) \approx 0$, the system being completely reflecting.

For intermediate gate potential V_G, the conductance $g_0(V_G)$ becomes more important as shown in Fig. 5.3. The amplitude of the conductance grows for increasing U. However, the conductance g_0 cannot exceed $g_{\max} = 1$, as the two strips are coupled only via the internal nano-system hopping term t_d.

Analogous to the one-dimensional case the peak can be split into two distinct peaks by increasing U or t_d.

In order to favor the non-local effect, we restrict ourselves in this chapter to small values of t_d, for which the nano-system conductance develops only a single peak as a function of V_G. During the calculation of the tip-dependent values, we will adjust the gate potential V_G to the value V_* corresponding to the conductance maximum without the tip, since non-local effect is most important for $V_G \approx V^*$.

5.4.2 Effect of the tip upon the Hartree-Fock self-energies Σ^{HF}

The non-local effect is induced by the dependence of the Hartree-Fock corrections upon the tip position. In Fig. 5.4, the relative changes $\delta\Sigma^{\mathrm{F}}$ for the Fock self-energy

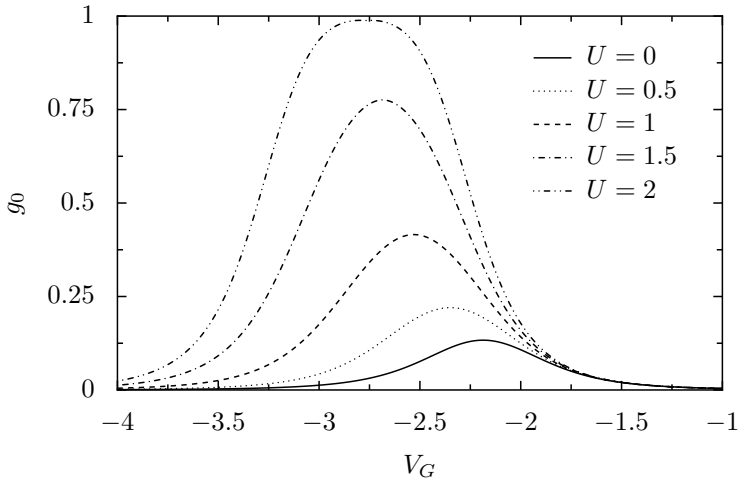

Figure 5.3: The conductance of the nano-system without tip: As function of the gate potential V_G, the conductance g_0 is shown for different interaction strengths $U = 0$, 0.5, 1, 1.5 and 2. The parameters are $t_d = 0.1$, $E_F = -3.57$ and $\mathcal{L}_y = 301$. As the hopping term t_d and the Fermi Energy E_F are small, only one peak exists for $g_0(V_G)$. For larger values of t_d, it will split into two distinct peaks, analogous to the situation with 1 dimensional leads.

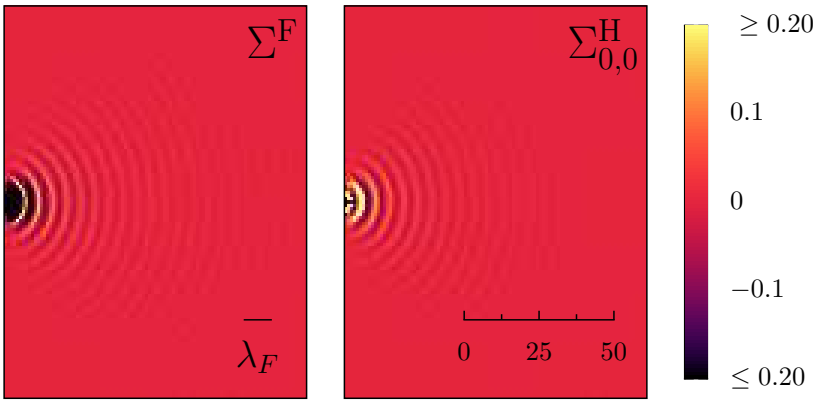

Figure 5.4: The influence of the tip on the Hartree-Fock self-energies of the nano-system: The relative change $\delta\Sigma^{\mathrm{HF}} = (\Sigma^{\mathrm{HF}} - \Sigma^{\mathrm{HF}_0})/\Sigma^{\mathrm{HF}}_0$ is shown as a function for the tip position (x_T, y_T). Σ^{HF}_0 refers to the unperturbed value without tip. The interaction strength is set to $U = 1.7$, the hopping term $t_d = 0.01$. Left image: The correction for the Fock term $\delta\Sigma^{\mathrm{F}}$, $\Sigma^{\mathrm{F}}_0 = -0.1204$. Right image: The correction for the Hartree-Term $\delta\Sigma^{\mathrm{H}}_{\mathbf{0}}$ on the left nano-system site $\mathbf{0}$, $\Sigma^{\mathrm{F}}_{\mathbf{0}\,0} = 0.5285$. The tip potential V_T is given by $V_T = -2$.

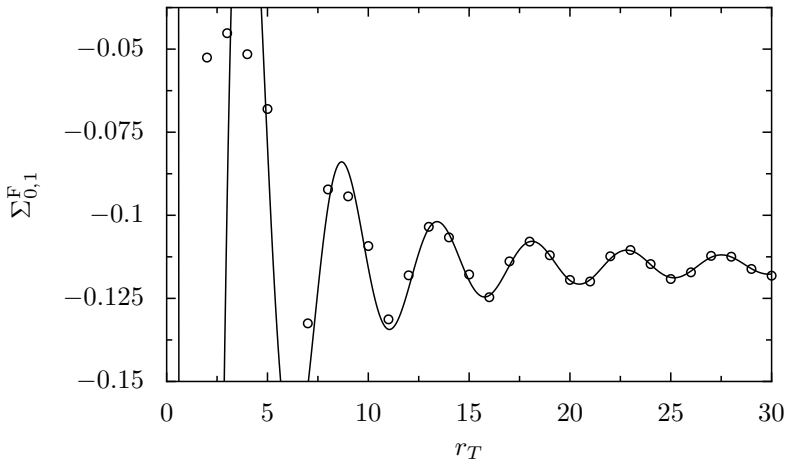

Figure 5.5: The Fock self-energy Σ^{F} as a function of the tip position r_T for $\theta_T = 0$. The parameters are $V_T = -2$, $U = 1.7$ and $t_d = 0.01$. The circles give the calculated Hartree-Fock-results, the line is an asymptotic fit with Eq. (5.11) with $\Sigma^{\mathrm{F}}_0 = -0.115$, $a = 2.379$ and $\delta = 0.765$.

(left part of Fig. 5.4) and for the Hartree self-energy $\delta\Sigma^{\mathrm{H}}_{\mathbf{0}}$ (right part of Fig. 5.4), are shown as function of the tip position. These relative changes are defined as

$$\delta\Sigma^{\mathrm{HF}} = \frac{\Sigma^{\mathrm{HF}} - \Sigma^{\mathrm{HF}}_0}{\Sigma^{\mathrm{HF}}_0} \tag{5.10}$$

where Σ^{HF} refers to the value with tip, while Σ^{HF}_0 is obtained without the tip. The images show two principal effects: First, both the Hartree and the Fock self-energies Σ^{H} and Σ^{H} exhibit oscillations of period $\lambda_F/2$. Second, these oscillations decay when the distance r_T between the nano-system and the tip is increased.

In order to analyze the decay of $\delta\Sigma^{\mathrm{HF}}(r_T, \theta_T)$ more precisely, we focus on the horizontal line with $\theta_T = 0$. The Fock self-energy $\Sigma^{\mathrm{F}}(r_T, 0)$ along this line is shown in Fig. 5.5 as a function of r_T. Apart from the first few sites ($r_T \lesssim 5$), the decay of $\delta\Sigma^{\mathrm{F}}$ can be described by a fit of the form

$$\delta\Sigma^{\mathrm{F}}(r_T, \theta_T = 0) = a\frac{\cos(2k_F r_T + \delta)}{r_T^2}\,. \tag{5.11}$$

This is the expected behavior for Friedel oscillations in a two-dimensional electron gas (see section 1.1.2). In Fig. 5.5, the data are asymptotically fitted by Eq. (5.11).

The asymptotic decay of the oscillations of the Hartree self-energies $\Sigma^{\mathrm{H}}_{\mathbf{0},\mathbf{1}}$ can be described by the same fitting function Eq. (5.11). When $\theta_T \neq 0$, the fit is only possible for small values of θ_T. For large angles $\theta_T \approx \pm\pi/2$, when the tip is positioned almost vertical to the nano-system, focussing effects become important, and the Hartree-Fock self-energies converge faster towards their asymptotic values.

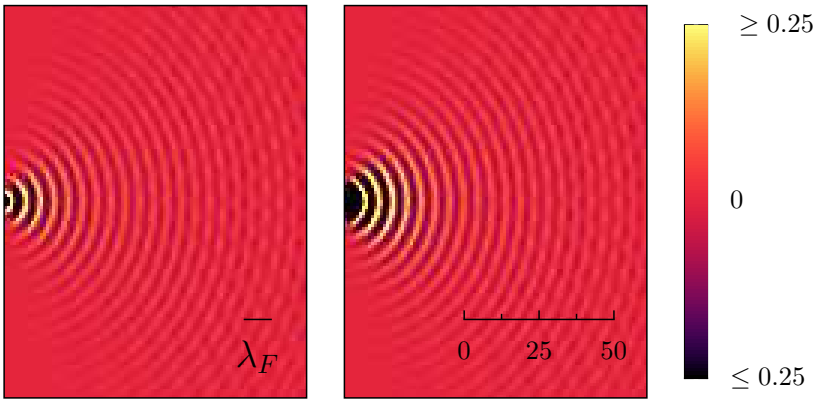

Figure 5.6: Influence of the tip on the total conductance g: The relative change $\delta g = (g - g_0)/g_0$ is shown as function for the tip position (x_T, y_T). g_0 gives the conductance without tip ($V_T = 0$). The hopping term is $t_d = 0.01$, the tip potential$V_T = -2$. Left part: The relative change δg for $U = 0$, the conductance without tip being given by $g_0(U = 0) = 0.00143$. Right part: The relative change δg for $U = 1.7$, the conductance without tip is given by $g_0(U = 1.7) = 0.1878$.

5.4.3 Effect of the tip upon the conductance g

In Fig. 5.6, the effect of the tip upon the conductance g through the model is given as a function of the tip position (x_T, y_T). The left image shows the relative correction $\delta g = (g - g_0)/g_0$ without interaction $U = 0$. One observes conductance oscillations with a period of half the Fermi wavelength $\lambda_F/2$, even without interaction inside the nano-system. These oscillations result from the interferences at the Fermi energy between the two independent scatterers (tip and nano-system) and decay polynomially when the distance r_T is increased. The precise decay function depends on the angle θ_T. Around $\theta_T \approx 0$, the oscillations of $\delta g(U = 0)$ decay asymptotically as $1/r_T$, while they decay much faster for large angles $\theta_T \approx \pm\pi/2$. For $\theta_T = 0$, the asymptotic fit

$$\delta g(U = 0, r_T) = \alpha \frac{\cos(k_F r_T - \delta)}{r_T} \tag{5.12}$$

is shown as a function of r_T in Fig. 5.7. One can see that the fit indeed reproduces the numerical data for $r_T \gtrsim 0.5$.

When the electron-electron interactions inside the nano-system are important, the effect of the tip upon the total conductance falls off in a different way. The resulting conductance g is shown in the right image in Fig. 5.6 for $U = 1.7$ as a function of the tip position. At a first glance, two effects of the interaction can be detected: First, the conductance g through the model is greatly enhanced. This is

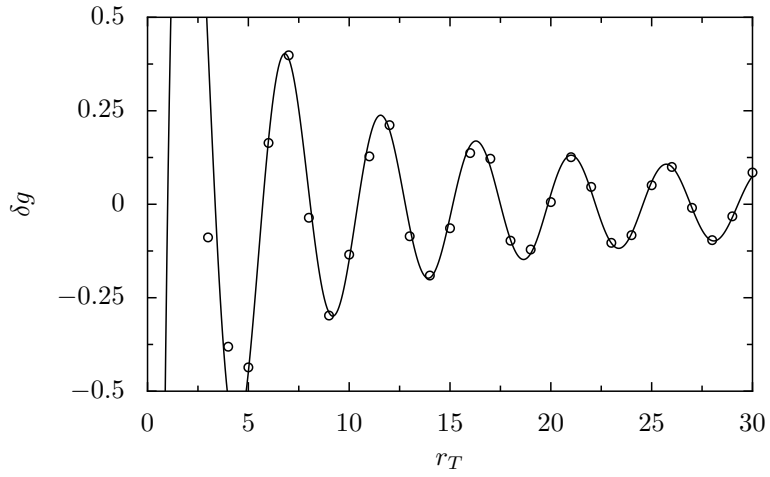

Figure 5.7: Decay of the effect of the tip upon the conductance without interaction ($U = 0$): Along the line $\theta_T = 0$, the tip-dependent oscillations of the conductance g decay as $1/r_T$. Using the same parameters as in the left image of Fig. 5.6, $\delta g(r_T, \theta_T = 0)$ is shown as a function of r_T (circles). The line gives the fit (5.12) with $\alpha = 0.11$ and $\delta = 1.2$.

an effect of the Exchange-correction, which increases the effective hopping term t_d inside the nano-system by Σ^{F}, thus increasing the effective transmission probability of the nano-system. Second, the conductance oscillations induced by the tip are much more pronounced in the vicinity of the nano-system. This results from the influence of the tip upon the Hartree-Fock self-energies Σ^{HF}, which was discussed in section 5.4.2. This influence decays as $1/r_T^2$, thus it is mainly important in the vicinity of the nano-system.

Let us study the influence of the tip upon g for $\theta_T = 0$. In order to describe the effects of the tip upon the conductance oscillations, we use the function

$$\frac{a_1 \cos(2k_F r_T + \delta_1)}{r_T} + \frac{a_2 \cos(2k_F r_T + \delta_2)}{r_T^2} \tag{5.13}$$

in order to fit the oscillations of the conductance $g(U \neq 0, r_T)$ as a function of the tip position r_T. The four adjustable fitting-parameters are a_1, a_2, δ_1 and δ_2.

This fit can be explained as follows:

- The $1/r_T$-term is used to describe the decay of the first part of the oscillations, which is created by the interferences at the Fermi energy between tip and nano-system. This term dominates the asymptotic behavior of the oscillations.
- The $1/r_T^2$-term is used to describe the non-local contribution, which exists due to the dependence of the Hartree-Fock self-energies upon the tip position.

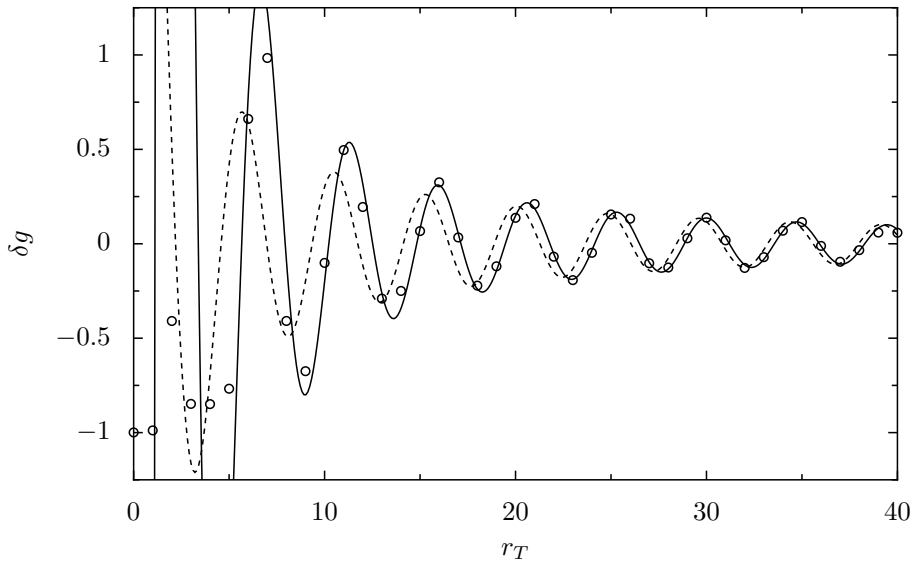

Figure 5.8: Decay of the effect of the tip upon the conductance g with $U = 1.7$. For $\theta_T = 0$, the relative change δg of the conductance is shown as a function of r_T. For large r_T, the conductance oscillations can be described by an $1/r_T$-decay (dashed line) as in the case without interaction. For small distances r_T, this fails, but an additional $1/r_T^2$-decay (solid line) is necessary to fit the data. The same parameters as in Fig. 5.6 are used. The fits are given by Eq. (5.13) with $a_1 = -0.676$ and $\delta_1 = 1.664$. The dashed line is calculated with $a_2 = 0$, the solid line by $a_2 = -7.605$ and $\delta_2 = 0.120$.

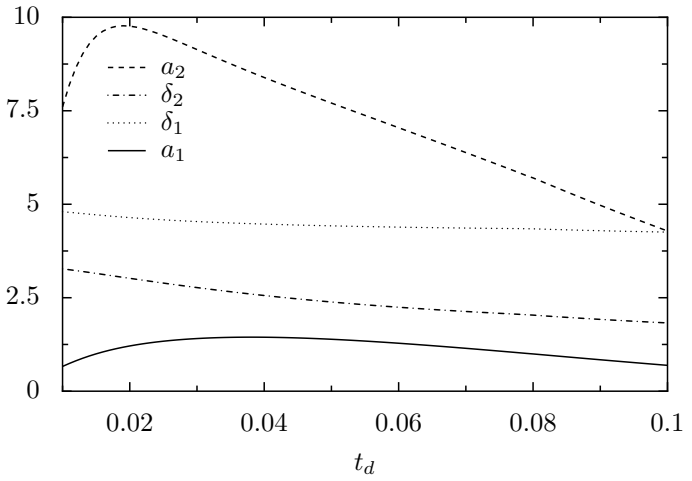

Figure 5.9: For a fixed interaction $U = 1.7$, the four fitting parameters of Eq. 5.13 are shown as function of the hopping term t_d: For large values of t_d, the $1/r_T^2$-term vanished (a_2 being given by the dashed line).

It results from the Friedel-oscillations induced by the tip, which change $\Sigma^{\mathrm{H}F}$. This term dominates for small r_T.

Both terms give oscillations of periodicity $\lambda_F/2$ which are reproduced by the factors $\cos(2k_F r_T + \delta_{1,2})$ in Eq. (5.13). In general, the two phase shifts δ_1 and δ_2 are different. Therefor, in addition to the crossover from the $1/r_T^2$-decay to the $1/r_T$-decay, a phase shift of the fringes in Figs. 5.6 and 5.8 can be observed when r_T is increased.

In Fig. 5.8, we show the effect of the tip upon g as a function of r_T for $\theta_T = 0$, in the presence of an interaction $U = 1.7$ inside the nano-system. The two lines show the fit (5.13) including the effect of the interaction (solid line), and the asymptotic fit obtained from setting $a_2 = 0$ (dashed line). For large values of r_T, the effect of the tip upon the Hartree-Fock parameters is negligible, and the dashed line reproduces the data, as without interaction. When the tip is put in the vicinity of the nano-system, a crossover happens from the $1/r_T$-decay (described by a_1 and δ_1) to the $1/r_T^2$-decay (described by a_2 and δ_2). For these small values of r_T the effect of the tip is mainly driven by Σ^{HF}, and not by the quantum interferences at the Fermi energy. Also the phase shift of the oscillations from δ_1 to δ_2 can be seen Fig. 5.8, which happens at the crossover from the $1/r_T$-decay to the $1/r_T^2$-decay.

To study the importance of the non-local effect in the SGM images, we study $g(r_T)$ as a function of the tip position when r_T for $\theta_T = 0$ for different values of t_d and U. For each set of values (t_d, U), we used Eq. (5.13) to fit the numerical data. The figures 5.9 and 5.10 show the dependence of the four fitting parameters a_1, a_2, δ_1 and δ_2 describing the $1/r_T$-decay and the $1/r_T^2$-decay.

In Fig. 5.9, these four parameters are shown as function of t_d for $U = 1.7$. One can

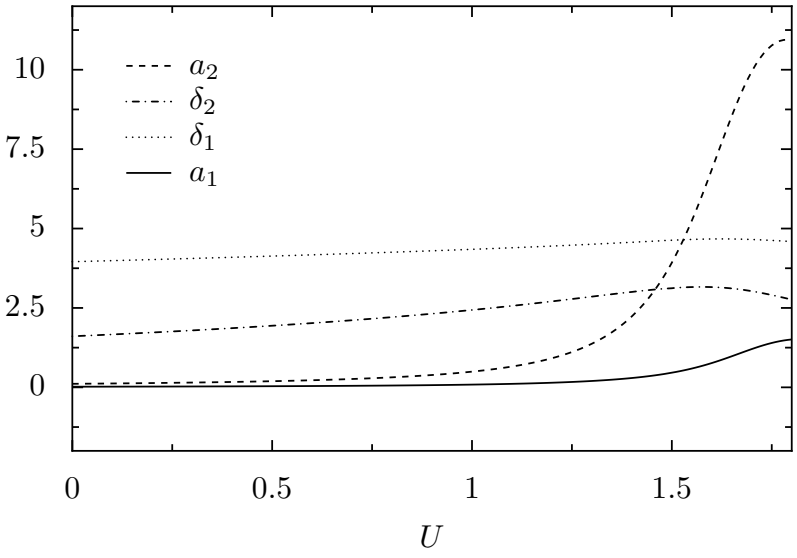

Figure 5.10: For a fixed hopping term $t_d = 0.02$, the four fitting parameters of Eq. 5.13 are shown as function of the interaction U: Around $U \approx 1.25$, the interaction effects become very important, a_2 (dashed line) growing much larger than a_1 (solid line).

clearly see that $a_2 > a_1$ for all values shown in Fig. 5.9. The biggest ratio of a_2/a_1 is located around $t_d = 0.02$. For this value of t_d, the importance of the non-local effect is maximal. For smaller values of t_d, we start to cut completely the two strips and $g = 0$. For larger values of t_d, the non-local effects and a_2/a_1 decrease, as discussed in chapter 2.

In Fig. 5.10, the four parameters are shown as function of U for $t_d = 0.02$. We can see that for small values of U, the non-local effects are almost negligible, whereas the parameter a_2, which shows the size of the non-local effect, exceeds a_1 when U is increased above $\gtrsim 1.25$.

5.5 Lattice effects and focussing

In the last section, we studied a small Fermi energy $E_F = -3.57$, which is low enough to having negligible lattice effects. If the Fermi energy is set to larger values, lattice effects become important, giving rise to completely different physics.

In this section, we study the influence of the lattice by changing the Fermi energy E_F. For larger values of E_F, strong focussing effects can take place.

In Fig. 5.11, the conductance of the nano-system as function of the gate voltage V_G is shown for different Fermi energies in the absence of the tip ($V_T = 0$). The figure shows the results for $U = 0$ and for a small hopping term of $t_d = 0.02$ inside the

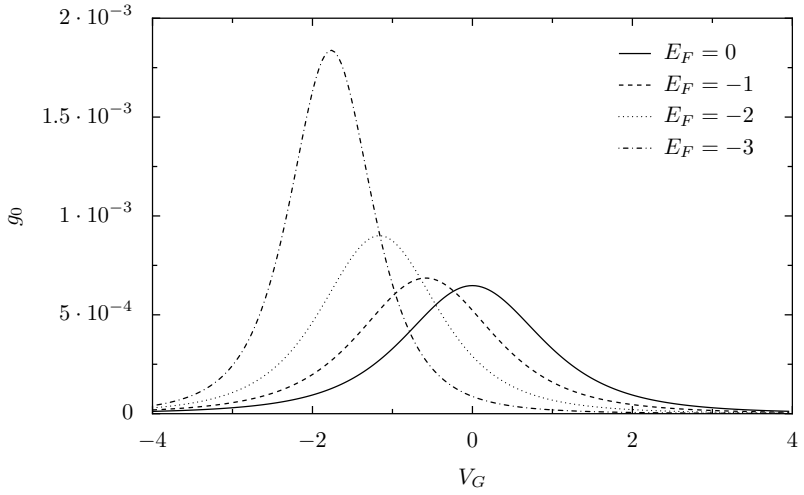

Figure 5.11: Conductance g for two-dimensional leads for different Fermi energies $E_F = -0$, $E_F = -1$, $E_F = -2$ and $E_F = -3$. The nano-system is given by $t_d = 0.02$ and $U = 0$. The leads have $\mathcal{L}_y = 101$ sites in transverse direction. The calculations are done without tip ($V_T = 0$) and without interaction inside the nano-system ($U = 0$).

nano-system. For this small hopping term, the conductance without tip $g_0(U = 0)$ is small for all Fermi energies shown in Fig. 5.11. Decreasing the Fermi energies results in an increased height of the conductance peak for $g_0(V_G)$.

For Fermi energies E_F larger than $E_F \approx -3$, the focussing effects become important and can be observed in the presence of the tip. This is shown in Figs. 5.12 and 5.13, where the relative change $\delta g(U = 0)$ of the conductance without interaction and the Fock self-energy $\Sigma^{\mathrm{F}}(U = 1.7)$ in the presence of local interactions have been calculated for increasing Fermi energies $E_F = -3$, -2, -1 and 0.

Fig. 5.12 shows the resulting conductance for $U = 0$ and strips with $\mathcal{L}_y = 101$ sites in transverse direction. For the low Fermi energy $E_F = -3$, the model has a similar behavior as shown in Fig. 5.6. However, when the Fermi energy is increased, the conductance starts to focus around $\theta_T \approx \pm\pi/2$. At half filling, the conductance depends only on the tip for $\theta_T = \pm\pi/2$. In other directions, the influence of the tip upon the conductance $g(U = 0)$ decays very quickly. However, if the tip is placed on one of the two diagonals $\theta_T = \pm\pi/2$, the conductance is almost independent of the distance r_T between the nano-system and the tip.

If the electron-electron interaction inside the nano-system becomes important, we obtain similar focussing effects for the non-local effect. We show in Fig. 5.13 the relative change $\delta\Sigma^{\mathrm{F}}$ of the Fock self-energy as a function of the tip position for $U = 1.7$. The Hartree self-energies Σ^{H} show a similar behavior as Σ^{F}. At the low Fermi energy $E_F = -3$, the oscillations are independent of θ_T, if θ_T is not too big.

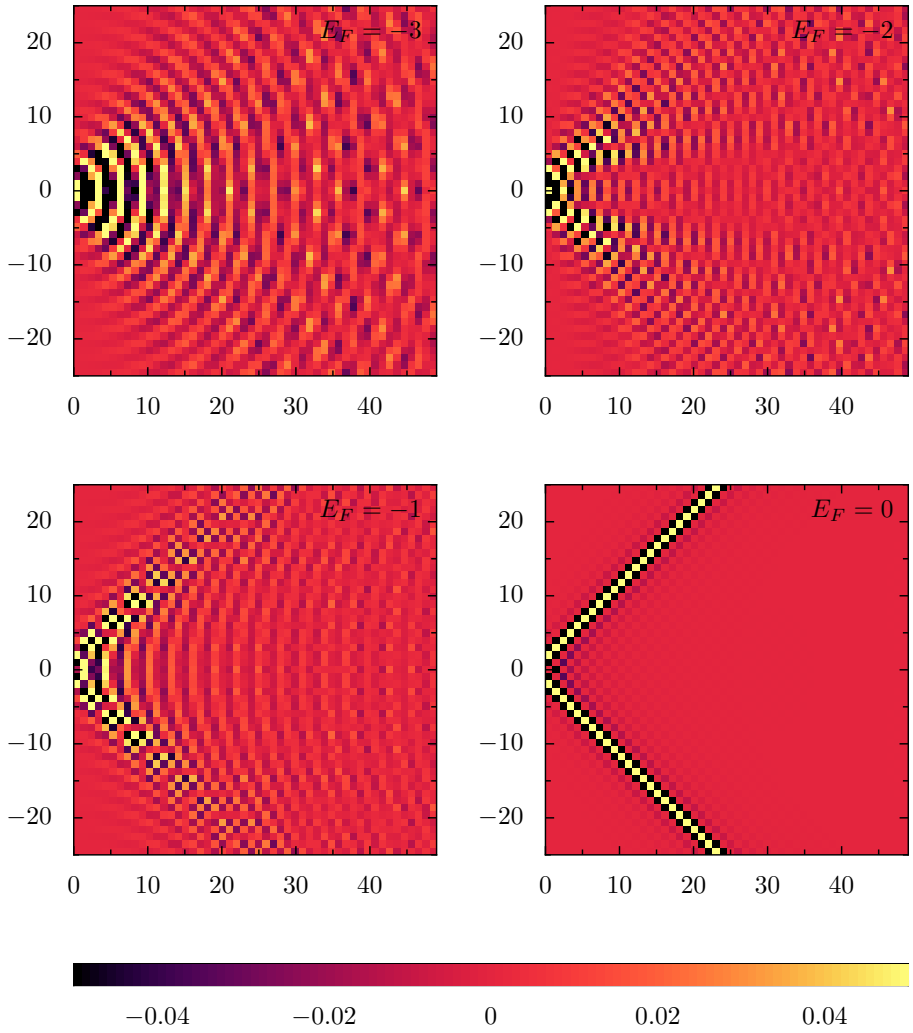

Figure 5.12: The relative change of the quantum conductance δg for $U = 0$. For larger Fermi energies, large focussing effects exists. The images show the relative change δg as a function of the tip position, with $\mathcal{L}_y = 101$, $t_d = 0.02$ and $V_T = +2$. The gate potential $V_G = V^*$ is adjusted to maximize the conductance without tip: $V_G(0) = -0.001$, $V_G(-1) = -0.58$, $V_G(-2) = -1.16$, $V_G(-3) = -1.77$. The conductance $g_0(E_F)$ without tip is obtained as $g_0(0) = 0.00065$, $g_0(-1) = 0.00069$, $g_0(-2) = 0.0009$, $g_0(-3) = 0.00184$.

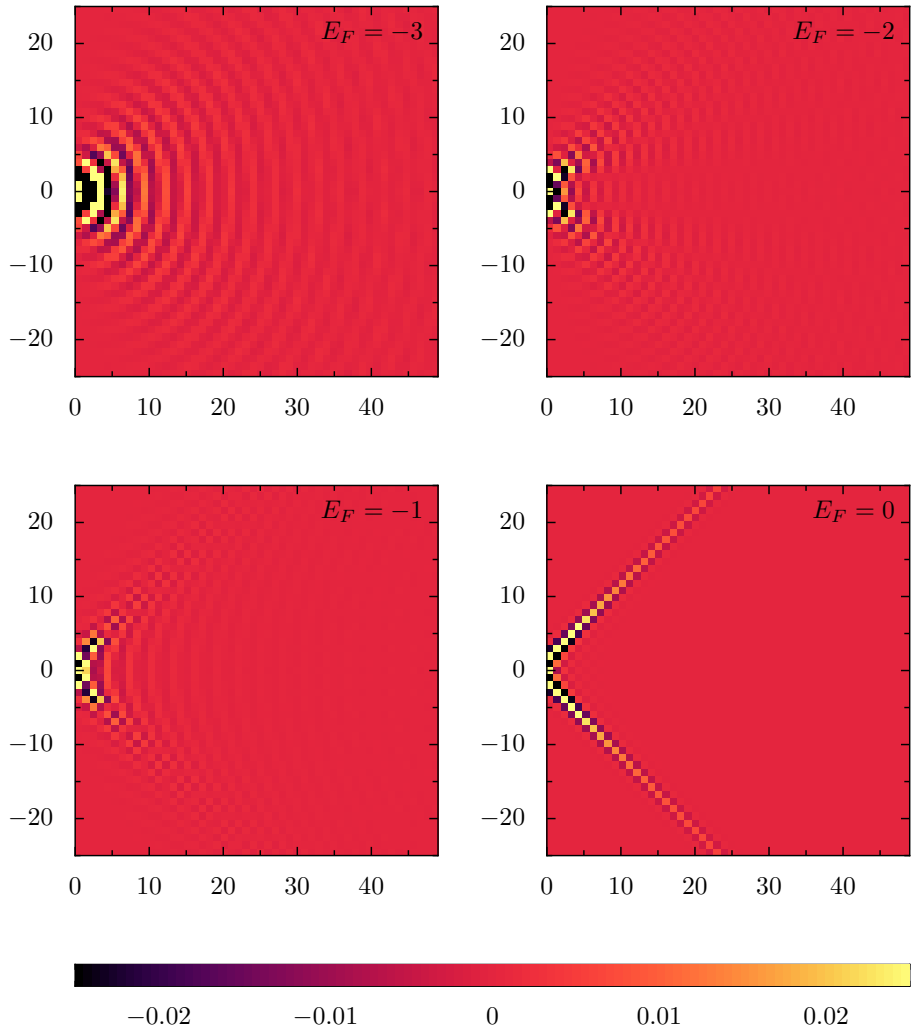

Figure 5.13: The Fock self-energy Σ^{F} with interaction ($U = 1.7$). For higher energies, large focussing effects exists as consequence of the finite lattice. The images show the relative change $\delta\Sigma^{\mathrm{F}}$ as a function of the tip position on the two-dimensional lead with $\mathcal{L}_y = 101$. The nano-system is modelled with $t_d = 0.02$, $V_G = V^*$ adjusted to maximize the conductance. We use a repulsive tip potential $V_T = +2$. The E_F-depending potentials $V_G(E_F)$ are given by: $V_G(0) = -0.001$, $V_G(-1) = -0.58$, $V_G(-2) = -1.16$, $V_G(-3) = -1.77$. The values without tip are given by $\Sigma^{\mathrm{F}}(0) = -0.0158$, $\Sigma^{\mathrm{F}}(-1) = -0.0166$, $\Sigma^{\mathrm{F}}(-2) = -0.0200$, $\Sigma^{\mathrm{F}}(-3) = -0.0359$.

For $E_F = 0$, the Hartree-Fock self-energies are only influenced by the tip when it is place on one of the diagonals $\theta_T \approx \pm\pi/2$.

However, the decay of $\delta\Sigma^{\mathrm{HF}}$ is different to the decay of $\delta g(U = 0)$ shown in Fig. 5.12. At $E_F = -3$, the correction of the Hartree-Fock self-energies decays as $1/r_T^2$. At half filling ($E_F = 0$), the decay along the diagonals can be described approximately by $1/r_T$, such that the behavior for $\theta_T \approx \pm\pi/2$ at half is similar to the one-dimensional case discussed at the beginning of this chapter: As the one-body contribution by the tip to the conductance g stays constant, the decay of δg is a pure many-body term and exists only in the presence of electron-electron interaction.

5.6 Towards improved models

In this work, we used a minimal model in order to describe the quantum point contact inside which the electrons interact. In this simple model, we showed the importance of the non-local contribution to the SGM images if the electron-electron interactions are important inside the quantum point contact. However, the nano-system used to model the QPC is not adequate to reproduce the properties of an real quantum point contact, its conductance is always smaller than $g_{\max} = 1$.

Moreover, the disorder and the interaction effects in the two-dimensional leads are ignored, as we assuming perfect leads without electron-electron disorder. Thus, the branched electron flow observed in the SGM images does not appear in our calculations.

These two restrictions can be overcome. A. Lassl *et al.* recently studied the transport properties of a single Quantum Point Contact [42], not including an external tip potential. They used a more realistic model to describe the QPC and included the spin degree of freedom. The interaction is taken into account at the Hartree-Fock level in their study. In these calculations, relevant featured of the 0.7-structure are reproduced at zero temperature. As A. Lassl *et al.* used the non-equilibrium Green's function approach and describe the leads by appropriate self-energies, it is possible to use a similar model to describe SGM-images, if one includes the potential of the AFM tip in the self-energies which describe the leads.

Another model was studied by G. Metalidis *et al.* [48]: they developed an algorithm which can be used to obtain the self-energy describing the lead as a function of the tip position very efficiently. With this approach, the branched electron flow observed in the experimental SGM images was reproduced theoretically [48]. However, G. Metalidis *et al.* ignored the electron-electron interactions in their setup.

In order to understand the importance of the non-local effect discussed in our work upon the SGM images, it will be necessary to combine these two approaches. Beside an increase of the numerical calculation time, this will introduce no fundamental problems.

In this section, we show a first step to a more realistic modelling of the QPC: The

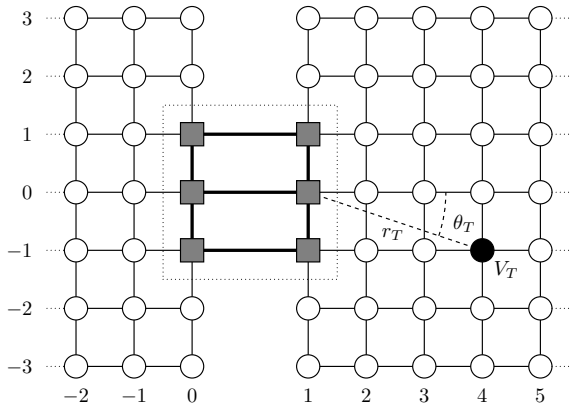

Figure 5.14: The model with $\mathcal{N}_y = 2N_y + 1 = 3$ links inside the nano-system. The hopping terms inside the nano-system are given by t_d (thick lines). Inside the nano-system, a repulsive nearest neighbour interaction U exists.

model is sketched in Fig. 5.14. Instead of one single link between the two strips, we use $\mathcal{N}_y = 2N_y + 1$ links to connect the left and the right strip. Nearest-neighbour interaction U acts between all the sites of this bigger nano-system with $2\mathcal{N}_y$ sites, indicated by squares in Fig. 5.14. The Hamiltonian of the nano-system is given by

$$\begin{aligned} H_S^{N_y} = &-t_d \left(\sum_{y=-N_y}^{N_y} c_{0,y}^\dagger c_{1,y} + \sum_{x=0}^{1} \sum_{y=-N_y}^{N_y-1} c_{x,y}^\dagger c_{x,y+1} + \text{H.c.} \right) \\ &+ U \left(\sum_{y=-N_y}^{N_y} n_{0,y} n_{1,y} + \sum_{x=0}^{1} \sum_{y=-N_y}^{N_y-1} n_{x,y} n_{x,y+1} \right) + V_G \sum_{x=0}^{1} \sum_{y=-N_y}^{N_y-1} n_{x,y}, \end{aligned} \tag{5.14}$$

where $\mathcal{N}_y = 2N_y + 1$ gives the number of links between the two strips.

When $\mathcal{N}_y > 1$, one changes

- The self-energies $\sigma_{L,R}$ describing the influence of the strips upon the nano-system are $\mathcal{N}_y \times \mathcal{N}_y$ matrices (instead of 1×1 matrices).
- The model has $2\mathcal{N}_y$ Hartree terms and $3\mathcal{N}_y - 2$ Fock-terms, which are defined by $5\mathcal{N}_y - 2$ coupled equations (instead of 3 equations).

Because of this, the numerical calculations become much heavier.

This model allows us to obtain a conductance $g > 1$, nevertheless the conductance is limited to $g_{\max} = \mathcal{N}_y$.

Fig. 5.15 shows the relative change of the conductance g, when the tip is scanned over the right strip. The size of the nano-system is indicated by the grey box in the images. Both the case with interaction $U = 1$ and without interaction $U = 0$ are

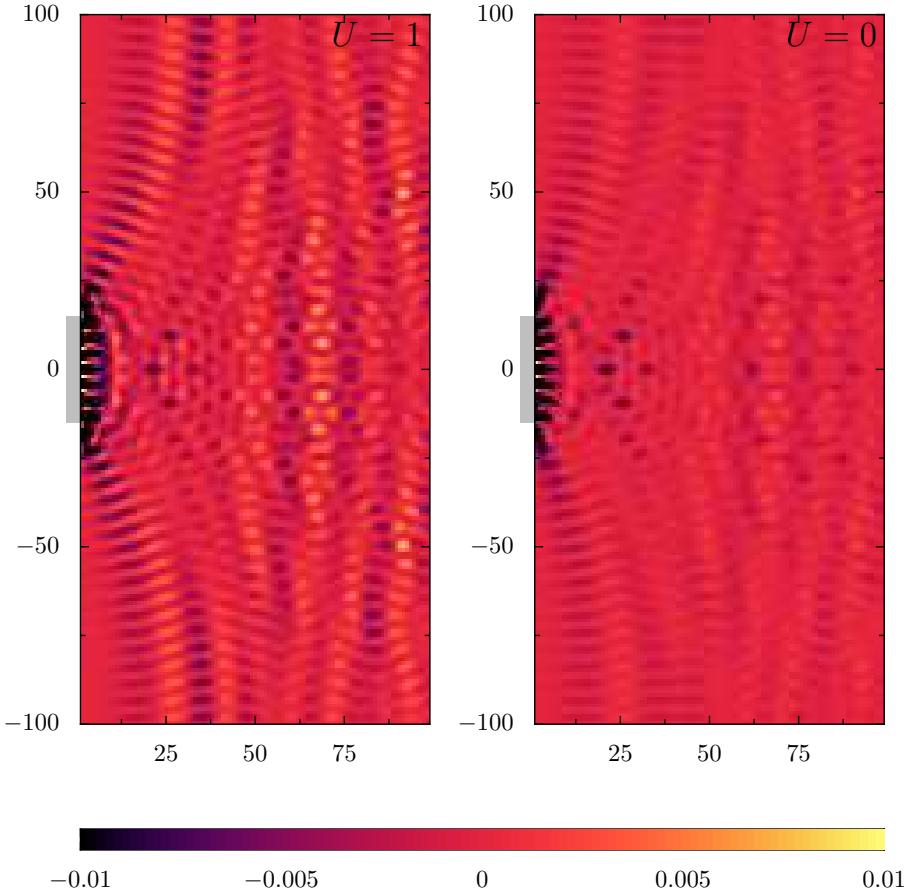

Figure 5.15: The relative change δg of the quantum conductance g for a nano-system with $N = 31$ links connecting the two strips as shown in Fig. 5.14. The transverse size is given by $\mathcal{L}_y = 201$. The other parameters are set to $E_F = -3.57$, $td = 0.02$, $V_T = 2$. The images are calculated for interaction strengths $U = 0$ and $U = 1$, $V_G(U) = V^*(U)$ maximizing the conductance g_0 without tip.

shown in the left and the right part of Fig. 5.15. As it was the case for $\mathcal{N}_y = 1$, the interaction enhances both the conductance and the relative size of the conductance oscillations for different tip positions.

These are preliminary results which have to be studied in a future work.

5.7 Conclusion and outlook

In this chapter, we have shown that images made by scanning gate microscopy contain informations about the strength of electron-electron interaction inside a local nano-system. During the study, disorder and electron-electron interactions in the strips have been neglected. At zero temperature, a $1/r_T^2$-decay of the conductance oscillations around the nano-structure can be observed in the SGM images, if the electron-electron interaction is important inside the nano-system. The ratio of the amplitudes a_2/a_1 and the difference between the phase shifts $\delta_2 - \delta_1$ which appear in the fit function Eq. (5.13) allow to determine the value of U which acts inside the nano-system.

Many parameters contribute to the amplitude of the $1/r_T^2$-decay. In order to obtain a big signal, and to be able to detect the $1/r_T^2$-decay, the following conditions have to be fulfilled: Of course, the interaction U inside the nano-system has to be important compared to the other energy scales influencing the physics inside the nano-system (large r_s factor). The oscillations of the density and the correlation function, which are created by the charged tip, should be large. This can be achieved by using a large tip potential V_T and placing the tip in the vicinity of the quantum point contact. To allow these oscillations to enter into the nano-system, it has to be strongly coupled to the lead. Finally, the effect depends on the fact that these oscillations change the internal state of the nano-system. This has been already discussed in chapter 2.

In order to extract informations about the interaction strength, it is necessary to compare the $1/r_T$-decay and the $1/r_T^2$-decay. Thus the tip should be in the vicinity of the nano-system. In real experiments, this creates an additional difficulty, as the gate electrodes needed to create the studied nano-structure are placed on top of the sample very often, thus preventing to move the AFM tip very close to the nano-structure. But it is also possible to create samples with a clean surface, using wet etching to create trenches defining the structure [4]. In these samples it is possible to make SGM images of the tip being placed on top of the nano-structure.

In real measurements, the leads will have a disordered potential, which changes also the $1/r_T$ decay of the oscillations even in the absence of interactions. In the experimental images [69, 70], the electrons form narrow, branched strands. Topinka *et al.* explain these branches by focussing of the electron paths by ripples in the disorder potential.

Using more realistic models of a quantum point contact it can be shown that the

different transmission modes are focussed into different directions [77]. It will be interesting, to make SGM images in the vicinity of a quantum point contact (QPC) for different gate potentials: Between the conductance plateaus, the internal state of the QPC is more sensitive to the positioning of the tip. For an almost closed quantum point contact, an anomaly in the conductance curve $g(V_G)$ appears around the conductance value $g \approx 0.7$. This is the so-called "0.7-anomaly" [68]. It is explained very often as an interaction-induced effect [66]. This would indicate that electron-electron interactions are important inside the QPC, leading to important non-local effects upon the conductance. It will be very interesting to study the non-local effect induced by the tip upon an QPC which is biased on the 0.7-anomaly.

6 Summary and Outlook

In this thesis we have studied the influence of electron-electron interaction upon the quantum conductance of spinless nano-structures. We ignored the electron-electron interactions in the leads (assuming a small r_S factor) and took the interactions into account in the nano-structure only. We used Landauer-Büttiker conductance formula to obtain the conductance at zero temperature. The scattering properties of the interacting region at a Fermi energy E_F can be described by an effective one-body scattering matrix [50]. If the interactions become important, this effective scattering matrix becomes non-local, depending on the scattering properties of the attached leads: If an external scatterer is introduced in the vicinity of the nano-structure into one of the leads, the scattering matrix describing the interacting structure will be changed by the second scatterer. In this thesis, we studied this effect both numerically and analytically, using the Hartree-Fock approximation to describe the interactions.

Hartree-Fock theory allows to understand the non-local effect: The external scatterer induces Friedel oscillations of the density $\langle c_x^\dagger c_x \rangle$ and of the correlation function $\langle c_{x+1}^\dagger c_x \rangle$ inside the nano-structure. These oscillations change the Hartree- and Fock-correction induced by interactions in the nano-structure.

In chapter 2, we introduced the nano-system used as interacting nano-structure. We have seen that although we are using a very simple model, it shows already quite complex physics: as a function of its parameters different regimes can emerge. A central parameter is the hopping term t_d used to coupled the two sites of nano-system. While the effective scattering matrix is independent of external scatterers for large t_d, a small t_d can make the effective transmission of the nano-system highly sensitive to external scatterers. We studied the validity of Hartree-Fock calculations for this problem. In section 2.4.1 it is shown that Hartree-Fock works remarkably well to describe the conductance of such a small nano-system, when $t_d = 1$. However in the limit $t_d \to 0$, an orbital Kondo effect can appear in our model due to inversion symmetry, and the validity of the Hartree-Fock approximation breaks down.

In chapter 3 we studied two identical nano-systems with internal electron-electron interactions connected by an non-interacting lead of length L_C. For this model, it is possible to give the analytic expression for the expectation values $\langle c_x^\dagger c_x \rangle$ and $\langle c_{x+1}^\dagger c_x \rangle$ appearing in the Hartree-Fock equations. When L_C is not too large, the non-local correction to the total conductance can be important. We show that for finite temperature this correction is suppressed when $L_C > L_T$, L_T being the thermal length. Comparing the results with exact DMRG results, we show that the

non-local correction upon the conductance is described correctly by Hartree-Fock, even for relatively large interaction strengths. However, the importance of the non-local effect is underestimated by the Hartree-Fock approximation. This effective coupling between effective scattering matrices for spinless particles is reminiscent of the RKKY-interaction, which couples local magnetic moments via the conduction electrons.

In order to observe this non-local contribution to the conductance it is not necessary to have electron-electron interactions inside both scatterers. The oscillations of $\langle c_x^\dagger c_x \rangle$ and $\langle c_{x+1}^\dagger c_x \rangle$ which influence the transmission properties of an scatterer with local electron interactions, can also be induced by a pure one-body scatterer. In chapter 4 we replaced the second scatterer by an attached ring, threaded by a magnetic flux Φ, which induces flux-dependent oscillations in the lead. In this setup, the dependence of the total conductance on the flux Φ is due to two effects: First, the scattering properties of the Aharonov-Bohm scatterer depend on Φ. Second, if the electrons interact inside the nano-system, the scattering properties of the nano-system depend also on Φ. By adjusting the geometry of the attached ring it is possible to suppress the first effect at the Fermi energy, such that the remaining flux-dependence of the total conductance is a pure many-body effect.

In chapter 5, we extend our study to a two-dimensional model. For two-dimensional models, it is much more justified to neglect the electron-electron interactions in the leads than in the one-dimensional case, where a Luttinger liquid is formed. Using the same nano-system as studied in the previous chapters, we now contact it to two-dimensional leads. The external scatterer is given by a local potential V_T at a distance r_T from the nano-system, which can be moved in the leads. The conductance through the two-dimensional model is measured as a function of the position of V_T. This is a simple model for a measurement made by Scanning Gate Microscopy [69]. The conductance obtained by our model shows fringes spaced by half the Fermi wave length λ_F, which decrease as r_T is increased. Analyzing the images, we observe two different length-dependences: Without interaction the conductance decays as $1/r_T$. A local interaction inside the nano-system adds an additional $1/r_T^2$ decay, which can be seen for small r_T. These different decays provide a method to detect the importance of the interaction inside the nano-system.

The two-dimensional SGM setup being described by a simple model in chapter 5, a more realistic analysis will be interesting. In a real experiment, the interacting nano-system could be given by an almost closed Quantum Point Contact (QPC). Having a low electron density inside the QPC, the electron-electron interactions are important, especially if the QPC is biased at the 0.7 structure. Using the non-equilibrium Green's function technique, a more realistic model of a quantum point contact has been studied by A. Lassl *et al.* [42]. Taking into account the electron-electron interaction inside the quantum point contact at the Hartree-Fock level, they reproduced the relevant features of the 0.7 structure.

G. Metalidis *et al.* [48] developed a recursive Green's function formalism for non-

interacting models to efficiently simulate images made by Scanning Gate Microscopy, including disorder in the leads. Using this technique, they obtained images similar to the experimentally obtained SGM images. The disordered leads allow to reproduce the branched electron flow observed in [70].

It will be interesting to combine these two approaches in order to study Scanning Gate Microscopy measurements of the electron flow through a quantum point contact with local electron-electron interaction inside the QPC. If these numerical calculations show that it is possible to detect the effect of the non-local contribution upon the quantum conductance of the SGM-setup, it can be tried to detect the non-local effect in experimental images made by Scanning Gate Microscopy.

7 Publications

1. Yoichi Asada, Axel Freyn and Jean-Louis Pichard, "Conductance of nano-systems with interactions coupled via conduction electrons: effect of indirect exchange interactions", *Eur. Phys. J. B*, **2006**, 53, 109-120.

2. Axel Freyn and Jean-Louis Pichard, "Effect of Measurement Probes upon the Conductance of an Interacting Nanosystem: Detection of an Attached Ring by Nonlocal Many-Body Effects", *Phys. Rev. Lett.*, **2007**, 98, 186401-186404.

3. Axel Freyn and Jean-Louis Pichard, "Effect of flux-dependent Friedel oscillations upon the effective transmission of an interacting nano-system", *Eur. Phys. J. B*, **2007**, 58, 279-290.

4. Axel Freyn, Ioannis Kleftogiannis and Jean-Louis Pichard, "Scanning Gate Microscopy of a Nanostructure Where Electrons Interact", *Phys. Rev. Lett.*, **2008**, 100, 226802.

5. Dietmar Weinmann, Rodolfo Jalabert, Axel Freyn, Gert-Ludwig Ingold and Jean-Louis Pichard, "Detection of interaction-induced nonlocal effects using perfectly transmitting nanostructures", *unpublished*, **2008**, arXiv:0803.2780

Bibliography

[1] M. Abramowitz and I. A. Stegun, editors. *Handbook of mathematical functions, with formulas, graphs, and mathematical tables*. Dover Publications, 1965.

[2] Y. Aharonov and D. Bohm. Further Considerations on Electromagnetic Potentials in the Quantum Theory. *Phys. Rev.*, 123:1511 – 1524, 1961.

[3] P. W. Anderson. Localized Magnetic States in Metals. *Phys. Rev.*, 124(1):41 – 53, October 1961.

[4] N. Aoki, A. Burke, C. R. da Cunha, R. Akis, D. K. Ferry, and Y. Ochiai. Study of quantum point contact via low temperature scanning gate microscopy. *Journal of Physics: Conference Series*, 38:79–82, 2006.

[5] Y. Asada. Numerical calculation of the landauer conductance through an interacting electron system in the hartree-fock approximation. arxiv:cond-mat/0603147v1, March 2006.

[6] Y. Asada, A. Freyn, and J.-L. Pichard. Conductance of nano-systems with interactions coupled via conduction electrons: effect of indirect exchange interactions. *Eur. Phys. J. B*, 53(1):109–120, September 2006.

[7] N. W. Ashcroft and N. D. Mermin. *Solid State Physics*. Brooks Cole, 1976.

[8] A. Bachtold, M. S. Fuhrer, S. Plyasunov, M. Forero, E. H. Anderson, A. Zettl, and P. L. McEuen. Scanned probe microscopy of electronic transport in carbon nanotubes. *Phys. Rev. Lett.*, 84(26):6082–6085, June 2000.

[9] J. Bardeen, L. Cooper, and J. Schrieffer. Theory of Superconductivity. *Phys. Rev.*, 108(5):1175–1204, 1957.

[10] G. Binnig and H. Rohrer. Scanning tunneling microscopy. *IBM J. Res. Dev.*, 30(4):355, 1986.

[11] G. Binnig and H. Rohrer. Scanning tunneling microscopy. *Rev. Mod. Phys.*, 59(3):615–625, 1987.

[12] A. Blandin and J. Friedel. Propriétés magnétiques des alliages dilués. Interactions magnétiques et antiferromagnétisme dans les alliages du type métal noble-métal de transition. *J. Phys. Rad.*, 20:160–168, 1959.

[13] H. Bruus, V. V. Cheianov, and K. Flensberg. The anomalous 0.5 and 0.7 conductance plateaus in quantum point contacts. *Physica E*, 10:97–102, May 2001.

[14] R. Bulla, T. A. Costi, and T. Pruschke. Numerical renormalization group method for quantum impurity systems. *Rev. Mod. Phys.*, 80:395, 2008.

[15] M. Büttiker. Four-Terminal Phase-Coherent Conductance. *Phys. Rev. Lett.*, 57(14):1761–1764, 1986.

[16] M. Büttiker, Y. Imry, and M. Y. Azbel. Quantum oscillations in one-dimensional normal-metal rings. *Phys. Rev. A*, 30(4):1982–1989, October 1984.

[17] M. Büttiker, Y. Imry, R. Landauer, and S. Pinhas. Generalized many-channel conductance formula with application to small rings. *Phys. Rev. B*, 31(10):6207 – 6215, May 1985.

[18] D. Calvetti, G. H. Golub, W. B. Gragg, and L. Reichel. Computation of Gauss-Kronrod quadrature rules. *Math. Comp.*, 69(231):1035–1052, February 2000.

[19] P. S. Cornaglia and C. A. Balseiro. On the magnetic nature of quantum point contacts. *Europhysics Letters*, 67(4):634–640, August 2004.

[20] C. R. da Cunha, N. Aoki, T. Morimoto, Y. Ochiai, R. Akis, and D. K. Ferry. Imaging of quantum interference patterns within a quantum point contact. *Appl. Phys. Lett.*, 89:242109, December 2006.

[21] S. Datta. *Electronic Transport in Mesoscopic Systems*. Cambridge Studies in Semiconductor Physics and Microelectronic Engineering. Cambridge University Press, 1997.

[22] H.-L. Engquist and P. W. Anderson. Definition and measurement of the electrical and thermal resistances. *Phys. Rev. B*, 24(2):1151 – 1154, July 1981.

[23] M. A. Eriksson, R. G. Beck, M. Topinka, J. A. Katine, R. M. Westervelt, K. L. Campman, and A. C. Gossard. Cryogenic scanning probe characterization of semiconductor nanostructures. *Appl. Phys. Lett.*, 69(5):671, July 1996.

[24] J. Favand and F. Mila. Comparison of tunneling through molecules with mott-hubbard and with dimerization gaps. *Eur. Phys. J. B*, 2(3):293–299, Mai 1998.

[25] D. K. Ferry and S. M. Goodnick. *Transport in Nanostructures*. Cambridge studies in semiconductor physics and microelectronic engineering. Cambridge University Press, 1997.

[26] A. L. Fetter and J. D. Walecka. *Quantum Theory of Many-Particle Systems*. Dover Publications, 2003.

[27] B. Hackens, F. Martins, T. Ouisse, H. Sellier, S. Bollaert, X. Wallart, A. Cappy, J. Chevrier, V. Bayot, and S. Huant. Imaging and controlling electron transport inside a quantum ring. *Nature Physics*, 2(12):826 – 830, December 2006.

[28] A. C. Hewson. *The Kondo Problem to Heavy Fermions*. Cambridge Studies in Magnetism. Cambridge University Press, 1997.

[29] K. Hirose, Y. Meir, and N. S. Wingreen. Local moment formation in quantum point contacts. *Phys. Rev. Lett.*, 90(2):026804, January 2003.

[30] W. Hofstetter and G. Zarand. Singlet–triplet transition in lateral quantum dots: A numerical renormalization group study. *Phys. Rev. B*, 69(23):235301, June 2004.

[31] Y. Imry. *Introduction to Mesoscopic Physics*. Oxford University Press, 1997.

[32] Y. Imry and R. Landauer. Conductance viewed as transmission. *Rev. Mod. Phys.*, 71(2):S306–S312, Mar 1999.

[33] M. P. Jura, M. A. Topinka, L. Urban, A. Yazdani, H. Shtrikman, L. N. Pfeiffer, K. W. West, and D. Goldhaber-Gordon. Unexpected features of branched flow through high-mobility two-dimensional electron gases. *Nature Physics*, 3(12):841 – 845, December 2007.

[34] M. A. Kastner. The single-electron transistor. *Rev. Mod. Phys.*, 64(3):849, July 1992.

[35] T. Kasuya. A theory of metallic ferro- and antiferromagnetism on Zener's model. *Prog. Theor. Phys.*, 16(1):45–57, 1956.

[36] C. Kittel. *Quantum Theory of Solids*. Wiley, 1987.

[37] J. Kondo. Resistance minimum in dilute magnetic alloys. *Progress of Theoretical Physics*, 32(1):37–49, 1964.

[38] H. R. Krishna-murthy, J. W. Wilkins, and K. G. Wilson. Renormalization-group approach to the anderson model of dilute magnetic alloys. i. static properties for the symmetric case. *Phys. Rev. B*, 21(3):1003 – 1043, 1980.

[39] H. R. Krishna-murthy, J. W. Wilkins, and K. G. Wilson. Renormalization-group approach to the anderson model of dilute magnetic alloys. ii. static properties for the asymmetric case. *Phys. Rev. B*, 21(3):1044 – 1083, 1980.

[40] R. Landauer. Spatial variation of currents and fields due to localized scatterers in metallic conduction. *IBM J. Res. Dev.*, 1(3):223, July 1957.

[41] R. Landauer. Electrical resistance of disordered one-dimensional lattices. *Phil. Mag.*, 21(172):863–687, april 1970.

[42] A. Lassl, P. Schlagheck, and K. Richter. Effects of short-range interactions on transport through quantum point contacts: A numerical approach. *Phys. Rev. B*, 75:045346, January 2007.

[43] B. J. LeRoy, A. C. Bleszynski, K. E. Aidala, R. M. Westervelt, A. Kalben, E. J. Heller, S. E. J. Shaw, K. D. Maranowski, and A. C. Gossard. Imaging electron interferometer. *Phys. Rev. Lett.*, 94:126801, April 2005.

[44] A. MacKinnon. The conductivity of the one-dimensional disordered anderson model: a new numerical method. *J. Phys. C*, 13(35):L1031–L1034, December 1980.

[45] F. Martins, B. Hackens, M. G. Pala, T. Ouisse, H. Sellier, X. Wallart, S. Bollaert, A. Cappy, J. Chevrier, V. Bayot, and S. Huant. Imaging electron wave functions inside open quantum rings. *Phys. Rev. Lett.*, 99:136807, 2007.

[46] V. Meden and U. Schollwöck. Conductance of interacting nanowires. *Phys. Rev. B*, 67(19):193303, May 2003.

[47] Y. Meir, K. Hirose, and N. S. Wingreen. Kondo model for the "0.7 anomaly" in transport through a quantum point contact. *Phys. Rev. Lett.*, 89(19):196802, November 2002.

[48] G. Metalidis and P. Bruno. Green's function technique for studying electron flow in two-dimensional mesoscopic samples. *Phys. Rev. B*, 72:235304, December 2005.

[49] R. A. Molina, P. Schmitteckert, D. Weinmann, R. A. Jalabert, G.-L. Ingold, and J.-L. Pichard. Residual conductance of correlated one-dimensional nanosystems: A numerical approach. *Eur. Phys. J. B*, 39(1):107, Jun 2004.

[50] R. A. Molina, D. Weinmann, R. A. Jalabert, G.-L. Ingold, and J.-L. Pichard. Conductance through a one-dimensional correlated system: Relation to persistent currents and the role of the contacts. *Phys. Rev. B*, 67(23):235306, Jun 2003.

[51] R. A. Molina, D. Weinmann, and J.-L. Pichard. Length-dependent oscillations of the conductance through atomic chains: The importance of electronic correlations. *Europhys. Lett.*, 67(1):96–102, July 2004.

[52] R. A. Molina, D. Weinmann, and J.-L. Pichard. Interacting electron systems between fermi leads: effective one-body transmissions and correlation clouds. *Eur. Phys. J. B*, 48(2):243–247, November 2005.

[53] J. Moré, B. S. Garbow, and K. E. Hillstrom. User guide for minpack-1. Technical report, Argonne National Laboratory Report, 1980.

[54] A. Oguri and A. C. Hewson. NRG approach to the transport through a finite hubbard chain connected to reservoirs. *J. Phys. Soc. Jpn.*, 74(3):988–996, March 2005.

[55] M. G. Pala, B. Hackens, F. Martins, H. Sellier, V. Bayot, and S. Huant. Local density of states in mesoscopic samples from scanning gate microscopy. *Phys. Rev. B*, 77:125310, 2008.

[56] I. Peschel, editor. *Density-Matrix Renormalization: A new Numerical Method in Physics*, volume 528 of *Lecture notes in physics*. Springer Berlin Heidelberg, 1999.

[57] A. Pioda, S. Kičin, T. Ihn, M. Sigrist, A. Fuhrer, K. Ensslin, A. Weichselbaum, S. E. Ulloa, M. Reinwald, and W. Wegscheider. Spatially resolved manipulation of single electrons in quantum dots using a scanned probe. *Phys. Rev. Lett.*, 93(21):216801, Nov 2004.

[58] W. H. Press, B. P. Flannery, S. A. Teukolsky, and W. T. Vetterling. *Numerical Recipes in FORTRAN 77: The Art of Scientific Computing*. Cambridge University Press, September 1992.

[59] D. Reilly, Y. Zhanga, and L. DiCarloa. Phenomenology of the 0.7 conductance feature. *Physica E*, 34:27–30, August 2006.

[60] D. J. Reilly. Phenomenological model for the 0.7 conductance feature in quantum wires. *Phys. Rev. B*, 72:033309, 2005.

[61] T. Rejec and A. Ramšak. Formulas for zero-temperature conductance through a region with interaction. *Phys. Rev. B*, 68(3):035342, July 2003.

[62] M. A. Ruderman and C. Kittel. Indirect exchange coupling of nuclear magnetic moments by conduction electrons. *Phys. Rev.*, 96:99 – 102, 1954.

[63] S. Sanvito, C. J. Lambert, J. H. Jefferson, and A. M. Bratkovsky. General green's-function formalism for transport calculations with spd hamiltonians and giant magnetoresistance in co- and ni-based magnetic multilayers. *Phys. Rev. B*, 59:11936 – 11948, August 1999.

[64] L. Schweitzer, B. Kramer, and A. MacKinnon. Magnetic field and electron states in two-dimensional disordered systems. *J. Phys. C: Solid State Phys.*, 17(23):4111–4125, August 1984.

[65] W. J. Skocpol, P. M. Mankiewich, R. E. Howard, L. D. Jackel, and D. M. Tennant. Nonlocal potential measurements of quantum conductors. *Phys. Rev. Lett.*, 58(22):2347 – 2350, June 1987.

[66] C. Sloggett, A. I. Milstein, and O. P. Sushkov. Correlated electron current and temperature dependence of the conductance of a quantum point contact. *Eur. Phys. J. B*, 61(4):427–432, February 2008.

[67] O. P. Sushkov. Conductance anomalies in a one-dimensional quantum contact. *Phys. Rev. B*, 64(15):155319, Sep 2001.

[68] K. J. Thomas, J. T. Nicholls, M. Y. Simmons, M. Pepper, D. R. Mace, and D. A. Ritchie. Possible spin polarization in a one-dimensional electron gas. *Phys. Rev. Lett.*, 77(1):135–138, 1996.

[69] M. A. Topinka, B. J. LeRoy, S. E. J. Shaw, E. J. Heller, R. M. Westervelt, K. D. Maranowski, and A. C. Gossard. Imaging Coherent Electron Flow from a Quantum Point Contact. *Science*, 289(5488):2323–2326, 2000.

[70] M. A. Topinka, B. J. LeRoy, R. M. Westervelt, S. E. J. Shaw, R. Fleischmann, E. J. Heller, K. D. Maranowski, and A. C. Gossard. Coherent branched flow in a two-dimensional electron gas. *Nature*, 410:183–186, March 2001.

[71] B. J. van Wees, H. van Houten, C. W. J. Beenakker, J. G. Williamson, L. P. Kouwenhoven, D. van der Marel, and C. T. Foxon. Quantized conductance of point contacts in a two-dimensional electron gas. *Phys. Rev. Lett.*, 60(9):848–850, February 1988.

[72] G. Vasseur, D. Weinmann, and R. A. Jalabert. Coulomb blockade without potential barriers. *Eur. Phys. J. B*, 51(2):267–275, Mai 2006.

[73] J. H. V. Vleck. Note on the interactions between the spins of magnetic ions or nuclei in metals. *Rev. Mod. Phys*, 34(4):681 – 686, 1962.

[74] C.-K. Wang and K.-F. Berggren. Spin splitting of subbands in quasi-one-dimensional electron quantum channels. *Phys. Rev. B*, 54(20):R14257–R14260, Nov 1996.

[75] S. Washburn. *Mesoscopic Phenomena in Solids*, pages 1–36. North Holland, 1991.

[76] D. Weinmann, R. A. Jalabert, A. Freyn, G.-L. Ingold, and J.-L. Pichard. Detection of interaction-induced nonlocal effects using perfectly transmitting nanostructures. arXiv:0803.2780v1 [cond-mat.mes-hall], March 2008.

[77] R. M. Westervelt, M. A. Topinka, B. J. LeRoy, A. C. Bleszynski, K. Aidala, S. E. J. Shaw, E. J. Heller, K. D. Maranowski, and A. C. Gossard. Imaging electron waves. *Physica E*, 24(1-2):63–69, August 2004.

[78] S. R. White. Density matrix formulation for quantum renormalization groups. *Phys. Rev. Lett.*, 69(19):2863–2866, Nov 1992.

[79] S. R. White. Density-matrix algorithms for quantum renormalization groups. *Phys. Rev. B*, 48(14):10345–10356, Oct 1993.

[80] K. G. Wilson. The renormalization group: Critical phenomena and the kondo problem. *Rev. Mod. Phys*, 47(4):773–839, October 1975.

[81] M. T. Woodside and P. L. McEuen. Scanned probe imaging of single-electron charge states in nanotube quantum dots. *Science*, 296(5570):1098 – 1101, May 2002.

[82] K. Yosida. Magnetic Properties of Cu-Mn Alloys. *Phys. Rev.*, 106(5):893 – 898, 1957.

A Appendix

In the appendix, additional technical details regqrding the calculation methods will be given. At first, section A.1 gives the details of the extrapolation technique used in the one-dimensional models. Section A.3 contains a short reminder of the Green's function theory used in this work, while section A.3 describes the explicit derivation of the retarded and advanced Green's function for a semi-infinite lead, which is used ruring the nurmerical calculations . The recursive Green's function algorithm used to calculate the Green's function including the charged tip is described in section A.4. The last two numerical operations, the determination of the self-energy describing a lead with or without the AFM tip when it is coupled to the nano-system and the numerical integration over the nano-system Green's function elements, are discussed in sections A.5 and A.6. Finally in section A.7 we will describe the techniques used to obtain the self-consistent solution of the Hartree-Fock equations 2.10-2.12 numerically, both for the one- and two-dimensional case.

A.1 Extrapolation method to determine the HF parameters

In the one-dimensional case we calculated the Hartree-Fock parameters describing an infinite system by extrapolating the results for finite models of size $N = N_R + N_L + N_S$, where N_R and N_L give the lengths of the two ideal leads and N_S is the size of the system, including the second scatterer, e. g. in chapter 3, $N_S = 4 + L_C$. In the limit $N \to \infty$, the eigenvalues and expectation values of this model Hamiltonian converge towards the correct results for infinite chains as $\propto 1/N$. Doing these calculations for different lengths N_L and N_R, one detects oscillations as shown in Fig. A.1, which all converge to the same asymptotic value. At half filling ($k_F = \pi/2$), the function oscillate between four different values. In order to optimize the extrapolation procedure, we do the Hartree-Fock calculations for four consecutive lengths N, $N+1$, $N+2$ and $N+3$. This gives the four curves shown in Fig. A.1 for the Hartree-Fock parameter v. At other filling factors, the oscillating behavior becomes more complex, e. g. at $k_F = \pi/4$ there appear 16 different curves.

This oscillating behavior can be used to optimize the numerical convergence: At half filling, we determine these four curves and fit them independently with $v_i(N) = v_i + \alpha_i 1/N_i$. The extrapolated value for the Hartree-Fock parameters v can then be obtained as the mean value $v = 1/4 \sum_i v_i$, the differences between the v_i indicating

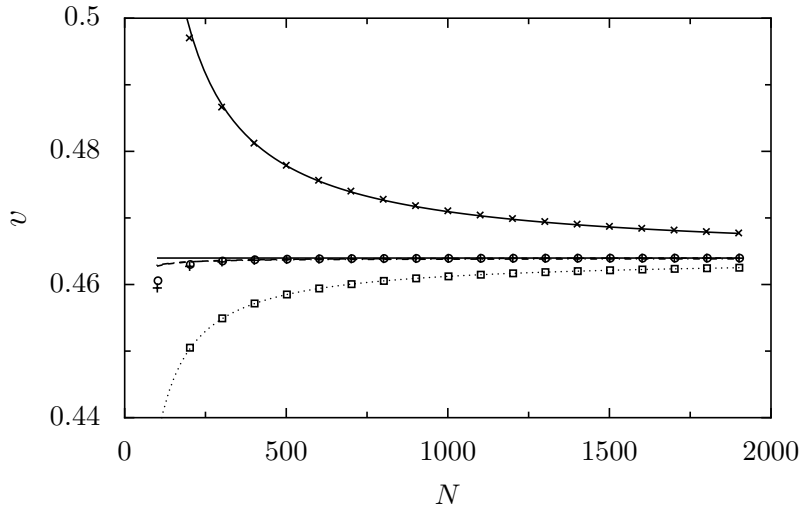

Figure A.1: Effective hopping term v of a nano-system coupled to two finite one-dimensional leads of respective lengths N_L and N_R ($N_L \approx N_R$) as a function of the total length $N = N_L + N_R + 2$, for $k_F = \pi/2$, $U = 2$, $t_\mathrm{h} = t_\mathrm{c} = 1$ and $t_\mathrm{d} = 0.1$. The different lengths are given by: $N_L = N_R = 2n$ (×), $N_L = N_R - 1 = 2n$ (+), $N_L = N_R = 2n + 1$ (□), $N_L = N_R - 1 = 2n + 1$ (○).

the quality of the extrapolation. Usually, we used sizes of up to $N = 2000$ sites to obtain the extrapolated values.

A.2 Definition of the Green's functions

In this appendix, the zero-temperature Green's function are defined. We set $\hbar = 1$.

In our models, we neglect electron-electron interactions in the leads. For non-interacting fermions, the retarded and advanced Green's functions describing the leads are given by

$$G^r(r, r', \epsilon) = \sum_n \frac{\psi_n(r)\psi_n^*(r')}{\epsilon - \epsilon_n + \mathrm{i}\eta} \tag{A.1}$$

$$G^a(r, r', \epsilon) = \sum_n \frac{\psi_n(r)\psi_n^*(r')}{\epsilon - \epsilon_n - \mathrm{i}\eta}, \tag{A.2}$$

where the sum n runs over all single particle eigenstates, $\psi_n(r)$ denotes the single particle eigenfunction with the energy ϵ_n, and η is an infinitesimal positive real number.

These Green's functions can also be expressed equivalently by the inverse of an

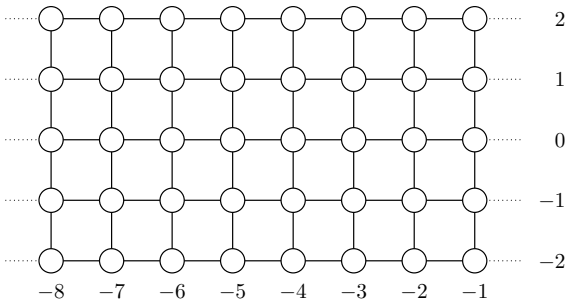

Figure A.2: The two-dimensional semi-infinite left lead, stretching from $x = -\infty$ to $x = -1$. The transverse width is given by $\mathcal{L}_y = 2L_y + 1 = 5$.

operator as

$$G^r(r, r', \epsilon) = \langle r|(\epsilon - H + \mathrm{i}\eta)^{-1}|r'\rangle \tag{A.3}$$
$$G^r(r, r', \epsilon) = \langle r|(\epsilon - H + \mathrm{i}\eta)^{-1}|r'\rangle, \tag{A.4}$$

where H is the single particle Hamiltonian describing the problem. As these two definitions are equivalent, we can use both during the calculations.

A.3 Green's function for a semi-infinite lead

In this appendix, the retarded and advanced Green's functions for a semi-infinite two-dimensional lead are calculated. Additionally, some related matrices, which are needed to describe the lead in the Green's function formalism at zero temperature are given. For simplicity, we look at the left lead only, which extends from $x = -\infty$ to $x = -1$. The Green's functions for the right lead can be derived analogously. The semi-infinite lead (sketched in Fig. A.2) is described by the Hamiltonian

$$H_L = -t_L \left(\sum_{x=-\infty}^{-1} \sum_{y=-L_y}^{L_y-1} (c^\dagger_{x,y} c_{x,y+1} + H.c.) + \sum_{x=-\infty}^{-2} \sum_{y=-L_y}^{L_y} (c^\dagger_{x,y} c_{x+1,y} + H.c.) \right), \tag{A.5}$$

which contains hopping terms in longitudinal and transverse direction. The hopping amplitude t_L is set to $t_L = 1$ in the following, defining the energy scale. For this ideal lead, the eigenfunctions and the appropriate energies can be given analytically in terms of the transverse and longitudinal eigenstates:

$$\psi_{k_x,n_y}(x, y) = \psi^x_{k_x}(x)\psi^y_{n_y}(y) \tag{A.6}$$
$$E_{k_x,n_y} = E^x_{k_x} + E^y_{n_y}., \tag{A.7}$$

The longitudinal ($\psi^x_{k_x}$) and transverse ($\psi^y_{n_y}$) eigenstates of the lead are plane waves with appropriate boundary conditions: in transverse direction, we use hard wall boundaries, which imply $\psi^y_{n_y}(L_y+1) = \psi^y_{n_y}(-L_y-1) = 0$. In longitudinal direction, a hard wall boundary is given at $x = 0$. Thus we can write the eigenstates as

$$\psi^x_{k_x}(x) = \sqrt{\frac{2}{\pi}}\sin(k_x x) \tag{A.8}$$

$$\psi^y_{n_y}(y) = \sqrt{\frac{1}{L_y+1}}\cos\left(\frac{\pi n_y}{2L_y+2}y\right), \tag{A.9}$$

where the corresponding energies for the states in x- and y-direction are given by

$$E^x_{k_x}(x) = -2\cos(k_x) \tag{A.10}$$

$$E^y_{n_y}(y) = -2\cos\left(\frac{\pi(n_y+1)}{2L_y+2}\right), \tag{A.11}$$

$n_y = 1, \ldots \mathcal{L}_y$ denotes the transverse modes in y-direction, and $k_x \in [0:\pi]$ gives the wave vector in x-direction.

Using Eq. (A.1), the Green's function of the semi-infinite lead can be written as

$$G^L_{x,y;x',y'}(z) = \sum_{n_y=0}^{\mathcal{L}_y}\int_0^\pi \mathrm{d}k_x \frac{\psi_{k_x,n_y}(x,y)\psi_{n_y,k_x}(x',y')^*}{z - E_{k_x,n_y}}, \tag{A.12}$$

where z denotes a complex energy. For $z = \epsilon \pm \mathrm{i}\eta$ with $\eta \to 0$ the usual retarded / advanced Green's function is obtained. But during the numerical calculations, we need to evaluate the Green's function also far away from the real axis, so z can also have an non-negligible imaginary part in the calculations. The indices $x, x' \leq -1$ and $-L_y \leq y, y' \leq L_y$ indicate the sites in the lead between which the Green's function is evaluated.

For our calculations we only need to determine the surface elements of the Green's function. This are the sites, where where the lead will be coupled to the nano-system, given by $x = x' = -1$. For these element, the integration can be performed analytically. We obtain

$$G^L_{-1,y;-1,y'}(z) = \sum_{n_y=0}^{\mathcal{L}_y}\psi^y_{n_y}(y)\psi^y_{n_y}(y')^* f^r\left(z - E^y_{n_y}\right), \tag{A.13}$$

where the function $f^r(z)$ is given by

$$f^r(z) = \begin{cases} \frac{z}{2} + \frac{\sqrt{4-z^2}}{4\pi}\left(\ln(2-z) - \ln(2+z) - 2\ln(\frac{z-2}{\sqrt{4-z^2}})\right) & z \notin \mathbb{R} \\ \frac{z}{2} + \frac{1}{2}\sqrt{z^2-4} & z \in \mathbb{R}, z \leq -2 \\ \frac{z}{2} - \frac{\mathrm{i}}{2}\sqrt{4-z^2} & z \in \mathbb{R}, -2 < z < 2 \\ \frac{z}{2} - \frac{1}{2}\sqrt{z^2-4} & z \in \mathbb{R}, z \leq 2. \end{cases} \tag{A.14}$$

The values for $f^r(z)$ on the real axis are given for the retarded Green's function $z = \epsilon + \mathrm{i}\eta$. For the advanced function, we get the complex conjugated results for real values of z:

$$f^a(z) = \begin{cases} \frac{z}{2} + \frac{\sqrt{4-z^2}}{4\pi}\left(\ln(2-z) - \ln(2+z) - 2\ln(\frac{z-2}{\sqrt{4-z^2}})\right) & z \notin \mathbb{R} \\ \frac{z}{2} + \frac{1}{2}\sqrt{z^2-4} & z \in \mathbb{R}, z \leq -2 \\ \frac{z}{2} + \frac{\mathrm{i}}{2}\sqrt{4-z^2} & z \in \mathbb{R}, -2 < z < 2 \\ \frac{z}{2} - \frac{1}{2}\sqrt{z^2-4} & z \in \mathbb{R}, z \leq 2. \end{cases} \tag{A.15}$$

Once these surface elements are known, it is possible to calculate the retarded and advanced self-energies $\Sigma^{L,r}$ and $\Sigma^{L,l}$, which are needed to describe the influence of this lead upon another system, when the lead is coupled at the sites $x = 1$ to that system. Given the coupling Hamiltonian between the system and the lead

$$H^{L,S} = -t_{LS} \sum_{y=-L_y}^{L_y} \left(c^\dagger_{-1,y} c_{0,y} + H.c. \right), \tag{A.16}$$

the self-energies on the sites $x = 0$ which include the effect of the lead are given by

$$\Sigma^{L,r}_{y,y'}(z) = t^2_{LS} G^{L,r}_{-1,y;-1,y'}(z) \tag{A.17}$$

$$\Sigma^{L,a}_{y,y'}(z) = t^2_{LS} G^{L,a}_{-1,y;-1,y'}(z). \tag{A.18}$$

In this appendix, we also set the hopping amplitude t_{LS} describing the coupling between the lead and the system to $t_{LS} = 1$. In order to express the Landauer-Büttiker conductance [17], we will also need the matrix Γ^L describing the transfer of the propagating modes of the lead between the system and the lead. This matrix is defined by

$$\begin{aligned} \Gamma^L_{y,y'}(\epsilon) &= \mathrm{i}\left(G^{L,r}_{-1,y;-1,y'}(z) - G^{L,a}_{-1,y;-1,y'}(z) \right) \\ &= \sum_{n_y}{}' \psi^y_{k_y}(y) \psi^y_{k_y}(y') 2\sin(k^x_{n_y}) \end{aligned} \tag{A.19}$$

The summation is only taken over those modes which propagate in the lead. These modes are determined by the condition $-2 < \epsilon - E^y_{n_y} < 2$, the states with $|\epsilon - E^y_{n_y}| > 2$ are localized and decay exponentially in y-direction.

The coupling to the second lead on the right side is described by analogous equations. We assume it extends from $x = L_x + 1$ to $x = \infty$:

$$H_R = -t_R \left(\sum_{x=L_x+1}^{\infty} \sum_{y=-L_y}^{L_y-1} (c^\dagger_{x,y} c_{x,y+1} + H.c.) + \sum_{x=L_x+1}^{\infty} \sum_{y=-L_y}^{L_y} (c^\dagger_{x,y} c_{x+1,y} + H.c.) \right), \tag{A.20}$$

The surface elements of the Green's function for this lead are given by

$$G^{Rr/a}_{L_x+1,y;L_x+1,y'}(z) = \sum_{n_y=0}^{\mathcal{L}_y} \psi^y_{n_y}(y)\psi^y_{n_y}(y')^* f^{r/a}\left(z - E^y_{n_y}\right). \tag{A.21}$$

Using the coupling Hamiltonian

$$H^{S,R} = -t_{SR} \sum_{y=-L_y}^{L_y} \left(c^\dagger_{L_x,y} c_{L_x+1,y} + H.c.\right) \tag{A.22}$$

to couple this lead to the right side of the system, we get the self-energies as

$$\Sigma^{R,r}_{y,y'}(z) = t^2_{SR} G^{R,r}_{L_x+1,y;L_x+1,y'}(z) \tag{A.23}$$

$$\Sigma^{R,a}_{y,y'}(z) = t^2_{SR} G^{R,a}_{L_x+1,y;L_x+1,y'}(z). \tag{A.24}$$

Again, we use $t_{SR} = 1$.

Finally, Γ^R is given by

$$\begin{aligned}\Gamma^R_{y,y'}(\epsilon) &= \mathrm{i}\left(G^{R,r}_{L_x+1,y;L_x+1,y'}(z) - G^{R,a}_{L_x+1,y;L_x+1,y'}(z)\right) \\ &= {\sum_{n_y}}' \psi^y_{k_y}(y)\psi^y_{k_y}(y') 2\sin(k^x_{n_y})\end{aligned} \tag{A.25}$$

For leads with more general properties, when an analytical calculation of the self-energy is not possible, the algorithm sketched in [63] can be used in order to calculate the self-energy describing the lead.

A.4 Recursive Green's function algorithm

The recursive Green's function algorithm (RGF) [25, 44, 63, 64] is a technique which allows to calculate numerically some or all elements of the Green's functions of big systems. We use it for two purposes: First, in order to include the tip-potential V_t into the self-energy $\sigma_L(z)$, which is needed for the Hartree-Fock calculations. Second, in order to calculate the Green's function elements necessary to describe the transport trough the complete system, including the tip. This will be needed to obtain the Landauer-Büttiker conductance [17].

The recursive Green's function algorithm (RGF) is based on the Dyson equation

$$\begin{aligned}G =& G^0 + G^0 V G \\ G =& G^0 + G V G^0,\end{aligned} \tag{A.26}$$

which relates the Green's function G of a perturbed system with Hamiltonian $H = H^0 + V$ to the Green's function G^0 of the unperturbed system with the Hamiltonian

H^0. The Dyson equation is valid for arbitrary perturbations V, which are added to the unperturbed Hamiltonian $H_0 0$

The RGF algorithm is useful to calculate some or all Green's function elements for a quasi one-dimensional system. It consists in recursively adding the different slices in x-direction to the system, treating the coupling between the old part of the system and the newly added slice as perturbation. It can be easily used for all two-dimensional leads described by an Hamiltonian of the form:

$$\begin{aligned} H = &\sum_{x=1}^{\mathcal{L}_x}\sum_{y=1}^{\mathcal{L}_y} \epsilon_{x,y} n_{x,y} \\ &- \sum_{x=1}^{\mathcal{L}_x}\sum_{y=1}^{\mathcal{L}_y-1} \left(t_{x,y;x,y+1} c^\dagger_{x,y} c_{x,y+1} + \text{H.c.} \right) \\ &- \sum_{x=1}^{\mathcal{L}_x-1}\sum_{y=1}^{\mathcal{L}_y} \left(t_{x,y;x+1,y} c^\dagger_{x,y} c_{x+1,y} + \text{H.c.} \right), \end{aligned} \tag{A.27}$$

where $\epsilon_{x,y}$ is the potential at site (x, y), and $t_{x,y;x',y'}$ give the hopping term between the site (x, y) and (x', y'). It is crucial not to have long range hopping terms in x-direction, but only hopping terms between sites with $x' = \pm x$. Long range hopping terms in y-direction are no problem.

We separate the system in x-direction into one slice for each value x. These slices are described by Hamiltonians

$$H_x = \sum_{y=1}^{\mathcal{L}_y} \epsilon_{x,y} n_{x,y} - \sum_{y=1}^{\mathcal{L}y-1} \left(t_{x,y;x,y+1} c^\dagger_{x,y} c_{x,y+1} + \text{H.c.} \right), \tag{A.28}$$

containing only the site potentials and the hopping terms in y-direction. The matrices

$$V^{(x,x+1)} = -\sum_{y=1}^{\mathcal{L}_y} (t_{x,y;x+1,y} c^\dagger_{x,y} c_{x+1,y} + \text{H.c.}) \tag{A.29}$$

give the couplings between the different slices x and $x + 1$. H_{x_0,x_1} denotes the Hamiltonian describing all slices with $x_0 \leq x \leq x_1$ coupled together, the remaining slices added without coupling in x-direction

$$H_{x_0,x_1} = \sum_{x=x_0}^{x_1} H_x + \sum_{x=x_0}^{x_1-1} (V_{x,x+1} + V_{x+1,x}) + \sum_{x=x_1+1}^{\mathcal{L}_x} H_x \,. \tag{A.30}$$

$G^{(1,x_1)}$ denotes the Green's function describing the coupled system from $x = 1$ to $x = x_1$ together with the separated slices for $x > x_1$. Lower indices are used to indicate submatrices for given values of x: $G^{(1,x_1)}$ is a matrix of size $\mathcal{L}_y * \mathcal{L}_x$ containing

all elements of the Green's function for the system described by H_{1,x_1}, $G^{(1,x_1)}_{x,x'}$ denotes the submatrix of size $\mathcal{L}_y$, which contains the elements $\langle x, y|G^{(1,x_1)}|x', y'\rangle$ for given x, y.

The recursive procedure consists in calculating the elements of $G^{(1,L_x+1)}$ from the known elements of $G^{(1,L_x)}$.

The surface elements of the new Green's function $G^{(1,L_x+1)}$ can be obtained as

$$G^{(1,L_x+1)}_{L_x+1,L_x+1} = \left(z - H_{L_x+1} - V^{(L_x,L_x+1)}_{L_x+1,L_x} G^{(1,L_x)}_{L_x,L_x} V^{(L_x,L_x+1)}_{L_x,L_x+1}\right)^{-1}, \tag{A.31}$$

describing the coupling of the slice $1 \leq x \leq L_x$ to the slice with $x = L_x + 1$ with the appropriate self-energy $\Sigma_{1,L_x} = V_{L_x+1,L_x} G^{(1,L_x)}_{L_x,L_x} V_{L_x,L_x+1}$. The complex energy, at which the Green's function is evaluated, is given by z. For $z \to 0^+$, one obtains the retarded Green's function G^r, for $z \to 0^-$, one obtains the advanced Green's function G^a.

To obtain the other elements, we use the Dyson equation and obtain for $x, x' \leq L_x$

$$\begin{aligned} G^{(1,L_x+1)}_{L_x+1,x} =& G^{(1,L_x)}_{L_x+1,x} + \sum_{\xi,\xi'} G^{(1,L_x+1)}_{L_x+1,\xi} V^{(L_x,L_x+1)}_{\xi,\xi'} G^{(1,L_x)}_{\xi',x} \\ =& 0 + G^{(1,L_x+1)}_{L_x+1,L_x+1} V^{(L_x,L_x+1)}_{L_x+1,L_x} G^{(1,L_x)}_{L_x,x}, \end{aligned} \tag{A.32}$$

$$\begin{aligned} G^{(1,L_x+1)}_{x,L_x+1} =& G^{(1,L_x)}_{x,L_x+1} + \sum_{\xi,\xi'} G^{(1,L_x)}_{x,\xi} V^{(L_x,L_x+1)}_{\xi,\xi'} G^{(1,L_x+1)}_{\xi',L_x+1} \\ =& 0 + G^{(1,L_x)}_{x,L_x} V^{(L_x,L_x+1)}_{L_x,L_x+1} G^{(1,L_x+1)}_{L_x+1,L_x+1}, \end{aligned} \tag{A.33}$$

$$\begin{aligned} G^{(1,L_x+1)}_{x,x'} =& G^{(1,L_x)}_{x,x'} + \sum_{\xi,\xi'} G^{(1,L_x)}_{x,\xi} V^{(L_x,L_x+1)}_{\xi,\xi'} G^{(1,L_x+1)}_{\xi',L_x+1} \\ =& G^{(1,L_x)}_{x,x'} + G^{(1,L_x)}_{x,L_x} V^{(L_x,L_x+1)}_{L_x,L_x+1} G^{(1,L_x+1)}_{L_x+1,x'}. \end{aligned} \tag{A.34}$$

The initial condition for the recursive Green's function method is the Green's function for the first slide,

$$G^{(1,1)}_{1,1} = (E - H_1)^{-1}. \tag{A.35}$$

When the system is coupled to semi-infinite leads, the effects of the attached leads can be described in terms of self-energies Σ^L and Σ^R (Appendix A.3) [21]. The left self-energy has to be included into the initial condition Eq. (A.35) as

$$G^{(1,1)}_{1,1} = (E - H_1 - \Sigma^L)^{-1}, \tag{A.36}$$

the right self-energy has to be added into Eq. (A.31) when the right-most slice $L_x + 1 = \mathcal{L}_x$ is added, resulting in

$$G^{(1,\mathcal{L}_x)}_{\mathcal{L}_x,\mathcal{L}_x} = \left(z - H_{\mathcal{L}_x} - \Sigma^R - V^{(\mathcal{L}_x-1,\mathcal{L}_x)}_{\mathcal{L}_x,\mathcal{L}_x-1} G^{(1,\mathcal{L}_x-1)}_{\mathcal{L}_x-1,\mathcal{L}_x-1} V^{(\mathcal{L}_x-1,\mathcal{L}_x)}_{\mathcal{L}_x-1,\mathcal{L}_x}\right)^{-1}. \tag{A.37}$$

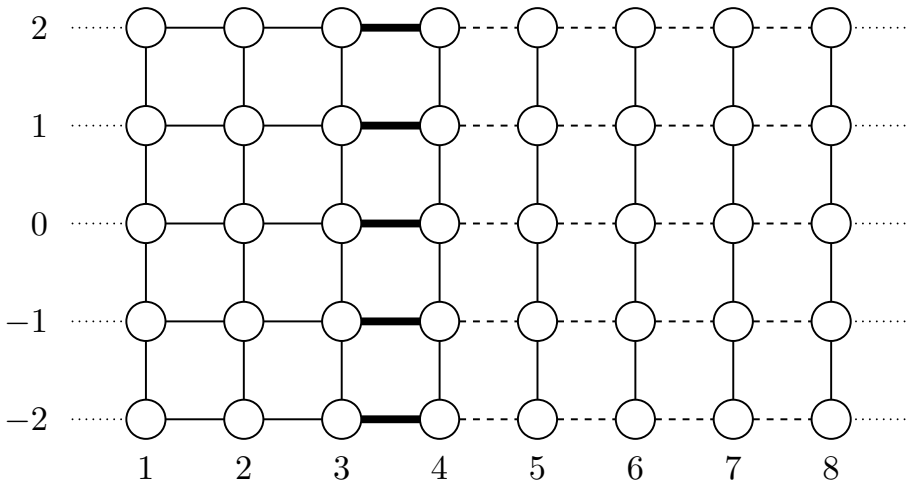

Figure A.3: Basic principle for the RGF-algorithm. In the 3-th iteration, the coupling Hamiltonian $V_{3,4}$, describing the horizontal couplings between the slices $x = 3$ and $x = 4$ is used to connect the slice $x = 4$ to the system $x \leq 3$. The new Green's function elements for the combined Hamiltonian $x \leq 4$ can be calculated using the formulas (A.31)-(A.34).

The equations (A.31)-(A.34) give the necessary formulas to calculate all $(\mathcal{L}_x\mathcal{L}_y)^2$ elements of the Green's function $G^{(1,\mathcal{L}_x)}$. However, in most cases it is not necessary to calculate all these elements but a small subset is sufficient. In these situations, a huge factor in calculation time can be saved, if only the necessary elements are calculated:

- When the Landauer-Büttiker conductance of the system is calculated, only the Green's function elements describing the transport trough the strip, including the tip, are needed. This is the submatrix $G^{(1,\mathcal{L}_x)}_{1,\mathcal{L}_x}$ of the complete Green's function. In order to obtain this submatrix, it is sufficient to calculate the submatrices $G^{(1,L_x)}_{1,L_x}$ and $G^{(1,L_x)}_{L_x,L_x}$ during the recursion procedure.

- To complete the numerical integration of the Hartree-Fock equations, only the Green's function elements at the left end of the strip ($G^{(1,\mathcal{L}_x)}_{1,1}$) are needed. The fastest way to obtain these elements is to apply the RGF-algorithm in the other direction: Starting at the right end with $G^{(\mathcal{L}_x,\mathcal{L}_x)}$, slices are added recursively at the left side. As we only need the elements at the surface, it is sufficient to calculate the surface elements $G^{(L_x,\mathcal{L}_x)}_{L_x,L_x}$ during the recursion, by the use of Eq. (A.31).

For our specific model, there are some additional possible optimizations of this general algorithm. Most of the numerical calculation time is spent in calculating the self-energy describing the right lead as a function of the tip position. Having no

disorder in the lead, we can use the following procedure to obtain the results for one vertical tip position y_T and all horizontal tip positions $1 \leq x_T \leq x_{T,\max}$ in one run:

- We calculate the self-energy describing the semi-infinite lead.
- We add a vertical slice including the tip to the semi-infinite lead and calculate the surface-elements of this slice. This gives the self-energies for $x_T = 1$.
- We add a perfect vertical slice at the left of the tip and calculate the surface elements of this new model. This shifts effectively the tip to $x_T = 2$ and gives the self-energies for $x_T = 2$.
- We add iteratively new slices and calculate the appropriate self-energies, until $x_T = x_{T,\max}$ is reached.

When there is disorder in the leads, this simple procedure cannot be used anymore. However, G. Metalidis *et al.* discussed a recursive Green's function algorithm optimized to obtain the Green's function as a function of the tip position [48], which can be used in the presence of disorder in the leads.

A.5 Self-energy of the coupling of a $2d$-strip to the nano-system

During the solution of the Hartree-Fock equations for the two-dimensional model, a numerical integration of the Green's function elements inside the nano-system has to be performed. During this calculation, we want to reduce numerical efforts by only calculating the Green's function elements which are really needed, that is inside the nano-system. The remaining part of the model (the left and the right strip) is described by the self-energies $\sigma_L(z)$ and $\sigma_R(z, V_t, x_t, y_t)$ which are added to the nano-systems Green's function. Using this procedure, the Green's function $G_{\text{sys}}(z)$ which has to be calculated is reduced to a 2×2 matrix.

Calculating these self-energies $\sigma_{L,R}$ is done in two steps: First, the Green's functions of the two-dimensional strips have to be evaluated on all sites which are directly coupled to the nano-system. Second, the self-energies $\sigma_{L,R}$ can be calculated.

The first step is done using the recursive Green's function algorithm described in section A.4, starting at $x_{\max} = x_T$ and stopping at $x_{\min} = 2$. Then, the strip is completed, adding the sites with $x = 1$, except the central site $(x, y) = (1, 0)$, which belongs to the nano-system.

For the right lead, including the tip potential V_T, the self-energy σ_R is then given by

$$\sigma_R = V_{SR}^{\dagger} G^R V_{SR}, \tag{A.38}$$

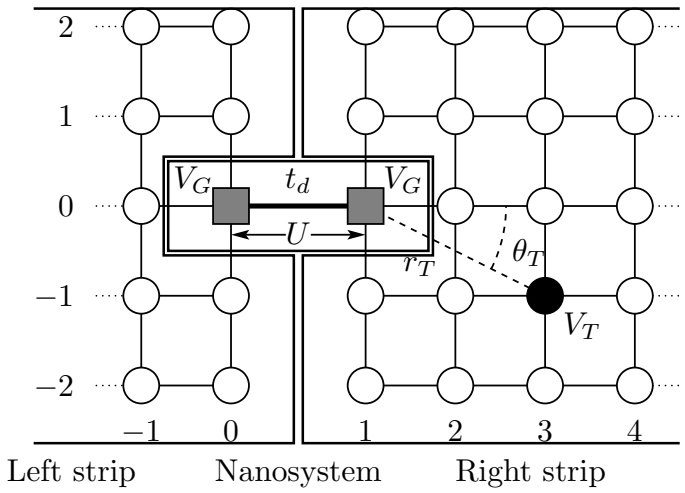

Figure A.4: The "strips" contain all sites except the nano-system sites $(x, y) = (0, 0)$ and $(1, 0)$. Using this definition, the Hartree-Fock calculation inside the nano-system can be done using only 2×2-matrices, thus decreasing the numerical effort needed to obtain a self-consistent solution.

V_{SR} denoting the coupling between the nano-system and the right strip,

$$V_{SR} = -c^{\dagger}_{1,0}(c_{2,0} + c_{1,-1} + c_{1,1}) + \text{H.c.}. \tag{A.39}$$

Combining Eqs. A.38 and A.39, the self-energy σ_R is given by the sum over all 9 Green's function elements which are defined between the three sites $(2, 0)$, $(1, -1)$ and $(1, 1)$,

$$\sigma_R = \sum_{i,j=(1,-1),(1,1),(2,0)} G^R_{i,j}. \tag{A.40}$$

The self-energy σ_L describing the coupling to the left lead can be calculated analogously, using the three points $(-1, 0)$, $(0, -1)$ and $(0, 1)$.

A.6 Numerical integration of the Green's function

In order to solve the Hartree-Fock equations (5.5)-(5.7) self-consistently, we have to integrate the Green's function elements G inside the nano-system. In the two-dimensional case, this integration has to be done numerically, as the analytical formulas for the Green's function elements are unknown, the Green's function being calculated by the recursive Green's function method. Instead of doing the original integration $\int_{-\infty}^{E_F} \mathrm{d}E G_{i,j}(E \pm \mathrm{i}\eta)$ with $\eta \to 0$ to obtain the correct results for the retarded $(E + \mathrm{i}\eta)$ or the advanced $(E - \mathrm{i}\eta)$ Green's function directly, there are some possible simplifications which decrease the calculation time:

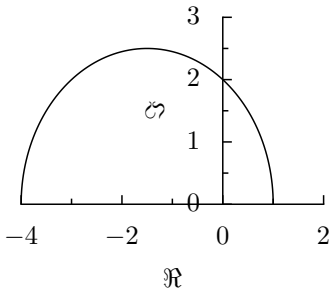

Figure A.5: The numerical integration of the Green's function elements is done on a half-circle in the upper half of the complex plane, from $z = -4 + O^{+}\mathrm{i}$ until $z = E_F + 0^{+}\mathrm{i}$. As there are no poles in the plane except on the real axis, an arbitrary integration path can be chosen.

First, only the imaginary part of the integral appears in the Hartree-Fock equations. In the absence of magnetic fields, the Green's functions are completely real for energies below the band ($E < -4$). In addition, there are no poles of the Green's function on the real axis for $-\infty < E < -4$. Because of this, we know that the integral for $-\infty < E < -4$ vanishes for all elements of the Green's function

$$\Im\left(\int_{-\infty}^{-4} \mathrm{d}E G_{i,j}(E \pm \mathrm{i}\eta)\right) = \Im\left(\int_{-\infty}^{-4} \mathrm{d}E G_{i,j}(E)\right) = 0. \tag{A.41}$$

Thus it is sufficient to start the numerical integration at $E = -4$.

Second, instead of doing the integration along the real axis with a vanishing imaginary contribution $\mathrm{i}\eta$, and taking the limit $\eta \to 0$, we can use the fact that all poles of the Green's functions are situated on the real axis. This means, that we can use contour integration and select an arbitrary integration path in the upper (for the retarded Green's function) or lower (for the advanced Green's function) part of the complex plane instead. For all possible paths in the appropriate half of the complex plane which start at $E = -4$ and end at $E = E_F$, we will obtain the same result. Some tests showed, that fastest numerical convergence is achieved by using a half-circle in the upper plane (Fig. A.5) as integration path.

Integration is a common task in numerical calculations, such that many algorithms with different characteristics have been developed [58]. All have in common that the continuous integration is replaced by a discrete sum. The algorithms differ in the way how the sums are defined and on which points x_i the function has to be evaluated. In general, very good results can be obtained by approximating the function $f(x)$ by a series of polynomials, and then summing over these polynomials [1].

We are using Gauss-Kronrod formula [18, 58] for the integration on the half circle in the complex plane, with an increasing number of points $N = 10, 21, 43, 87, 175$, in order to be able to detect when the numerical integration converges. For $N = 175$

points, the results were converged to a relative precision $\leq 10^{-9}$. Using Gauss-Kronrod points for the integration has the advantage that the results for n points can be used again in the calculation of the result for $2n+1$ points, thus decreasing the numerical calculation time.

A.7 Numerical solution of the Hartree-Fock equations

The models studied in this thesis are describe by 1 to 3 Hartree-Fock parameters, which have to be defined as solution of a system of one to three coupled Hartree-Fock equations. We use two different algorithms for the one- and two-dimensional problems.

In the one-dimensional case, each evaluation of the expectation values $\langle c_0^\dagger c_0 \rangle$, $\langle c_0^\dagger c_1 \rangle$ and $\langle c_1^\dagger c_1 \rangle$ for a given set of parameters v, V_0 and V_1 is time consuming, as we have to perform the extrapolation procedure described in A.1. In order to solve the Hartree-Fock equations (2.10)-(2.12), it is necessary to evaluate these expectation functions for different sets of v, V_0 and V_1. We use an optimization of Newton's method [58], the so-called "Powell's Hybrid method" [53] in order to solve this system of non-linear equations numerically.

In two dimension, where we use the Green's function formulation of the Hartree-Fock theory, the effort needed to calculate the Hartree-Fock self-energies (5.5)-(5.7) is independent of the model size once the self-energies σ_L and σ_R are calculated. In this situation, an iterative procedure is numerically faster: We start from a first set of Hartree-Fock self-energies $\Sigma_{\mathbf{0}}^{\mathrm{H},0}$, $\Sigma_{\mathbf{1}}^{\mathrm{H},0}$ and $\Sigma^{\mathrm{F},0}$, and integrate the Green's function elements inside the nano-system. Then Eqs. (5.5)-(5.7) are used to obtain the Hartree-Fock self-energies $\Sigma_{\mathbf{0}}^{\mathrm{H},1}$, $\Sigma_{\mathbf{1}}^{\mathrm{H},1}$, $\Sigma^{\mathrm{F},1}$. This iteration is continued until the self-energies are converged to their values $\Sigma_{\mathbf{0}}^{\mathrm{H}}$, $\Sigma_{\mathbf{1}}^{\mathrm{H}}$, Σ^{F}. In general, this iterative scheme is not guaranteed to converge, it can have also oscillatory solutions, where e. g. $\Sigma_{\mathbf{H}F}^{2n}$ and $\Sigma_{\mathbf{H}F}^{2n+1}$ converge to different asymptotic values. To overcome this problem, some more advanced algorithms for solving Hartree-Fock-like equations have been developed. However, in our model these advanced algorithms are not necessary. If an iteration did not converge, we can easily restart it, using different starting parameters $\Sigma_{\mathbf{0}}^{\mathrm{H},1}$, $\Sigma_{\mathbf{1}}^{\mathrm{H},1}$ and $\Sigma^{\mathrm{F},1}$.